1. TIDAL SYNCHRONIZATION OF THE ROTATION OF EARLY MAIN SEQUENCE STARS IN CLOSE BINARIES.
2. THE RINGS OF URANUS: RESULTS OF THE 1978 APRIL 10 OCCULTATION.
3. ON THE RESONANCE THEORY OF THE RINGS OF URANUS.

Thesis by

Philip David Nicholson

In Partial Fulfillment of the Requirements

for the Degree of

Doctor of Philosophy

California Institute of Technology

Pasadena, California

1979

(Submitted September 25, 1978)

To my parents, with love;

To Dr. B.J. O'Mara, my undergraduate physics Lecturer, who enjoined me to seek my fortune across the Pacific.

ACKNOWLEDGEMENTS

To Dr. Peter Goldreich, I am indebted for many things: for his strong encouragement of an Australian student to come to California; for many hours of detailed discussions covering almost all aspects of this work, in his capacity as both my academic and thesis advisor; for encouragement and useful criticism; and last, but not least, for an insight into the way an expert "does theory". Dr. Goldreich and I collaborated on the work which forms Part 3 of this thesis, and he provided the initial stimulus for the occultation observations reported in Part 2.

Dr. Duane Muhleman provided my introduction to the analysis of observational data during my early years as a graduate student. Since then, we have had many useful discussions, and this work has benefitted from his criticisms.

The work reported in Part 2 of this thesis represents the contributions of several people besides the writer, to all of whom I am most grateful. Dr. Gerry Neugebauer, Keith Matthews, and Gordon Forrester provided and/or constructed the instrumentation necessary for successful occultation observations at 2.2μm, while Drs. Eric Persson and Robert Zinn actually carried out the observations in Chile. The Hale Observatories kindly provided the necessary time on the Du Pont telescope at Las Campanas, on somewhat shorter notice than is customary. Dr. Maarten Schmidt generously offered us simultaneous observing time on the Hale telescope at Mount Palomar, although the weather chose to be

unco-operative. Assistance in this project was also provided by Carolyn Porco, Dr. Jay Elias, M. Aaronson, M. Clark, A. Guerra, F. Peralta, L. Papic, and R. Lucinio.

I acknowledge many fascinating discussions with Dr. Guiseppe Colombo, concerning the rings of Uranus, from which the initial concept for the model of the ϵ ring presented here emerged.

For several discussions which clarified my understanding of dynamical tides in rotating stars, I am grateful to Drs. Tony Dobrovolskis and Andrew Ingersoll. In various stages of this research, assistance has been rendered by Barbara Noyes, Dr. George Preston, and Dr. James Elliot.

To Jo Ann, my wife, who has shouldered much more than her fair share of domestic responsibilities during the final stages of this work, while simultaneously providing editorial assistance in its preparation, go my deepest thanks.

For much of the final preparation of this thesis, I owe thanks to Kay Campbell, Hallee Kelso and Delmine Da Costa.

My work at Caltech has been largely supported by NASA grant NGL 05-002-003. Additional support, for the investigations reported in Part 2, was provided by NASA grants NGL 05-002-140 and NGL 05-002-207, and NSF grants AST 76-22676, AST 77-20516, and AST 76-24281. My studies in the U.S. were made possible, in part, by an Australian-American Fulbright Travel Grant and a Gowrie Travelling Scholarship.

PREFACE

This thesis represents three separate investigations, one of which deals with close binary stellar systems and the other two with the rings of Uranus.

Part 1 is an unpublished theoretical study of the synchronization of rotational and orbital motions of early type main sequence stars in close binaries.

Part 2 concerns the observation and analysis of a stellar occultation by the rings of Uranus. The observations were made by Drs. Eric Persson, Gerry Neugebauer, and Keith Matthews, while the writer is responsible for the data analysis and for the construction of the model for the ϵ ring. This work is to be published, as presented here, in the October 1978 issue of the Astronomical Journal.

Part 3 is a quantitative analysis of a resonance model proposed for the rings of Uranus. This work was carried out in collaboration with Dr. Peter Goldreich, and has been published as a Letter to Nature (Nature 269 (1977) pp. 783-785).

ABSTRACT

Part 1:

The rotational synchronization of an early type main sequence star in a close binary system has been attributed to radiative damping of the dynamical component of the tide raised in the star by its companion (Zahn, 1975, 1977). An investigation of the dynamical tide is presented here, which includes the heretofore neglected effects of stellar rotation. Foremost among these effects is the splitting of the tidal response into a set of modes whose latitudinal structures are controlled by the solutions of Laplace's tidal equation.

An approximate analytic expression is derived for the rate of tidal energy dissipation associated with each of these modes, which in turn determines the rate of synchronization of the star's rotation with its orbital motion. This analytic result is supported by a numerical analysis of the dynamical tide raised in a 5 $M_\odot$ star. Combination of analytic and numerical results yields synchronization timescales for stars in the mass range 2 $M_\odot$ - 10 $M_\odot$. These timescales are a factor of 10 shorter than those obtained by Zahn, and are in good agreement with the observational data concerning synchronism among early type stars in close binaries. It is suggested, however, that the final stages of synchronization are controlled by another mechanism: the slow stellar expansion which accompanies the later stages of main sequence evolution.

Part 2:

Observations of the 1978 April 10 stellar occultation by the rings of Uranus are presented. Nine rings were observed and their radii and widths are calculated. Rings η, γ, and δ are found to be most likely circular and coplanar, in agreement with previous analyses; the remaining rings are either non-circular or slightly inclined. The width of the ϵ ring is a linear function of its radius from the center of Uranus, projected onto the satellites' orbital plane; this suggests that it forms one continuous non-circular ring. The optical depth profile of the ϵ ring has not changed significantly since 1977 March. A model of this ring which fits all available observations adequately is that of a uniformly precessing Keplerian ellipse coplanar with the satellites' orbits. This model permits predictions of the radius and width of the ϵ ring for future occultations. The precession rate is used to determine J_2 for Uranus, on the assumption that precession is caused solely by the planetary oblateness and not by satellite-ring interactions.

Part 3:

A three-body resonance model proposed to account for the rings of Uranus is quantitatively analyzed and found to be unacceptable on several grounds. Calculation of the strengths of two-body and three-body resonances involving all known satellites of Uranus, and which fall in the neighborhood of the rings, reveals that the strongest resonances are the 4:1 and 5:1 resonances with Miranda, and the three-body resonances involving

Miranda and Ariel. Resonances invoked by the proposed model are much weaker. Despite the fact that four of these relatively strong resonances approximately coincide with rings 5, α, γ, and ϵ, they are too weak to explain the observed widths of the rings. Finally, the simple ring model of densely packed particles librating about a resonance is shown to be secularly unstable.

TABLE OF CONTENTS

FIGURES: Part 1

TABLES: Part 1

——— oOo ———

FIGURES: Part 2

TABLES: Part 2

———— oOo ————

FIGURE: Part 3

TABLE: Part 3

oOo

PART 1

TIDAL SYNCHRONIZATION OF THE ROTATION OF EARLY MAIN SEQUENCE STARS IN CLOSE BINARIES.

I. INTRODUCTION

Rotational velocities of stars in close binary systems are, on the average, considerably lower than those of single stars of the same spectral type. In fact, observations of an eclipsing binary, for which the radii of the stars may often be determined from analyses of the light and radial velocity curves, frequently indicate that one or both stellar rotation rates are almost synchronous with the orbital motion (Olson, 1968; Plavec, 1970).

While some form of interaction leading to such synchronization does not seem implausible for stars which are separated by only a few radii, the precise mechanism has been elusive. Tidal interaction, long considered the obvious candidate, may lead to a transfer of angular momentum from stellar rotation to the orbital motion of the system, but the tidal torque on, say, the primary depends on the phase lag between the tidal potential due to the secondary and the resulting tidal distortion of the primary. If this phase lag is zero, then the distortion of the primary is symmetric about the line of centers of the two stars, and there can be no tidal torque.

The amplitude of the phase lag depends, in turn, on the rate of mechanical energy dissipation in the system which is attributable to the tidal distortion. If the rotational angular velocity of the primary and the mean orbital motion of the binary system are denoted by Ω and ω respectively, and the primary's moment of inertia by I, then it may readily be shown (see section 5b) that the rate of

spin-down of the primary due to the tidal torque is given by

$$\dot{\Omega} = - \frac{\dot{E}}{I(\Omega - \omega)} \quad , \qquad (1.1)$$

where $\dot{E}$ is the rate of tidal dissipation of mechanical energy in the primary. The problem of calculating the rate of synchronization of rotational and orbital motions thus amounts to calculating the rate of tidal energy dissipation.

For main sequence stars with deep convective envelopes (i.e., spectral type F or later), it has been shown (Zahn, 1966, 1977) that convectively induced turbulent viscosity acting on the tidal currents flowing in the envelopes of these stars results in significant energy dissipation. The calculated rate of dissipation, while quite uncertain because of the limitations of the mixing length theory of convection, coupled with the long main sequence lifetimes of such stars (10^9-10^{11} yr), readily explains the occurrence of synchronism for late type stars in close binaries.

However, the great majority of stars in close binary systems that have had their rotational velocities measured are main sequence stars of spectral type A and B. Such stars possess stably stratified radiative envelopes and relatively small convective cores. Despite the high Reynolds number associated with tidal currents in the envelope of such a star, it is generally believed (e.g., Zahn, 1977) that the stable stratification prevents the growth of turbulence and the associated turbulent (or eddy) viscosity. The velocities of tidal currents in the core and the estimated turbulent viscosity

there are both small, and result in negligible energy dissipation. The action of "molecular" viscosity or radiative damping on the envelope currents is also insignificant (Zahn, 1977).

The only promising mechanism for tidal energy dissipation in early type main sequence stars has been advanced by Zahn (1975, 1977), and involves the "dynamical" tide. This term refers to that small part of the time dependent tidal distortion of a star which is not given by the equilibrium response of the star to a quasi-static tidal potential. The velocities and distortions associated with the dynamical tide are generally much smaller than those associated with the equilibrium component of the tide, and are usually neglected in studies of the dynamics of close binaries (e.g., Kopal, 1959).

Zahn was able to show, however, that the dynamical tide, which in the radiative envelope takes the form of radially propagating gravity waves, transports a significant flux of mechanical energy from the interior of the star to the surface layers. Radiative damping of these gravity waves in the stellar atmosphere may result in the loss of a large fraction of this energy from the binary system. Zahn's calculations indicated that the rate of transport and subsequent dissipation of mechanical energy by the dynamical tide was indeed sufficient to account for the synchronization of early type stars in binaries with orbital periods less than 2 or 3 days. This is in fair agreement with the observational evidence although somewhat greater dissipation rates than those calculated by Zahn are indicated.

The present work is essentially an independent version of Zahn's calculations, but with two major changes which bring the theory closer to the real world. Zahn has neglected the effect of rotation (via the coriolis force) on the dynamical tide, even though the rotational periods of non-synchronous early type stars in close binaries are of the order of 1 day or less. This has been remedied here, although some approximations have been made to keep the problem tractable. The second improvement is the replacement of Zahn's zero-temperature outer boundary condition for the stellar model used in the calculations by a more realistic finite temperature condition. This matter bears on the question of what fraction of the energy transported by the dynamical tide is dissipated in the stellar atmosphere.

In section II, the general theory of the dynamical tide in a rotating, early type main sequence star is developed. Particular attention is paid to those features of the theory which arise peculiarly as a consequence of stellar rotation, and have thus not previously been considered. Section III gives approximate analytic solutions for the functions describing the radial dependence of the dynamical tide, and concludes with an approximate analytic expression for the energy dissipation rate.

The analytic solutions of section III are supplemented, in section IV, by more accurate numerical solutions carried out for a 5 $M_\odot$ star (spectral type $\sim$ B6.5). In section V these numerical results, scaled to other stellar masses by use of the analytic

expressions developed in section III, are employed to describe the process of synchronization in a close binary. Synchronization time scales are calculated for a range of early type stars, and compared with the available observational data. Section VI enumerates the principal results, relating both to the extension of the theory of dynamical tides, and to the degree of success of the theory in accounting for synchronism in early type close binaries.

Throughout the theoretical development of sections II, III, IV, and V, the star suffering tidal distortion is referred to as the primary, and its companion as the secondary. The latter is treated as a point mass. No implication concerning the relative masses or luminosities of the two stars is intended. In the present terminology, each component of a real binary acts as both primary and secondary.

II. THE DYNAMICAL TIDE IN A ROTATING STAR.

a) The tidal potential

The first step in calculating the amplitude of either the equilibrium or the dynamical tide is to write an expression for the tidal potential, U, responsible for these distortions. It is assumed, for simplicity, that the rotation axis of the primary is normal to the orbit plane, and that the binary orbit is circular. We use a spherical polar co-ordinate system centered on, and rotating with, the primary. Colatitude, θ, is measured from the north rotation pole, and longitude, φ, is measured in the prograde direction with $\varphi = 0$ corresponding to the direction of the secondary at time $t = 0$. Under the above assumptions, the tidal potential may be written as

$$U(r,\theta,\varphi,t) = -\frac{GM_2}{a}\sum_{\ell=2}^{\infty}\sum_{m=0}^{\ell} T_\ell^m\,(r/a)^\ell\,P_\ell^m\,(\cos\theta)\,\cos(\sigma_m t + m\varphi) \quad , \tag{2.1}$$

where

$$T_\ell^m = (2-\delta_{m0})\,\frac{(\ell-m)!}{(\ell+m)!}\,P_\ell^m(0) \quad , \tag{2.2}$$

and

$$\sigma_m = m(\Omega-\omega) \quad . \tag{2.3}$$

M_2 is the mass of the secondary, and a the separation between the centers of primary and secondary. The functions P_ℓ^m are associated Legendre functions. Since $P_\ell^m(0) = 0$ if $\ell - m$ is odd, only even m terms appear for ℓ even, and only odd m for ℓ odd. As long as the tidal response of the star remains linear, each temporal Fourier component of the tide may be considered separately, and the results

subsequently summed. The dominant terms in the expansion of U, to which we will later restrict our attention, are given by

$$-\frac{GM_2}{a}\left(\frac{r}{a}\right)^2\left\{-\tfrac{1}{2}\,P_2^0(\cos\theta)+\tfrac{1}{4}\,P_2^2(\cos\theta)\cos(\sigma_2 t+2\varphi)\right\}\quad,\qquad(2.4)$$

where $$P_2^0(\cos\theta)=\tfrac{1}{2}(3\cos^2\theta-1)\quad,$$

and $$P_2^2(\cos\theta)=3(1-\cos^2\theta)\quad.$$

b) Derivation of the differential equations

The differential equations governing stellar tidal oscillations are derived from the familiar equations of motion of an inviscid, compressible fluid, including coriolis and centrifugal terms:

$$\frac{\partial}{\partial t}\ (\rho \underset{\sim}{v}) + (\underset{\sim}{v}\cdot\nabla)\ \rho \underset{\sim}{v} = -\nabla p - \rho\ \nabla V - 2\rho(\underset{\sim}{\Omega} \times \underset{\sim}{v}) \tag{2.5}$$

$$\frac{\partial \rho}{\partial t} = -\nabla\cdot(\rho \underset{\sim}{v}) \quad . \tag{2.6}$$

The symbols are defined as follows: ρ = density, $\underset{\sim}{v}$ = fluid velocity, p = pressure, $\underset{\sim}{\Omega}$ = stellar rotational angular velocity, and V = total potential, including the internal gravitational potential of the star and a centrifugal term, as well as the tidal potential. The last term in equation (2.5) is the coriolis acceleration. The third fundamental equation comes from the requirement that the oscillations be adiabatic:

$$\frac{1}{p}\left(\frac{\partial p}{\partial t} + \underset{\sim}{v}\cdot\nabla p\right) = \frac{\Gamma}{\rho}\left(\frac{\partial \rho}{\partial t} + \underset{\sim}{v}\cdot\nabla \rho\right) \quad , \tag{2.7}$$

where Γ is the ratio of specific heats.

Since the tidal oscillations are of very small amplitude, except in the stellar atmosphere, these basic equations may be linearized in terms of the small departures ($\delta\rho$, δp, δV) from the equilibrium conditions (ρ_0, p_0, V_0) which prevail in the absence of tidal forces. It is assumed that this equilibrium state has $\underset{\sim}{v}_0 = 0$. The linearized equations are:

$$\rho_0 \frac{\partial \underset{\sim}{v}}{\partial t} = -\nabla \delta p - \delta\rho \nabla V_0 - 2\rho_0 (\underset{\sim}{\Omega} \times \underset{\sim}{v}) - \rho_0 \nabla \delta V \tag{2.8}$$

$$\frac{\partial \delta\rho}{\partial t} = -\nabla \cdot (\rho_0 \underset{\sim}{v}) \tag{2.9}$$

$$\frac{1}{p_0}\left(\frac{\partial \delta p}{\partial t} + \underset{\sim}{v} \cdot \nabla p_0\right) = \frac{\Gamma}{\rho_0}\left(\frac{\partial \delta\rho}{\partial t} + \underset{\sim}{v} \cdot \nabla \rho_0\right) \quad . \tag{2.10}$$

The equilibrium potential, V_o, includes the gravitational and centrifugal potentials, while δV consists of two parts: the externally applied tidal potential, U, and the perturbations to the internal gravitational potential, δV^{int}, caused by the tidal density perturbations. A fourth differential equation (Poisson's equation) is thus necessary to relate δV^{int} and $\delta\rho$:

$$\nabla^2 \left[\delta V^{int}(r,\theta,\varphi)\right] = 4\pi G\, \delta\rho(r,\theta,\varphi) \quad . \tag{2.11}$$

The solution of these linearized equations may be accomplished by either of two methods. All of the normal modes of oscillation of the star might be identified, along with their natural frequencies, ω_{mnk}. These modes are characterized by three indices - one each for the longitudinal (m) and latitudinal (n) structure of the mode, and one for the radial structure (k). The fundamental radial mode has $\omega_{mno} \simeq \sqrt{G\bar{\rho}} \sim 2\pi/1^{hour}$, where $\bar{\rho}$ = average density of the star. Higher order radial modes are divided into two sets: p-modes ($k > 0$) with $\omega_{mnk} \to \infty$ as $k \to \infty$; and g-modes ($k < 0$) with $\omega_{mnk} \to 0$ as $k \to -\infty$. The number of radial nodes increases as $|k|$ increases. It is possible to consider the forcing of each of these normal modes by a particular temporal Fourier component of the tidal potential, denoted

by the subscript m, and then sum up all of the separate responses to obtain the total stellar distortion due to that Fourier component. This procedure, while conceptually straightforward, requires a detailed investigation of the normal modes of the star, and many separate forcing calculations. Ultimately, many of the forced modes would make only negligible contributions to the total response. We thus choose to employ a second, more direct procedure which does not explicitly take account of the normal modes. Before continuing, however, we digress to introduce a very useful approximation suggested by the above discussion.

Tidal forcing periods, $2\pi/\sigma_m$, in close binaries typically lie in the range ~ 12 to $\gtrsim 100$ hours, so $\sigma_m \ll \omega_{mn0}$. Thus, all of the p-modes and the low order g-modes are being forced at a frequency much lower than their natural frequencies, and the response of each of these modes is essentially a static or equilibrium response, which is independent of σ_m. Now the internal potential perturbation, δV^{int}, is largely controlled by the density perturbations associated with normal modes with few radial nodes (i.e., the low order p-modes and g-modes), as the gravitational field associated with a rapidly oscillating density component tends to cancel. Consequently, all of the <u>significant</u> individual normal mode contributions to δV^{int} are equilibrium responses, and thus δV^{int} itself may be approximated by the equilibrium stellar response to the tidal potential. In terms of the usual Love functions, $k_\ell(r)$, and for the m^{th} Fourier component of the tidal potential, this result is expressed by

$$\delta V_m^{int}(r,\theta) \simeq \sum_{\ell=m}^{\infty} k_\ell(r)\, U_\ell^m\,(r,\theta) \quad , \tag{2.12}$$

where U_ℓ^m represents the (ℓ,m) component of expression (2.1). The Love functions may be calculated from the density profile of the star, $\rho_0(r)$, by solving Poisson's equation (2.11) for the equilibrium tide. The m^{th} Fourier component of the total potential perturbation in equation (2.8) is thus given by

$$\delta V_m \simeq -\frac{GM_2}{a} \sum_{\ell=m}^{\infty} [1+k_\ell(r)]\, T_\ell^m (r/a)^\ell\, P_\ell^m\,(\cos\theta) \cos[\sigma_m t + m\varphi] \quad , \tag{2.13}$$

and the problem is reduced to the simultaneous solution of equations (2.8), (2.9), and (2.10).

Let us now return to the second method for obtaining this solution. The m^{th} temporal Fourier component of the tidal response is isolated, and all perturbed quantities assumed to have the time and longitude dependence $e^{i(\sigma_m t + m\varphi)}$, where σ_m is given by equation (2.3). The perturbing potential is given by equation (2.13). We now make two approximations which greatly simplify both the analytic and numerical solution of the equations.

(1) The equilibrium structure of the star is taken to be spherically symmetric, i.e., ρ_0, p_0, and V_0 are functions of

the radius, r, only. We are thus neglecting the rotational flattening of the star, a procedure which is valid as long as $\Omega^2 \ll G\bar{\rho}$, where $\bar{\rho}$ is the average stellar density.

(2) In calculating the coriolis force, $-2\rho_0 \underset{\sim}{\Omega} \times \underset{\sim}{v}$, only the radial component of $\underset{\sim}{\Omega}$, $\Omega \cos\theta \, \hat{\underset{\sim}{r}}$, is retained. This procedure is standard in the theory of planetary atmospheric tides, and essentially amounts to asserting that the radial component of the coriolis force is small compared with the perturbed radial gravitational force, $-\delta\rho \nabla V_0$. This is correct in the radiative envelope and in the stellar atmosphere, where the radial wavelength of the tidal oscillations is small compared with the horizontal wavelength (see section 2e). We will justify this statement *a posteriori* in Appendix 1. The above assertion is, however, incorrect when applied to the stellar core, and must consequently introduce some error in the solutions.

The principal reason for making approximation (2) above is that it leads to the separation of the equations in spherical polar co-ordinates. The details of this separation are relegated to Appendix 2, and the results simply quoted here. In the usual manner, an arbitrary separation constant, denoted by K, appears. Physical constraints imposed on the angular part of the solution restrict K to take any of an infinite set of discrete values, $\{K_{mn}\}$. Discussion of these constraints and of the form of the angular solutions is deferred to section 2c for convenience. The complete solution to equations (2.8, (2.9), and (2.10) may thus be written as a sum of

individual solutions corresponding to the different allowed values of K. The pressure perturbation and the radial component of the velocity take the form:

$$\delta p = \sum_n \delta p_{mn}(r)\, \Theta_{mn}(\theta)\, e^{i(\sigma_m t + m\varphi)} \quad , \tag{2.14}$$

and

$$(\underset{\sim}{v})_r = i\sigma_m \sum_n h_{mn}(r)\, \Theta_{mn}(\theta)\, e^{i(\sigma_m t + m\varphi)}; \tag{2.15}$$

while the density perturbation and the other two velocity components are given by similar expressions involving the functions δp_{mn}, h_{mn}, and Θ_{mn}, and their first derivatives. If, for the present, it is assumed that the functions $\Theta_{mn}(\theta)$ form a complete set in the interval $0 \le \theta \le \pi$ (see section 2c for a discussion of this point), the potential δV_m may be similarly expanded:

$$\delta V_m = \sum_n \delta V_{mn}(r)\, \Theta_{mn}(\theta)\, e^{i(\sigma_m t + m\varphi)} \quad . \tag{2.16}$$

The functions δp_{mn}, h_{mn}, and Θ_{mn} satisfy the following ordinary differential equations, in which the subscript m is largely suppressed:

$$p_0^{1/\Gamma} \frac{d}{dr}\left(p_0^{-1/\Gamma}\, \delta p_n\right) - \rho_0(\sigma^2 - N_v^2)\, h_n = -\rho_0 \frac{d}{dr}(\delta V_{mn}) \; ; \tag{2.17}$$

$$\frac{\sigma^2 \rho_0}{r^2 p_0^{1/\Gamma}} \frac{d}{dr}(r^2 p_0^{1/\Gamma} h_n) - \left(\frac{K_{mn}}{r^2} - \frac{\sigma^2 \rho_0}{\Gamma p_0}\right) \delta p_n = \frac{K_{mn}\rho_0}{r^2}\, \delta V_{mn} \; ; \tag{2.18}$$

$$\frac{d}{d\mu}\left(\frac{1-\mu^2}{f^2-\mu^2} \frac{d\Theta_n}{d\mu}\right) - \frac{1}{f^2-\mu^2}\left[\frac{m^2}{1-\mu^2} + \frac{m(f^2+\mu^2)}{f(f^2-\mu^2)}\right]\Theta_n + \frac{K_{mn}}{f^2}\, \Theta_n = 0. \tag{2.19}$$

In the third equation we have used the variable $\mu \equiv \cos\theta$, and the constant $f \equiv \frac{\sigma_m}{2\Omega}$. The quantity N_v is the Brunt-Väisälä frequency (the natural frequency for small-scale adiabatic vertical oscillations in a stratified fluid) and is given by

$$N_v^2 = -\frac{1}{\rho_0}\frac{dp_0}{dr}\frac{d}{dr}\left[\ell n \frac{p_0^{1/\Gamma}}{\rho_0}\right] \quad . \tag{2.20}$$

Cowling (1941), in his discussion of free oscillations in non-rotating stars, derived equations equivalent to (2.17) and (2.18), but with $K_{mn} = n(n+1)$ and with $\Theta_{mn}(\theta) = P_n^m(\cos\theta)$. Zahn (1975) used equations identical with Cowling's. The novel features introduced by rotation (via the coriolis force), namely the angular functions Θ_{mn} and their associated separation constants K_{mn}, are discussed in section 2c.

At this point, it is convenient to separate δp_{mn} and h_{mn} into what Zahn (1975) has referred to as "equilibrium" and "dynamical" components. The equilibrium component may be thought of as the response when all of the normal modes of the star are forced at a frequency much less than their resonant frequencies. It is obtained by setting $\sigma = 0$ in (2.17) and (2.18):

$$\left.\begin{aligned} \delta p_{mn}^{eq} &= -\rho_0\,\delta V_{mn} \quad , \\ \text{and} \qquad h_{mn}^{eq} &= \rho_0\,\delta V_{mn} \Big/ \frac{dp_0}{dr} = -\delta V_{mn}/g \end{aligned}\right\} \tag{2.21}$$

where g is the local gravitational acceleration. The "dynamical tide" is defined by the quantities:

$$\left.\begin{aligned} \delta p_{mn}^{dyn} &= \delta p_{mn} - \delta p_{mn}^{eq} \quad , \\ \text{and} \qquad h_{mn}^{dyn} &= h_{mn} - h_{mn}^{eq} \quad , \end{aligned}\right\} \tag{2.22}$$

which satisfy the same differential equations (2.17) and (2.18), but with the right hand sides changed to

$$\left.\begin{aligned} & \sigma^2 \rho_0 \, \delta V_{mn} \Big/ \frac{dp_0}{dr} \quad , \\ \text{and} \qquad & -\frac{\sigma^2 \rho_0}{r^2} \frac{d}{dr} \left(r^2 \rho_0 \, \delta V_{mn} \Big/ \frac{dp_0}{dr} \right) \end{aligned}\right. \tag{2.23}$$

respectively.

In section 3, approximate analytic solutions for δp_{mn}^{dyn} and h_{mn}^{dyn} are derived, whilst more accurate numerical solutions are obtained in section 4.

c) The angular part of the tidal oscillations

Equation (2.19), which is independent of the structure of the star and of the form of the perturbing potential δV_{mn}, is known as Laplace's tidal equation. Its solutions govern the oscillations of an ocean of uniform depth covering a rotating planet, and global atmospheric oscillations on a rotating planet. For a detailed review of the latter subject, see Chapman and Lindzen (1970). The solution of Laplace's tidal equation, subject to the physically necessary condition that all solutions be regular and bounded in the interval $0 \leq \theta \leq \pi$, is an eigenvalue problem. For the case of free oscillations of an ocean of depth D, the constant $\epsilon \equiv K/f^2$ is given by

$$\epsilon = \frac{4\Omega^2 R^2}{gD} \tag{2.24}$$

(R = planetary radius, g = surface gravity), and regular, bounded solutions exist only for certain discrete values of $f = \sigma/2\Omega$. The same applies to free atmospheric oscillations, but with D replaced by a length scale characteristic of the atmospheric structure. For an isothermal atmosphere with scale-height H, $D = \Gamma H$. When forced oscillations are considered, as in the present problem, the value of f is fixed by the forcing frequency and K (or ϵ) may take only certain discrete values, denoted K_{mn}. The solutions $\Theta_{mn}(\theta)$ which correspond to these eigenvalues are usually known as Hough functions, after a pioneer in the study of Laplace's tidal equation. Various notations

have been used for Hough functions and the related eigenvalues. In particular, workers such as Chapman and Lindzen (1970) who study atmospheric tides and oscillations use the "equivalent depth":

$$\mathcal{H}_{mn} \equiv \frac{4\Omega^2 R^2}{g\epsilon_{mn}} = \frac{\sigma_m^2 R^2}{gK_{mn}} \quad . \tag{2.25}$$

Longuet-Higgins (1967), in the most extensive published analysis of Laplace's tidal equation, uses the eigenvalue ϵ, Hough functions denoted by $Z(\theta)$, and the parameters $\lambda = -f$ and $s = m$.

The following brief description of Hough functions is adapted from Flattery (1967) and Longuet-Higgins (1967). For graphs of selected Hough functions, tables of eigenvalues, and various asymptotic approximations the reader is referred to the latter reference.

(1) As the operator $\mathcal{F}$, defined by rewriting equation (2.19) in the form

$$\mathcal{F}(\Theta) + \frac{K}{f^2}\Theta = 0 \quad , \tag{2.26}$$

is self-adjoint, the eigenvalues K_{mn} are real and the eigenfunctions Θ_{mn} orthogonal:

$$\int_{-1}^{1} \Theta_{mn}(\theta)\,\Theta_{mp}(\theta)\,d\mu = 0 \quad \text{if } n \neq p. \tag{2.27}$$

(2) For $|f| > 1$, equation (2.19) is a Sturm-Liouville equation. There are thus a countably infinite number of eigenvalues, all positive, with $K_{mn} \to \infty$ as $n \to \infty$. By convention, n takes the values

m, $m+1$, $m+2$, ... For any fixed m, the Hough functions form a complete set in the interval $0 \leq \theta \leq \pi$. That is, any regular bounded function $F(\theta)$ may be expanded in terms of these functions:

$$F(\theta) = \sum_{n=m}^{\infty} a_n \Theta_{mn}(\theta) \quad , \quad 0 \leq \theta \leq \pi \quad . \tag{2.28}$$

The expansion coefficients are given by

$$a_n = \int_{-1}^{1} F(\theta) \, \Theta_{mn}(\theta) \, d\mu \quad , \tag{2.29}$$

when the Hough functions are normalized to satisfy

$$\int_{-1}^{1} \Theta_{mn}(\theta)^2 \, d\mu = 1 \quad . \tag{2.30}$$

(3) For $|f| \leq 1$, equation (2.19) has two regular singularities (at $\mu = \pm f$) in the range $0 \leq \theta \leq \pi$, and does not rigorously satisfy the requirements for being a Sturm-Liouville equation. Nevertheless, the singularities are removable, and the eigenfunctions are assumed to form a complete set, though this has not been proved. Countably infinite sets of both positive and negative eigenvalues exist for $|f| \leq 1$, the index n conventionally taking the values $\pm m$, $\pm (m+1)$, $\pm (m+2)$, ... The plus signs correspond to solutions of the first class (Hough, 1898 ; Longuet-Higgins, 1967), or "gravitational modes" (Flattery, 1967), and are associated with positive eigenvalues. As $|f| \to 0$, the solutions of this class are concentrated towards $\mu = 0$, i.e., towards the equator of the rotating body. The minus signs

correspond to solutions of the second class, or "rotational modes," and are generally, though not always, associated with negative eigenvalues. For fixed f, there are only a finite number of positive second class eigenvalues. As $|f| \to 1$, the second class solutions are concentrated towards $\mu = \pm 1$, i.e., towards the poles. It is apparent that, if the Hough functions do form a complete set for $|f| \leq 1$, both positive and negative values of n must be included in equations (2.28) and (2.29).

(4) Solutions of the first class are symmetric about $\mu = 0$ for even values of $n - m$, and antisymmetric for odd $n - m$. The opposite holds for solutions of the second class. Since the tidal potential (2.1) contains only symmetric terms, we shall only be interested in symmetric Hough functions.

(5) In the limit $|f| \to \infty$, equation (2.19) becomes Legendre's equation, and the Hough functions are associated Legendre functions:

$$\Theta_{mn}(\theta) \to P_n^m(\mu).$$

The eigenvalues $K_{mn} \to n(n+1)$, independent of m. This limit corresponds to $\Omega \to 0$ while σ remains finite, i.e., to a non-rotating body. We thus recover the equations of Cowling (1941) and Zahn (1975) for a non-rotating star, referred to above in section 2b. Note that the expansion of the perturbing potential in equation (2.16) becomes trivial in this case, thus simplifying the calculations considerably.

d) Eigenvalues and projection coefficients

In this section the specific numerical properties of Hough functions which are of importance to the current investigation are collected. These involve the eigenvalues K_{mn} in equation (2.19), and the tidal potential coefficients δV_{mn} in equation (2.16). Only the dominant terms in the tidal potential, as given by expression (2.4), are included in this investigation. Inclusion of smaller higher order terms, while straightforward, seems superfluous in view of the approximations already made in section 2b. Since the first term in (2.4) (the T_2° term) has no time dependence, it contributes only to the equilibrium tide, and may be neglected. The second term (T_2^{2}) consists of a single Fourier component with m = 2.

In figure 1, the eigenvalues $K_{2,n}$ for $n = \pm 2, \pm 3, \pm 4,$ and ± 5 are displayed as functions of f in the range $-1.8 \leq f \leq 1.8$. For compactness, $|K|^{\frac{1}{2}}$ is plotted, but the sign of K is preserved; solid and dashed lines represent eigenvalues associated with symmetric and antisymmetric eigenfunctions respectively. The figure is based on tables given by Longuet-Higgins (1967). Referring to equation (2.3) and the definition of f, we see that $f = 1 - \omega/\Omega$ for m = 2. Consequently, for a binary whose orbital and rotational angular velocity vectors are parallel, f is initially less than, but close to, unity. As the rotational velocity slows towards synchronism, f decreases towards zero. We shall thus be concerned with the range $0 < f < 1$. In addition, negative eigenvalue solutions, while permissible, are

FIGURE 1: Eigenvalues of Laplace's tidal equation, K_{mn}, for m = 2 and n = ± 2, ± 3, ± 4, and ± 5. The abscissa is $f \equiv \sigma_2/2\Omega = (\Omega - \omega)/\Omega$, and the ordinate $|K_{mn}|^{\frac{1}{2}}$, with the sign of K_{mn} retained. Solid lines represent eigenvalues corresponding to symmetric eigenfunctions, dashed lines those corresponding to antisymmetric eigenfunctions. Positive and negative values of n correspond to Hough eigenfunctions of the first and second classes respectively. Note that, for the eigenfunctions of the second class, $K_{mn} \to -\infty$ as $f \to \pm 1$, and that for $|f| > 1$ only positive eigenvalues exist.

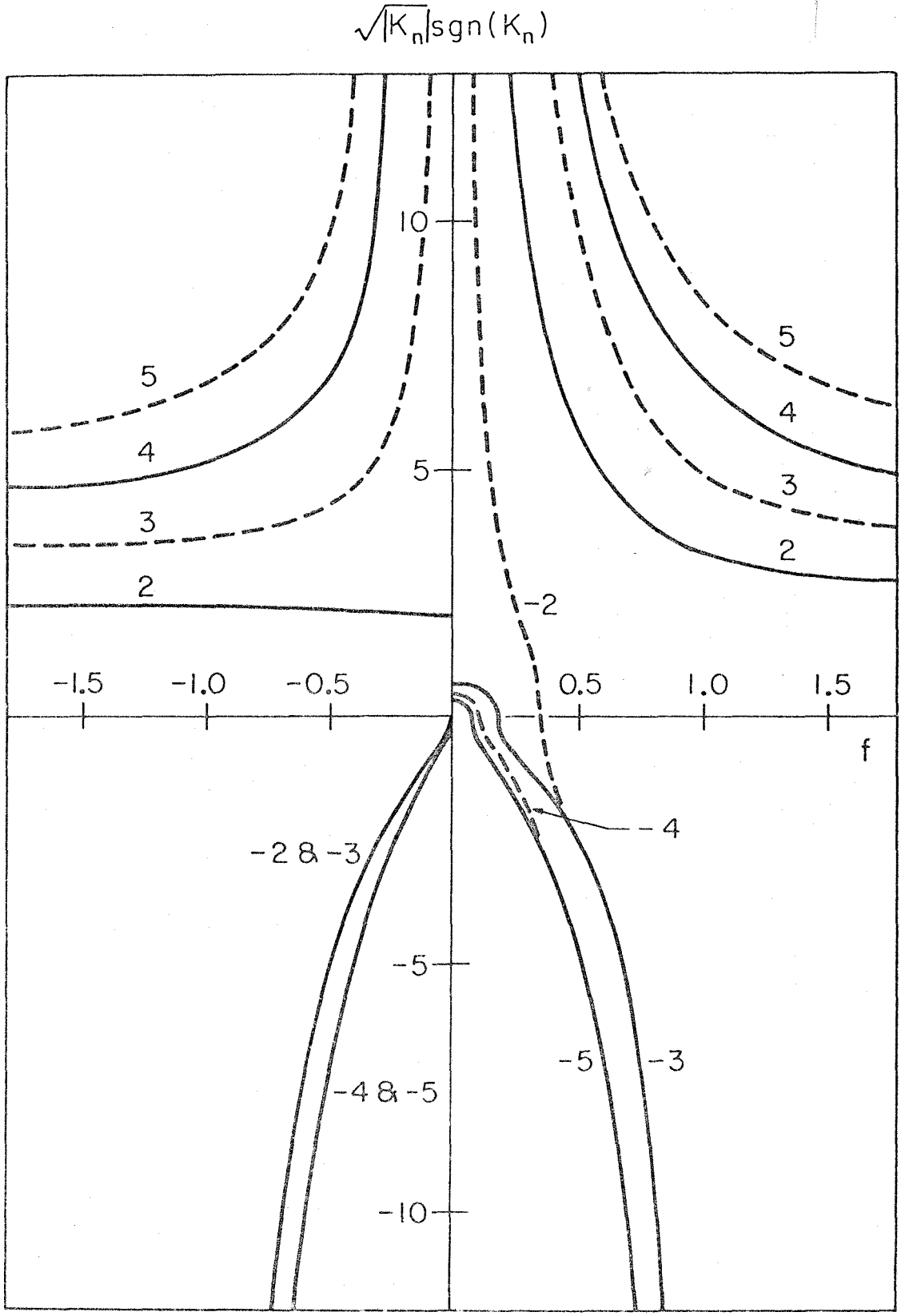
$\sqrt{|K_n|}\,sgn(K_n)$
10
5
-5
-10
-1.5
-1.0
-0.5
0.5
1.0
1.5
f
5
4
3
2
-2
-4
-2 & -3
-4 & -5
-5
-3

disregarded, since they contribute negligibly to energy dissipation by the dynamical tide. This is demonstrated by the WKB solutions obtained in section 2e. Finally, as noted in section 2c (4), only symmetric Hough modes are excited, since the tidal potential is symmetric. Figure 2 shows the first three eigenvalues corresponding to the solutions satisfying the above requirements, for the range $0.1 \leq f \leq 10$. For $f > 1/6$, only Hough functions of the first class need be considered, and the eigenvalues are well represented by the approximation (due to Longuet-Higgins, 1967):

$$K_{2,n} \simeq \frac{(2n-1)^2}{f^2} \tag{2.31}$$

for $0 < f \leq 1$. For $f < 1/6$, one or more symmetric Hough functions of the second class have positive eigenvalues and must thus be included in a complete analysis. In this investigation we will restrict f to be greater than 1/6, and not consider the final stages of synchronization.

The total perturbing potential is given by equation (2.13), with T_2^2 substituted from (2.4):

$$\delta V_2 \simeq - \frac{GM_2}{4a^3} (1 + k_2(r))\, r^2 P_2^2 (\cos\theta)\, e^{i(\sigma t + 2\varphi)} \quad , \tag{2.32}$$

where the subscript 2 has been dropped from σ. The Hough mode potential functions of (2.16), (2.17), and (2.18) are then obtained by application of (2.29):

$$\delta V_{2,n}(r) = \frac{3GM_2}{\sqrt{15}\, a^3} [1 + k_2(r)]\, r^2\, \mathscr{C}_n \quad , \tag{2.33}$$

FIGURE 2: Eigenvalues $K_{2,n}$ corresponding to the first three symmetric eigenfunctions of the first class, for $0.1 \leq f \leq 10$. The parameter ν is the positive root of the equation $\nu(\nu+1) = K_{2,n}$.

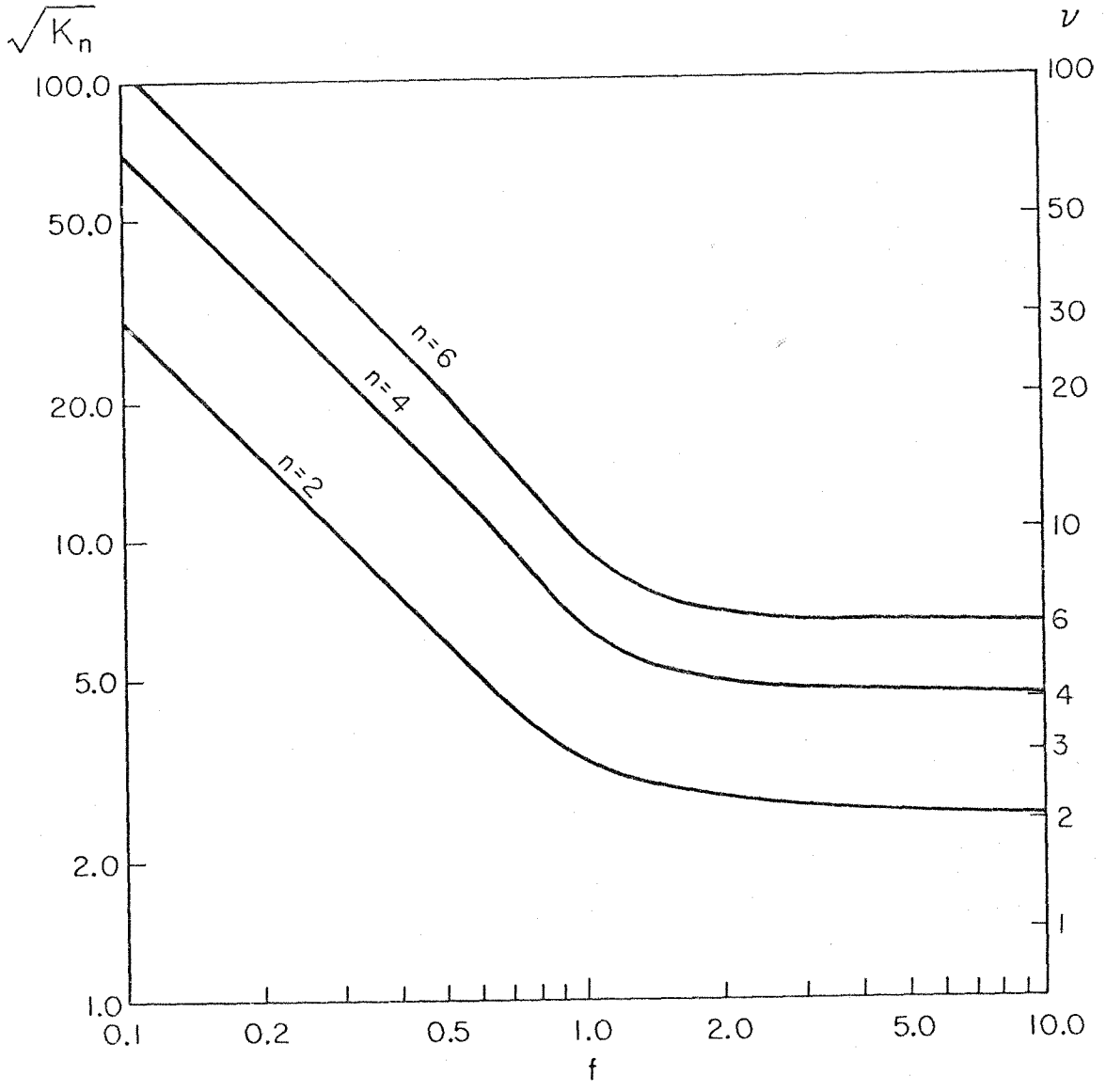
$\sqrt{K_n}$
ν
100.0
50.0
20.0
10.0
5.0
2.0
1.0
100
50
30
20
10
6
4
3
2
1
n=6
n=4
n=2
0.1
0.2
0.5
1.0
2.0
5.0
10.0
f

$$\text{with} \quad \mathscr{C}_n \equiv \int_{-1}^{1} \overline{P_2^2}(\mu)\, \Theta_{2,n}(\theta)\, d\mu \quad , \; n = 2, 4, 6, \ldots \; . \tag{2.34}$$

The normalized function $\overline{P_2^2}$ has been introduced to replace P_2^2:

$$\int_{-1}^{1} \left[\overline{P_2^2}(\mu)\right]^2 d\mu = 1 \quad ,$$
$$\overline{P_2^2}(\cos\theta) = \frac{\sqrt{15}}{4} \sin^2\theta \quad . \tag{2.35}$$

The projection coefficients, $\mathscr{C}_n$, are functions of the parameter f, and no complete tabulation of them has been published. Chapman and Lindzen (1970) provide tables up to n = 16 for values of f applicable to Earth atmospheric tides, namely f = 0.966, and f = 1.000. Graphs of the functions $\Theta_{2,2}$ and $\Theta_{2,4}$ given by Longuet-Higgins (1967) for a few specific values of the eigenvalue ϵ have been used to estimate $\mathscr{C}_2$ for f = 1.1, 0.54, and 0.31, and $\mathscr{C}_4$ for f = 0.81 and 0.47. Lastly, with the aid of asymptotic solutions of Laplace's tidal equation valid for $f \ll 1$, formulas have been derived for $\mathscr{C}_2$, $\mathscr{C}_4$, and $\mathscr{C}_6$ for small f. These asymptotic solutions are given in Appendix 3. All of these results are displayed in Figure 3. The dashed lines represent our adopted approximations for $\mathscr{C}_2$ and $\mathscr{C}_4$ as functions of f. These approximations do not seem likely to be in error by more than 50%. The rapid decrease of the $\mathscr{C}_n$'s as f decreases is due to the progressive concentration of the Hough functions towards $\mu = 0$. For $f \simeq 0$, Hough functions of the first class are essentially

Delta functions at $\mu = 0$. Meanwhile, the Hough functions of the second class are becoming less concentrated towards $\mu = \pm 1$ as f decreases. The coefficient $\mathscr{C}_{-3}$, for example, should be very small for $f \simeq 1$, but increase towards unity as $f \to 0$. This emphasizes the necessity of including these functions of the second class for very small values of f.

Finally we note that $\mathscr{C}_6$, $\mathscr{C}_8$, etc. are progressively smaller than $\mathscr{C}_2$ and $\mathscr{C}_4$. This is illustrated on Figure 3 for $f = 1$, and is an obvious consequence of the fact that, as n increases, the number of nodes of the Hough functions increases. For $f \simeq 1$, the coefficients are represented approximately by

$$\mathscr{C}_n \simeq \frac{32}{(\pi n)^2} \quad . \tag{2.36}$$

In this investigation, only $\mathscr{C}_2$ and $\mathscr{C}_4$ are retained.

FIGURE 3: The projection coefficients $\mathscr{C}_n$ defined by equation (2.34). Circles represent values tabulated by Chapman and Lindzen (1970) for f = 1.0 and f = 0.966, and originally calculated by Flattery (1967). Squares represent projection coefficients calculated from graphs of selected Hough functions given by Longuet-Higgins (1967). Asymptotic approximations for $f \ll 1$, given in Appendix 3, are shown as solid lines. The dashed lines indicate the approximate forms of $\mathscr{C}_2$ and $\mathscr{C}_4$ adopted for the present study.

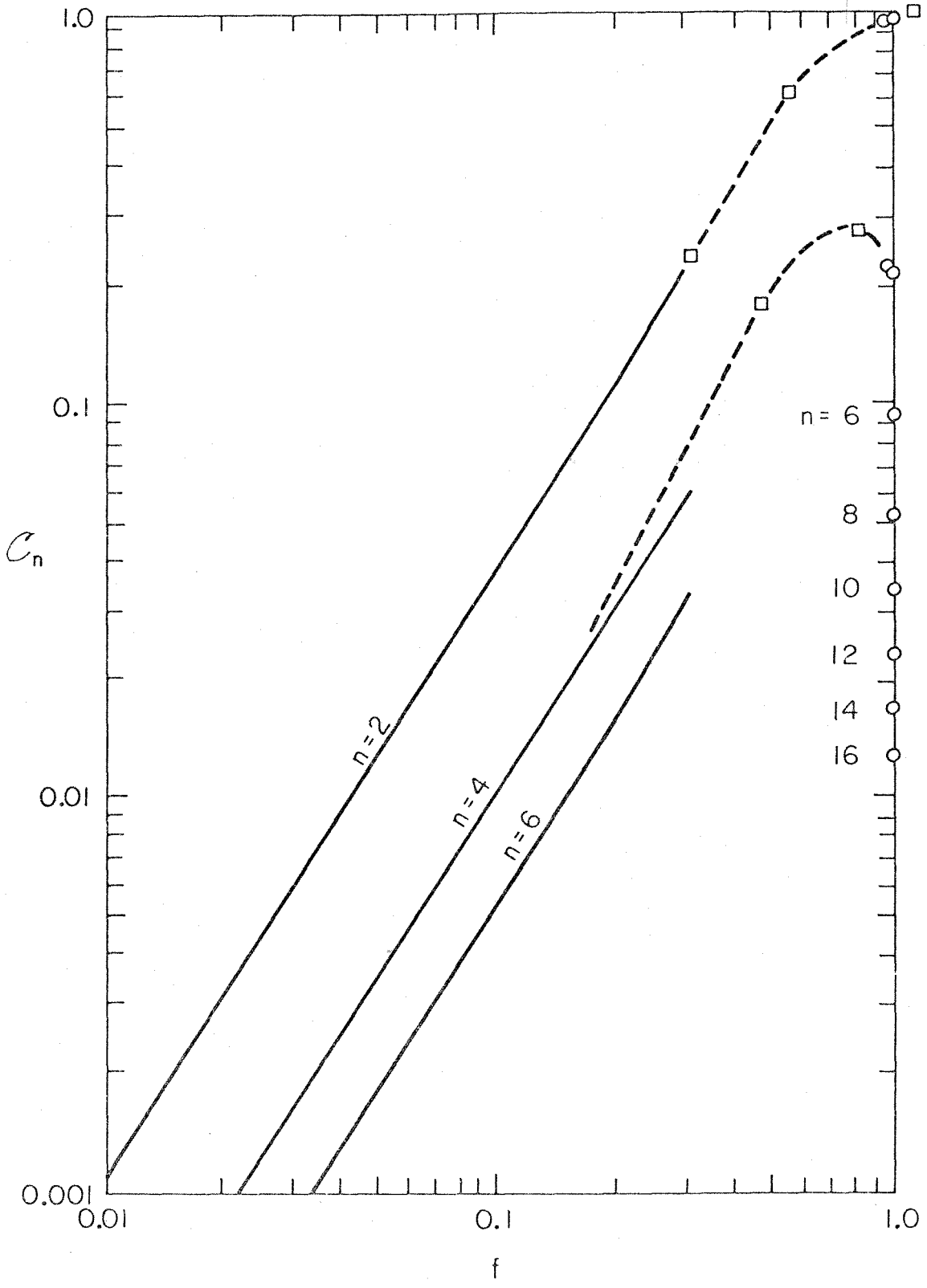
1.0
0.1
0.01
0.001
C_n
0.01
0.1
1.0
f
n=2
n=4
n=6
n = 6
8
10
12
14
16

e) WKB radial solutions and the energy flux

In this section, approximate WKB solutions are obtained for the radial functions δp_{mn} and h_{mn}. These solutions are valid only in the radiative envelope of the star, and break down near the core-envelope boundary and near the stellar surface. They do, however, provide a good approximation throughout a large part of the star, and provide a formula for calculating the mechanical energy flux carried by the dynamical tide. The subscript m will, henceforth, be suppressed and assumed to take the value 2.

Consider the homogeneous solutions of equations (2.17) and (2.18). Throughout the stellar interior

$$\frac{\sigma^2 \rho_0}{\Gamma p_0} \ll \frac{K_n}{r^2} \quad , \tag{2.37}$$

and the coefficient of δp_n in (2.18) may be simplified. For example, with conservative values for σ and K_n of 10^{-4} $\sec^{-1}$ and 10 respectively, and with the parameters of a typical (5 solar mass) early type star, the ratio of these quantities varies from 4×10^{-6} at the center, through 3×10^{-4} at the core-envelope boundary, to 4×10^{-3} in the middle of the envelope. In the stellar atmosphere the ratio approaches unity. Using (2.18) to eliminate δp_n, and introducing the new variable

$$w(r) \equiv r^2 \rho_0(r)^{\frac{1}{2}} h_n \quad , \tag{2.38}$$

we obtain the following second order differential equation:

$$\frac{d^2w}{dr^2} + \left(K_n \left[\frac{N_v^2}{\sigma^2} - 1 \right] + r^2 p_0^{1/\Gamma} \rho_0^{-\frac{1}{2}} \frac{d}{dr} \left[\rho_0 p_0^{-2/\Gamma} \frac{d}{dr} \left(p_0^{1/\Gamma} \rho_0^{-\frac{1}{2}} \right) \right] \right) \frac{w}{r^2} = 0 \tag{2.39}$$

Now, in the stellar envelope, $N_v \sim 10^{-3}$ sec^{-1}, while 10^{-5} sec$^{-1} < \sigma < 10^{-4}$ sec^{-1} for most cases of interest, so $N_v^2/\sigma^2 \sim 10^{3\pm1} \gg 1$. Also $K_n \sim 10$ to 10^2 typically for Hough functions of the first class (see Figure 2), and the term involving ρ_0 and p_0 is dimensionless and evidently of order unity. To a good approximation, then, (2.39) reduces to

$$\frac{d^2w}{dr^2} + \left(\frac{K_n N_v^2(r)}{\sigma^2} \right) \frac{w}{r^2} = 0 \quad , \; n = 2, 4, 6, \ldots \; . \tag{2.40}$$

Since the quantity in parentheses is $\gtrsim 10^3$, and varies slowly with r, the WKB technique is amply justified and the resulting independent solutions are given by

$$w_\pm \simeq A_\pm e^{i\epsilon_\pm} \left(\frac{r}{N_v(r)} \right)^{\frac{1}{2}} \exp \left\{ \pm i \frac{K_n^{\frac{1}{2}}}{\sigma} \int_{r_e}^{r} \frac{N_v(r')}{r'} dr' \right\} \quad , \tag{2.41}$$

where $A_\pm$ and $\epsilon_\pm$ are arbitrary real constants and r_e is the radius of the core-envelope boundary.

Using equations (2.38) and (2.18), we obtain the WKB solutions:

$$h_n^{\pm}(r) \simeq A_\pm e^{i\epsilon_\pm} \left[r^3 \rho_0(r) \, N_v(r) \right]^{-\frac{1}{2}} \exp \left\{ \pm i K_n^{\frac{1}{2}} g(r) \right\} , \tag{2.42}$$

and

$$\delta p_n^{\pm}(r) \simeq \pm i A_\pm e^{i\epsilon_\pm} \left[\frac{\sigma^2 \rho_0(r) N_v(r)}{K_n r} \right]^{\frac{1}{2}} \exp \left\{ \pm i K_n^{\frac{1}{2}} g(r) \right\} , \tag{2.43}$$

where

$$g(r) \equiv \frac{1}{\sigma} \int_{r_e}^{r} \frac{N_v(r')}{r'} \, dr' \tag{2.44}$$

Recalling the time dependence of the solutions, $e^{i\sigma t}$, we see that the two solutions corresponding to the $\pm$ sign represent waves propagating radially inwards and outwards respectively. The radial wavelength of these waves is given approximately by

$$\lambda \simeq \frac{2\pi\sigma r}{K_n^{\frac{1}{2}} N_v(r)} \tag{2.45}$$

$$\sim 10^{-2} r \text{ to } 10^{-1} r \quad ,$$

and they are an example of "gravity waves" (see Eckart, 1960).

So far we have assumed that $K_n > 0$. For Hough functions of the second class ($n \leq 0$), $K_n < 0$ for all odd n for $1/6 < f < 1$. In this case, the solutions of (2.40) are exponential functions of r. A positive exponential implies a very large amplitude surface oscillation, which is not physically acceptable. The negative exponential solution is acceptable, but the amplitude of such a mode of oscillation rapidly becomes negligible with increasing radius and the mode transfers negligible mechanical energy to the outer regions of the star. We thus neglect all modes with negative eigenvalues, as foreshadowed in section 2d.

Associated with these WKB solutions is a radial mechanical energy flux, analogous to the energy carried by a sound wave, given by:

$$F = \langle \mathrm{Re}\,(\delta p)\ \mathrm{Re}\,[(\underset{\sim}{v})_r] \rangle_{\text{time}} \quad . \tag{2.46}$$

With the aid of equations (2.14), (2.15), (2.42), and (2.43), we obtain for the total radial energy flux:

$$F = \frac{\sigma^2}{2r^2}\Bigg(\sum_n (A_+^n)^2 K_n^{-\frac{1}{2}} \Theta_n(\theta)^2 - \sum_n (A_-^n)^2 K_n^{-\frac{1}{2}} \Theta_n(\theta)^2 + \sum_n \sum_{\ell \neq n} K_n^{-\frac{1}{2}} \Theta_n(\theta)\, \Theta_\ell(\theta) \Bigg\{ A_+^n A_+^\ell \cos\left[\left(K_n^{\frac{1}{2}} - K_\ell^{\frac{1}{2}}\right) g(r) + \epsilon_+^n - \epsilon_+^\ell\right] + A_+^n A_-^\ell \cos\left[\left(K_n^{\frac{1}{2}} + K_\ell^{\frac{1}{2}}\right) g(r) + \epsilon_+^n - \epsilon_-^\ell\right] - A_-^n A_+^\ell \cos\left[\left(K_n^{\frac{1}{2}} + L_\ell^{\frac{1}{2}}\right) g(r) - \epsilon_-^n + \epsilon_+^\ell\right] - A_-^n A_-^\ell \cos\left[\left(K_\ell^{\frac{1}{2}} - K_n^{\frac{1}{2}}\right) g(r) + \epsilon_-^n - \epsilon_-^\ell\right] \Bigg\} \Bigg) \quad (2.47)$$

Since for given values of m and f, $K_n \neq K_\ell$ for $n \neq \ell$, the $A^n A^\ell$ terms in this expression oscillate with increasing radius. These terms also vanish when integrated over a sphere, because of the orthogonality of Hough functions. Thus they do not contribute to the overall transport of mechanical energy through the envelope. Restricting attention, therefore, to the first two terms, we see that the inward propagating gravity waves (A_+^n) transport energy outwards, and vice versa. This is a well-known property of gravity waves (see, for example, Eckart, 1960), and is a consequence of the radial component of the waves' group velocity being directed oppositely to the radial component of

their phase velocity. Note that the r^{-2} dependence of the flux implies that the total energy transported per second is independent of radius.

We shall see in section 3, and again in section 4, that these homogeneous WKB solutions are, in fact, excellent approximations to the complete forced solution in the stellar envelope. Thus, to compute the energy flux carried by the dynamical tide, it is only necessary to determine the coefficients $A_{\pm}^{n}$. These coefficients depend principally on three things: the amplitude of the tidally forced solutions, δp_n and h_n, in the core of the star; the properties of the core-envelope boundary; and the boundary conditions imposed on the envelope solution by the stellar atmosphere. We now proceed to a discussion of the latter problem.

f) Atmospheric boundary conditions

In his treatment of the dynamical tide in non-rotating stars, Zahn (1975) adopted a simplified polytropic outer boundary for his stellar models whereby the temperature goes to zero at a specified radius. As a consequence, the outward-propagating waves are completely reflected at this boundary, and a standing wave pattern is set up with $A_+^n = A_-^n$. Clearly there is no net transport of energy in this situation. To resolve this apparent problem, Zahn relaxed the requirement of adiabaticity, equation (2.7), in the optically thin stellar atmosphere, replacing it with the more complicated (and realistic) equations governing radiative damping of the waves. In the presence of atmospheric dissipation - such as radiative damping - the waves are no longer perfectly reflected back into the stellar interior. A_-^n is smaller than A_+^n, and there is a net outward flow of mechanical energy through the stellar envelope, which is ultimately deposited as heat in the stellar atmosphere or radiated directly to space.

However, if a more realistic atmospheric model is used, the outward propagating (in the group velocity sense) gravity waves are not necessarily reflected at all and may propagate outwards indefinitely. In this case, the amplitude of the waves increases as the gas pressure decreases, until the waves become nonlinear, possibly developing into shock waves. At this point the energy carried by the waves is likely to be dumped as heat into the gas, and ultimately radiated.

Of course, radiative damping of the waves occurs as well, and simply serves to increase the rate of dissipation of the waves' mechanical energy.

The conditions for propagation of gravity waves through, rather than their reflection by, the atmosphere of a rotating body are given by Chapman and Lindzen (1970) in chapter 3, equation (30). The functions $h_n(r)$ and $\delta p_n(r)$ are given by

$$h_n(r) = h_n^0 \exp\left(\frac{x}{2} + ikx\right) \quad ,$$

and

$$\delta p_n(r) = \delta p_n^0 \exp\left(-\frac{x}{2} + ikx\right) \quad ,$$

where $x = -\ell n\, p_0(r)$, h_n^0 and δp_n^0 are constants, and k is given by the dispersion relation:

$$k^2 = \frac{1}{4}\left[\frac{4H}{\mathscr{H}_n}\left(\frac{\Gamma - 1}{\Gamma} + \frac{dH}{dr}\right) - 1\right] \quad . \tag{2.48}$$

H(r) is the atmospheric pressure scale height, and $\mathscr{H}_n$ is the equivalent depth defined in equation (2.25). As an aside, we note the exponential growth of h_n and $\delta p_n/p_0$ with height, referred to above. Evidently, if the minimum temperature in the stellar atmosphere (at the top of the photosphere), T_{min}, is associated with a scale height H_{min}, then the n^{th} mode will not be reflected, provided

$$\left.\begin{aligned} &\mathscr{H}_n < \frac{4(\Gamma - 1)}{\Gamma} H_{min} \quad ; \\ &\text{i.e., provided} \\ &\sigma^2 < \frac{4(\Gamma - 1)\, K_n\, g\, H_{min}}{R^2} \quad , \end{aligned}\right\} \tag{2.49}$$

where R is the stellar radius. For m = 2 and $f \leq 1$, K_{mn} is given quite accurately by equation (2.31), and the condition for propagation of the n^{th} mode becomes:

$$\sigma f \equiv \frac{\sigma^2}{2\Omega} < \frac{2(2n-1)}{R} \left(\frac{(\Gamma - 1)\, g\, H_{min}}{\Gamma} \right)^{\frac{1}{2}} \quad . \tag{2.50}$$

Clearly, if the n^{th} mode propagates, so do the $(n+2)^{th}$, $(n+4)^{th}$, etc. Also, since both σ and f decrease during the process of synchronization, the number of propagating modes gradually increases.

If, for a particular mode, condition (2.50) is satisfied, then the boundary condition applied to the envelope solution is

$$A_-^n = 0 \quad , \tag{2.51}$$

i.e., no reflection of the energy flux by the atmosphere*. The outward energy flux is given by:

$$F_n = \frac{\sigma^2}{2r^2} K_n^{-\frac{1}{2}} (A_+^n)^2 \Theta_n(\theta)^2 \quad . \tag{2.52}$$

If condition (2.50) is not satisfied, outward propagating waves will be reflected at or below the level of T_{min}, and Zahn's boundary conditions involving radiative dissipation are appropriate. Following Zahn, we introduce the damping constant, γ, defined by

$$\left.\begin{aligned} A_+^n e^{i\epsilon_+} &= \tfrac{1}{2} A_n (1+\gamma) \\ A_-^n e^{i\epsilon_-} &= \tfrac{1}{2} A_n (1-\gamma) \quad . \end{aligned}\right\} \tag{2.53}$$

---

* This boundary condition is commonly known as the "radiation condition."

When $\gamma = 0$ (zero damping) $A_+^n = A_-^n$ and a standing wave pattern exists, with no net transport of energy. When $\gamma = 1$ (complete damping), $A_-^n = 0$ and the outward energy flux is given by equation (2.52), with $A_+^n = |A_n|$. For intermediate values of γ, the energy flux is

$$F_n = \frac{\sigma^2}{2r^2} K_n^{-\frac{1}{2}} \gamma |A_n|^2 \Theta_n(\theta)^2 \quad . \tag{2.54}$$

It may be shown (see Zahn, 1975, equation [2.38]) that, when γ is varied while all other stellar parameters are held constant, the constant A_n varies as:

$$A_n \propto (\sin \psi - i\gamma \cos \psi)^{-1} \tag{2.55}$$

where

$$\psi = \frac{K_n^{\frac{1}{2}}}{\sigma} \int_{r_e}^{r_a} \frac{N_v(r')}{r'} dr' + \text{constant} \quad . \tag{2.56}$$

Radii r_e and r_a are the radii of the core-envelope boundary and the reflecting layer in the stellar atmosphere respectively. Thus ψ is a measure of the total number of radial oscillations in the WKB solutions (2.42) and (2.43), and has a value of the order of 2π x (10 to 100). Substituting expression (2.55) in equation (2.54) for the energy flux, we obtain:

$$F_n = \frac{\gamma}{\sin^2 \psi + \gamma^2 \cos^2 \psi} F_n^0 \quad , \tag{2.57}$$

which is the same as Zahn's (1975) equation (2.50) and Zahn's (1977) equation (5.2).

As Ω, and hence σ, decrease during the process of synchronization, ψ increases steadily. Therefore, F_n oscillates between maxima F_n^0/γ and

minima γF_n^0. Zahn (1975) has pointed out that these maxima at $\psi = N\pi$ correspond to the tidal forcing frequency, σ, being in resonance with successive high order g-modes, i.e., normal modes of oscillation of the star. As γ approaches 1 (complete damping of the waves) these resonances become less and less important. Fortunately, if F_n is averaged over a range of time corresponding to an increase in ψ of 2π, the resulting average flux is almost independent of the damping constant γ. Neglecting the small variation in ω, equation (1.1) for the rotational evolution of the star may be written

$$-\frac{d\sigma}{dt} \simeq \frac{4\,\dot{E}(\sigma)}{I\sigma} \quad , \tag{2.58}$$

where $\dot{E}$ is proportional to F. Thus,

$$t' - t = \tfrac{1}{4} I \int_{\sigma}^{\sigma'} -\frac{\sigma}{\dot{E}(\sigma)}\, d\sigma$$

$$\propto -\int_{\sigma}^{\sigma'} \frac{\sigma}{F(\sigma)}\, d\sigma \sim -\langle\sigma\rangle \int_{\sigma}^{\sigma'} \frac{d\sigma}{F(\sigma)} \quad .$$

Now, the appropriate time-averaged value of F is given by

$$t' - t \propto -\frac{\langle\sigma\rangle}{\langle F\rangle}(\sigma' - \sigma) \quad ,$$

so

$$\langle F\rangle^{-1} = \frac{1}{\sigma' - \sigma} \int_{\sigma}^{\sigma'} \frac{d\sigma}{F(\sigma)} \quad . \tag{2.59}$$

Using expression (2.57) for F, and integrating over an interval corresponding to $\Delta\psi = 2\pi$, we obtain

$$\langle F \rangle \simeq \frac{2\gamma}{1+\gamma^2} F_n^0 \quad . \tag{2.60}$$

Zahn (1977) incorrectly obtained $\langle F \rangle = F_n^0$, by simply averaging expression (2.57) over ψ, and not taking into account the non-linear variation of σ (and hence ψ) with time due to the enhancement of $\frac{d\sigma}{dt}$ near the resonances. At any rate, for $\gamma \gtrsim 0.5$, $\langle F \rangle$ does not differ greatly from F_n^0, and is thus reasonably independent of the precise value of γ, as advertised above.

We will therefore *assume*, for the purpose of estimating the average flux, that $\gamma = 1$ and, in consequence, $\langle F \rangle = F_n^0$. The detailed atmospheric calculations necessary to obtain a realistic value for γ are not attempted here. Evidently, should such calculations show that $\gamma \ll 1$, the present estimate of the net energy flux carried by modes which do not satisfy the propagation condition, (2.50), must be reduced according to (2.60).

The relevant boundary condition to be applied to the envelope solution is obtained from (2.53), setting $\gamma = 1$: $A_-^n = 0$. This is the familiar radiation condition, (2.51), which also applies to modes which satisfy the propagation condition. We thus reach the important conclusion that, unless $\gamma \ll 1$, the radiation condition may be applied to all modes, whether porpagating or reflected, for the purpose of calculating the average net energy flux.

All solutions obtained in sections 3 and 4 satisfy the radiation condition. In section 4e, however, the conditions are discussed, under which the propagation condition (2.50) is satisfied for a $5M_\odot$ star, and the radiation condition thus rigorously applicable.

g) Summary

For each temporal Fourier component, $e^{i(\sigma_m t + m\varphi)}$, of the tidal potential, the response of the star is given as a sum of modes. The angular dependence of these modes is defined by Laplace's tidal equation (2.19), and the angular functions are known as Hough functions. The radial depencence of the tidal response is given, for each mode, in terms of the functions $\delta p_{mn}(r)$ and $h_{mn}(r)$, which satisfy the coupled equations (2.17) and (2.18). The constant K_{mn} in the latter equation is an eigenvalue which depends on the parameter f, as well as on the Fourier component (m) and the particular Hough mode (n).

The tidal potential, U, has been calculated for a circular orbit of zero inclination, and only the dominant term (2.4) in the potential has been retained. In consequence, only the m = 2 Fourier component appears in the tidal response of the star. The perturbing potential functions, $\delta V_{2,n}(r)$, which appear in the forcing terms (2.23) for the dynamical component of the tide, and in expression (2.21) for the equilibrium component, are given by equation (2.33), in terms of the projection coefficients $\mathscr{C}_n$. Negative eigenvalue modes (second class Hough functions) and modes higher than n = 4 are neglected.

In the radiative envelope of the star, the dynamical tide is well represented by the WKB solutions (2.42) and (2.43), which take the form of gravity waves propagating radially inwards and outwards. The mechanical energy flux carried by these waves is given by equation

(2.47) in terms of the unknown amplitudes $A_{\pm}^{n}$. These amplitudes depend on both the nature of the dynamical tide in the stellar core, and on the atmospheric boundary conditions. The latter depend strictly on whether each particular Hough mode propagates through the atmosphere or is reflected at some level (equations [2.49] and [2.50]). However, as long as radiative damping or some other dissipative mechanism is reasonably effective, the radiation condition (equation [2.51]) is an appropriate boundary condition and the net energy flux is given by (2.52).

III. ANALYTIC DEVELOPMENT

In this section approximate analytic solutions are obtained for the radial part of the dynamical tide, in both the stellar core and envelope. The solutions are matched at the core-envelope boundary, and boundary conditions are applied at the center of the star and in the outer part of the envelope (the radiation condition [2.51]). The mechanical energy flux is then calculated from equation (2.52).

The equations to be solved are (2.17) and (2.18), with the right-hand sides replaced by (2.23) for the dynamical tide.

a) Core solution

In the convective core, the pressure-density profile is essentially adiabatic, i.e., $p_0 \propto \rho_0^{\Gamma}$. Thus $N_v \simeq 0$ (see [2.20]) and N_v^2 may be neglected when compared with σ^2. Also, in the stellar interior, $\sigma^2 \rho_0 / \Gamma p_0 \ll K_n / r^2$, as discussed in section 2e. With these two simplifications, h_n^{dyn} is eliminated between (2.17) and (2.18), to yield the following equation for δp_n^{dyn}:

$$r^2 \frac{d^2 \delta p_n}{dr^2} + r \left(2 - \frac{r\rho_0'}{\rho_0} \right) \frac{d\delta p_n}{dr} - \left[K_n + \frac{2rp_0'}{\Gamma p_0} - \frac{\Gamma - 1}{\Gamma^2} \left(\frac{rp_0'}{p_0} \right)^2 - \frac{1}{\Gamma} \left(\frac{r\rho_0'}{\rho_0} \right) \left(\frac{rp_0'}{p_0} \right) + \frac{1}{\Gamma} \frac{r^2 p_0''}{p_0} \right] \delta p_n = \frac{\sigma^2 \rho_0^2 r^2}{\Gamma p_0} \delta V_{mn}(r) \quad . \tag{3.1}$$

The primes denote derivatives with respect to r, and the superscript "dyn" has been suppressed.

The adiabatic relation $p_0 \propto \rho_0^{\Gamma}$ implies that the core may be treated as a polytrope of index $(\Gamma - 1)^{-1}$. The density and pressure

profiles may then be expanded as power series in the dimensionless variable $x \equiv \alpha r$, where

$$\alpha = \left(\frac{2\pi G \rho_c^2}{3\Gamma p_c} \right)^{\frac{1}{2}} \quad ; \tag{3.2}$$

ρ_c and p_c are the central density and pressure respectively. The first few terms in the series are given by:

$$\left.\begin{aligned} \rho_0(r) &= \rho_c \left[1 - x^2 + \left(\frac{13}{10} - \frac{\Gamma}{2} \right) x^4 + O(x^6) \right] \quad , \\ p_0(r) &= p_c \left[1 - \Gamma x^2 + \frac{4\Gamma}{5} x^4 + O(x^6) \right] \quad . \end{aligned}\right\} \tag{3.3}$$

As may be seen from Table I, $x \simeq 0.7 \pm 0.1$ at the core-envelope boundary for stars in the mass range 2 to 10 solar masses.

By substituting these expressions for ρ_0 and p_0 into equation (3.1), along with expression (2.33) for $\delta V_{2,n}(r)$, a solution for δp_n is obtained in the form of a power series in x. It is convenient to introduce the constant ν, defined as the positive root of the equation

$$\nu(\nu+1) = K_n \quad . \tag{3.4}$$

The complete solution is a sum of a particular-integral solution and the general homogeneous solution. The first few terms in the expansion of these two components of the solution are, respectively:

$$\delta p_{nP} = \frac{3(1+\bar{k}_2)\, GM_2\, \mathscr{C}_n\, \sigma^2 \rho_c^2}{\sqrt{15}\; a^3\; (5+\nu)(4-\nu)\, \Gamma p_c}\; r^4 \left\{ 1 - \left[\frac{(5+\nu)(4-\nu)}{(7+\nu)(6-\nu)} \left(\Gamma - 1 + \frac{2\nu(\nu+1) - 24}{(2\nu+3)(2\nu-1)} \right) + \frac{2\nu(\nu+1) + 9}{(2\nu+3)(2\nu-1)} \right] x^2 + O(x^4) \right\} , \quad \nu \neq 4; \tag{3.5}$$

and

$$\delta p_{nH} = \xi_n r^{\nu} \left\{ 1 - \left(\frac{\nu+3}{2\nu+3} \right) x^2 - \frac{5+\nu}{2(5+2\nu)} \left(\Gamma - \frac{8}{5} - \frac{\nu+3}{2\nu+3} \right) x^4 + O(x^6) \right\} , \tag{3.6}$$

where ξ_n is an arbitrary constant. The Love function $k_2(r)$ has been approximated by its average value in the core, $\bar{k}_2$. A second independent homogeneous solution is obtained by substituting the negative root of (3.4) for ν in equation (3.6). However, this solution is unbounded as $r \to 0$, and is discarded. This constitutes the central boundary condition on the solutions. Note that for $\nu = 4$ δp_{nP} and δp_{nH} have the same r^4 behavior for small r, and that the coefficient of δp_{nP} is singular. In fact the correct form of the particular-integral solution for $\nu = 4$ has form

$$\delta p_{nP} \propto r^4 \ln r$$

for small r.

Expressions (3.5) and 3.6) are substituted in equation (2.17) to obtain the following power series solutions for the particular-integral and homogeneous components of h_n, respectively:

$$h_{nP} = \frac{3(1+\bar{k}_2)\ GM_2\, \mathscr{C}_n \rho_c}{\sqrt{15}\ a^3\ 2\Gamma\ \alpha^2 p_c} r \left\{ 1 + \left[\frac{3}{5} + \frac{8}{(5+\nu)(4-\nu)} \right] x^2 + O(x^4) \right\} , \tag{3.7}$$

and

$$h_{nH} = \frac{\xi_n \nu}{\sigma^2 \rho_c} r^{\nu-1} \left\{ 1 + \frac{\nu+2}{2\nu+3} x^2 + \frac{\nu+4}{2(5+2\nu)} \left(\Gamma - \frac{8}{5} + \frac{\nu+2}{2\nu+3} \right) x^4 + O(x^6) \right\} . \tag{3.8}$$

For convenience in manipulation, we denote the series $\left\{1 + ax^2 + bx^4 + \ldots\right\}$ in equations (3.5), (3.6), (3.7), and (3.8) respectively by Φ_1, Φ_2, Φ_3, and Φ_4. Each of these series is of order unity throughout the core, possibly approaching 2 or 3 at the core-envelope boundary where $x \simeq 0.7$.

The complete solution for the n^{th} mode of the dynamical tide in the core is:

$$\delta p_n^{dyn}(r) = \delta p_{nP} + \delta p_{nH} \quad ; \tag{3.9}$$

$$h_n^{dyn}(r) = h_{nP} + h_{nH} \quad . \tag{3.10}$$

b) Envelope solution

To obtain the solution for the dynamical tide in the envelope, we follow the procedure used in section 2e for the WKB solutions, introducing the variable $w(r) = r^2 \rho_0^{1/2} h_n^{dyn}$ (compare [2.38]). With the dynamical tide forcing terms given by (2.23), w(r) satisfies the approximate differential equation:

$$\frac{d^2w}{dr^2} + \left(\frac{K_n N_v^2(r)}{\sigma^2 r^2} \right) w =$$

$$\frac{K_n \rho_0^{3/2}}{p_0'} \delta V_{2,n} - \rho_0^{-1/2} p_0^{1/\Gamma} \frac{d}{dr} \left[\rho_0 p_0^{-1/\Gamma} \frac{d}{dr} \left(\frac{\rho_0 r^2}{p_0'} \delta V_{2,n} \right) \right], \qquad (3.11)$$

where $p_0' \equiv \frac{dp_0}{dr}$. The homogeneous part of this equation is, of course, identical with equation (2.40) from which the WKB solutions were derived. However, we must now consider the form of the solutions just outside the core-envelope boundary, $r = r_e$, in order to correctly match the core and envelope solutions. Far from this boundary, the WKB solutions may be used for the homogeneous solutions, and the particular-integral solution will be shown to be unimportant.

In the core, the pressure-density profile is essentially adiabatic, and $N_v^2 \simeq 0$ (see equation [2.20]). Outside the core, N_v^2 increases virtually linearly with r, until it stabilizes at about $r = 1.5\ r_e$ with a value of $\sim 10^{-6}$ sec^{-2}. This generalization is confirmed by Figure 4, which presents radial profiles of N_v^2 calculated from models of 2, 5, 7, and 10 solar mass stars. We are thus led, following Zahn (1975), to define a dimensionless parameter $v_n(\sigma, K_n)$ by setting

FIGURE 4: The linear variation of the square of the Brunt-Väisälä frequency with radius immediately outside the convective core, as exhibited by each of the stellar models in Table I.

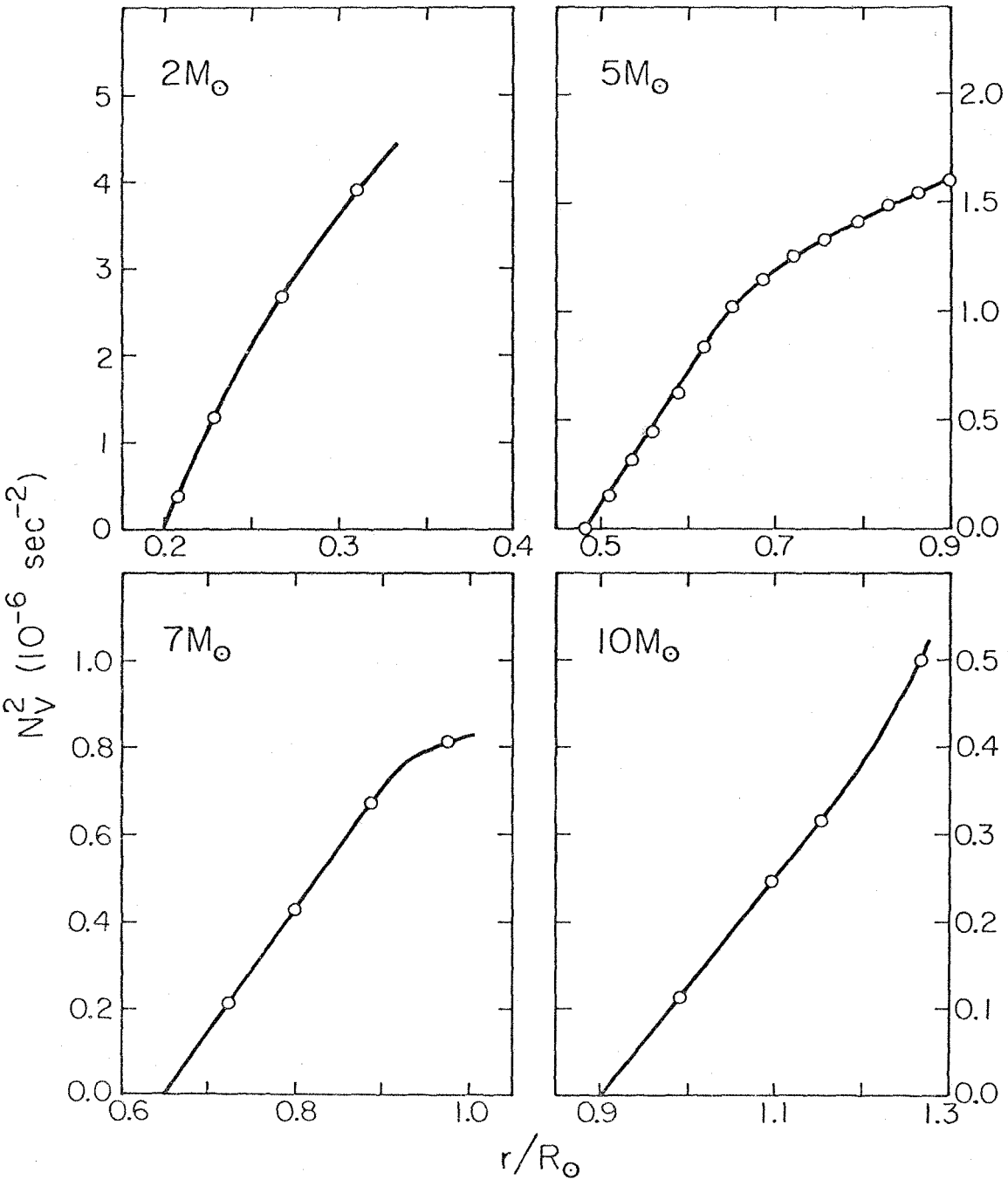
2M⊙
5M⊙
7M⊙
10M⊙
N_V^2 (10^{-6} sec^{-2})
r/R⊙
0
1
2
3
4
5
0.0
0.5
1.0
1.5
2.0
0.2
0.3
0.4
0.5
0.7
0.9
0.6
0.8
1.0
0.1
0.9
1.1
1.3

$$N_v^2 \simeq \frac{\sigma^2}{K_n} v_n^2 \left(\frac{r - r_e}{r_e} \right) \qquad (3.12)$$

$$\text{for } r_e \leq r \leqslant 1.5\ r_e \quad .$$

We also define a dimensionless independent variable z:

$$z \equiv v_n^{2/3} \left(\frac{r - r_e}{r_e} \right) \quad . \qquad (3.13)$$

Table I gives values of

$$\left[r \frac{dN_v^2}{dr} \right]_{r_e} = \frac{\sigma^2}{K_n} v_n^2$$

calculated from the profiles of Figure 4. The parameter v_n depends on σ and K_n, but for typical values of $\sigma = 5 \times 10^{-5}$ sec^{-1}, and $K_n = 100$, and for a 5 solar mass star, $v_n \simeq 350$, and $v_n^{2/3} \simeq 50$.

Equation (3.11) may now be written, for $r_e \leq r \leqslant 1.5\ r_e$, as:

$$\frac{d^2 w}{dz^2} + z w = \mathcal{Q}_n(z) \qquad (3.14)$$

where

$$\mathcal{Q}_n(z) = r_e^2 v_n^{-4/3} \times (\text{RHS of } [3.11]). \qquad (3.15)$$

The independent homogeneous solutions of this equation are the Airy functions Ai(-z) and Bi(-z) (Abramowitz and Stegun, p 446). The general homogeneous solution, in terms of the arbitrary constants γ_n and β_n, is:

$$w_H(z) = \gamma_n \text{ Ai}(-z) + \beta_n \text{ Bi}(-z) \quad . \qquad (3.16)$$

Airy functions may be written in terms of Bessel functions of order 1/3:

$$\left.\begin{aligned} \mathrm{Ai}(-z) &= \frac{z^{1/2}}{3}\left[J_{1/3}(\zeta) + J_{-1/3}(\zeta)\right] \quad , \\ \mathrm{Bi}(-z) &= \frac{z}{3}^{1/2}\left[J_{-1/3}(\zeta) - J_{1/3}(\zeta)\right] \quad , \end{aligned}\right\} \tag{3.17}$$

with $\zeta \equiv 2/3\ z^{3/2}$.

A particular-integral solution of equation (3.14) may be written in terms of these homogeneous solutions. We choose

$$w_P(z) = \pi\ \mathrm{Ai}(-z)\int_0^z \mathrm{Bi}(-z')\mathcal{Q}_n(z')\,dz'$$

$$- \pi\ \mathrm{Bi}(-z)\left[\int_0^z \mathrm{Ai}(-z')\mathcal{Q}_n(z')\,dz' - 2/3\,\mathcal{Q}_n(0)\right] . \tag{3.18}$$

These solutions are valid wherever $N_v^2(r)$ is given by equation (3.12), i.e., for $0 \le z \ll v_n^{2/3}/2 \sim 25$. Note that the function $\mathcal{Q}_n(z)$, which depends on $\rho_0(r)$ and $p_0(r)$, does not vary greatly over this range.

The asymptotic forms of w_H and w_P for $z \gg 1$ are governed by the corresponding asymptotic expressions for Airy functions (Abramowitz and Stegun, pp. 448, 449):

$$\left.\begin{aligned} \mathrm{Ai}(-z) &\simeq \frac{1}{\pi^{1/2}z^{1/4}}\ \sin\left(\zeta+\frac{\pi}{4}\right) \quad , & (3.19)\\ \mathrm{Bi}(-z) &\simeq \frac{1}{\pi^{1/2}z^{1/4}}\ \cos\left(\zeta+\frac{\pi}{4}\right) \quad , & (3.20)\\ \int_0^z \mathrm{Ai}(-z')dz' &\simeq \frac{2}{3} - \frac{1}{\pi^{1/4}z^{3/4}}\cos\left(\zeta+\frac{\pi}{4}\right) \quad , & (3.21)\\ \int_0^z \mathrm{Bi}(-z')dz' &\simeq \frac{1}{\pi^{1/2}z^{3/4}}\ \sin\left(\zeta+\frac{\pi}{4}\right) \quad . & (3.22) \end{aligned}\right\} \text{ for } z \gg 1$$

If $\mathcal{Q}_n(z)$ is approximated by its value at $z = 0$, the integrals in (3.18) may be evaluated using the above expressions to give:

$$w_P(z) \simeq \frac{\mathcal{Q}_n(0)}{z} \qquad \text{for } z \gg 1 \quad . \tag{3.23}$$

Thus w_P rapidly becomes much smaller than w_H as r increases, and may safely be neglected except in the immediate vicinity of the core-envelope boundary.

The complete solution for the dynamical tide in the inner envelope ($r_e \leq r \leq 1.5\ r_e$) is obtained from (3.16), (3.18), (2.18), and (2.23):

$$h_n^{dyn}(r) \simeq (r^2\rho_0^{1/2})^{-1}\left[\eta_n\,\mathrm{Ai}(-z) + \beta_n\,\mathrm{Bi}(-z) + w_P(z)\right] \quad , \tag{3.24}$$

$$\delta p_n^{dyn}(r) \simeq \frac{\sigma^2 v_n^{2/3}\rho_0^{1/2}}{K_n r_e}\left(\eta_n \frac{d}{dz}\left[\mathrm{Ai}(-z)\right] + \beta_n \frac{d}{dz}\left[\mathrm{Bi}(-z)\right] + \frac{dw_P(z)}{dz}\right) + \frac{\sigma^2\rho_0}{K_n}\frac{d}{dr}\left(\frac{r^2\rho_0\delta V_{2,n}}{p_0'}\right) \quad . \tag{3.25}$$

c) Boundary conditions

The boundary condition at the center of the star, i.e., that the solutions remain bounded as $r \to 0$, has already been satisfied by rejecting the negative root of equation (3.4). There are three boundary conditions that remain to be satisfied: continuity of h_n and δp_n at the core-envelope boundary, and the outer boundary condition on the envelope solution. The latter is supplied by the radiation condition, defined by equations (2.51) and (2.41). Application of these three conditions permits us to solve for the three arbitrary constants ξ_n, η_n, and β_n in the above radial solutions.

Consider first the outer boundary condition. Examination of the homogeneous terms in equations (3.24) and (3.25) for $z \gg 1$ reveals them to be, as expected, a special case of the WKB solutions (2.42) and (2.43), wherein r is set equal to r_e and N_v^2 is given by the linear relation (3.12):

$$K_n^{\frac{1}{2}} g(r) \equiv \frac{K_n^{\frac{1}{2}}}{\sigma} \int_{r_e}^{r} \frac{N_v(r')}{r'} dr' \simeq \frac{2}{3} z^{3/2} \equiv \zeta \quad .$$

If the arbitrary phases, $\epsilon_\pm$, of the WKB solutions are set equal to $\epsilon \pm \frac{\pi}{4}$, then the WKB and homogeneous inner envelope solutions are related by

$$\left.\begin{aligned} \eta_n &= i\, \mathscr{S}_n e^{i\epsilon} (A_+^n - A_-^n) \quad , \\ \text{and} \qquad \beta_n &= \mathscr{S}_n e^{i\epsilon} (A_+^n + A_-^n) \quad , \end{aligned}\right\} \tag{3.26}$$

where

$$\mathscr{S}_n \equiv \left(\frac{\pi K_n^{1/2} r_e}{\sigma v_n^{2/3}} \right)^{1/2} \quad . \tag{3.27}$$

In consequence of equation (3.23), the particular-integral terms in (3.24) and (3.25) involving $w_p(z)$ may be neglected for $z \gg 1$, and thus do not contribute significantly to the WKB amplitudes $A_{\pm}^{n}$. The last term in equation (3.25) for δp_n is not small compared with the homogeneous terms, but neither is it an oscillatory function of r, so it also does not contribute to $A_{\pm}^{n}$. Therefore, only the homogeneous terms in the envelope solution need be considered in the application of the radiation condition, and in the calculation of the net mechanical energy flux, F.

Applying the radiation condition, $A_{-}^{n} = 0$, to the relations (3.26), we obtain

$$\eta_n = i\beta_n \quad , \tag{3.28}$$

and

$$A_{+}^{n} = |\beta_n| \, \mathscr{S}_n^{-1} \quad . \tag{3.29}$$

Thus the mechanical energy flux, given by (2.52) in terms of A_{+}^{n}, may be calculated once $|\beta_n|$ is determined.

We now eliminate ξ_n and solve for β_n by requiring that δp_n and h_n be continuous at the core-envelope boundary, $r = r_e$. First, the envelope solutions must be evaluated at $z = 0$. Small z expansions of the Airy functions are given by Abramowitz and Stegun, p. 446:

$$\left.\begin{aligned} \mathrm{Ai}(-z) &\simeq c_1 + c_2 z \\ \mathrm{Bi}(-z) &\simeq \sqrt{3}\,(c_1 - c_2 z) \end{aligned}\right\} \tag{3.30}$$

where $$c_1 = [3^{2/3}\,\Gamma(\tfrac{2}{3})]^{-1} \simeq 0.355 \quad ,$$

and $$c_2 = [3^{1/3}\,\Gamma(\tfrac{1}{3})]^{-1} \simeq 0.259 \quad .$$

The homogeneous components of δp_n and h_n at $z = 0$ are thus determined. The first two terms in w_P are quadratic in z for $z \ll 1$, so

$$\left.\begin{aligned} w_P(z) &\simeq \frac{2\pi c_1}{\sqrt{3}}\,\mathcal{Q}_n(0) \quad , \\ \text{and} \quad \frac{dw_P(z)}{dz} &\simeq 0 \quad . \end{aligned}\right\} \tag{3.31}$$

The function $\mathcal{Q}_n$ may be expanded as a power series in the core variable $x \equiv \alpha r$, using equations (3.3) for $\rho_0(r)$ and $p_0(r)$. For $r = r_e$, we obtain

$$w_P\,(z=0) = \frac{3(1+\bar{k}_2)\,GM_2\,\mathcal{C}_n\,\pi\,c_1 r_e^{\,3}\,\rho_c^{\,3/2}\,(K_n - 6)}{\sqrt{15}\cdot\sqrt{3}\;\;v_n^{\,4/3}\,\alpha^2\,\Gamma\,p_c}\;\Phi_6(x_e) \quad , \tag{3.32}$$

where $\Phi_6(x)$ is of the form $\{1 + a\,x^2 + bx^4 + \ldots\}$. Again, $\bar{k}_2$ is the average value of the Love function in the core. Similarly, the particular-integral component of δp_n is expanded as a power series, to give:

$$\delta p_{nP}(z=0) = -\frac{3(1+\bar{k}_2)\,GM_2\,\mathcal{C}_n\,3\,\sigma^2\rho_c^{\,2}r_e^{\,2}}{\sqrt{15}\;\;a^3\;\;2\alpha^2\,\Gamma\,p_c\;\;\;K_n}\;\Phi_5(x_e) \quad , \tag{3.33}$$

where $\Phi_5(x)$ is also of the form $\{1 + ax^2 + bx^4 + \ldots\}$.

With these expressions in hand, and using the core solutions obtained in section 3a, it is a straightforward matter to match δp_n and h_n at the core-envelope boundary ($r = r_e$, $x = x_e$, or $z = 0$), eliminate

the constant ξ_n, and obtain the following expression for the constant β_n:

$$\beta_n = -\frac{9(1+\bar{k}_2)\, M_2 r_e^{\,3}\, \mathscr{C}_n}{4\sqrt{15}\,\pi\, v_n^{\,2/3}\, a^3 \rho_e^{\,1/2}} \left\{ -\frac{\Phi_3}{\Phi_4} + \frac{3\nu}{K_n}\,\frac{\Phi_5}{\Phi_2} + \frac{2\pi c_1 (K_n - 6)}{\sqrt{3}\; v_n^{\,4/3}} \left(\frac{\rho_c}{\rho_e}\right)^{1/2} \frac{\Phi_6}{\Phi_4} \right.$$

$$\left. + \frac{2\nu(\alpha r_e)^2}{(5+\nu)(4-\nu)}\,\frac{\Phi_1}{\Phi_2} \right\} \cdot \left[\frac{c_2(\sqrt{3}-i)}{(\nu+1)\Phi_2} + \left(\frac{\rho_c}{\rho_e}\right) \frac{c_1(\sqrt{3}+i)}{v_n^{\,2/3}\Phi_4} \right]^{-1} . \quad (3.34)$$

In this expression, $\rho_e \equiv \rho_0(r_e)$ and all Φ_i's are evaluated at $x = x_e$.

d) The mechanical energy flux

Except for the minor approximations made in the derivations of the differential equation (3.11) and of expression (3.23) for w_p, this is an exact solution of equations (2.17), (2.18), and (2.23) subject to the radiation condition. An accurate numerical result for β_n could be obtained if the six quantities $\Phi_i(x_e)$ were known. In principle they are given by power series in x (e.g., equations [3.5] to [3.8]) whose coefficients are calculable, but in practice $x_e \sim 0.7$ and the series converge rather slowly. An alternative procedure is to determine Φ_1 through Φ_4 by numerical solution of the differential equations in the core, and Φ_5 and Φ_6 from tabulated density and pressure profiles. This is essentially the course followed by Zahn (1975), in his combination analytical/numerical solution for the dynamical tide.

In order to obtain a completely analytic, albeit numerically approximate, estimate of β_n (and hence A_+^n and the energy flux) we make the approximation

$$\Phi_i(x_e) \simeq 1 \qquad , \qquad i = 1,2,\ldots,6 \qquad .$$

The expression for β_n is further simplified by neglecting the two small terms of order $\nu_n^{-4/3}$ and $\nu_n^{-2/3}$, and by setting $\frac{2\nu(\alpha r_e)^2}{(5+\nu)(4-\nu)}(\nu+1)$ equal to -1. The latter approximation is quite good for $\nu \geqslant 10$ (i.e., $K_n \geqslant 100$), and avoids the apparent singularity at $\nu = 4$. (Referring back to equation [3.5], we see that our particular-integral solution in the core is not valid for $\nu = 4$, and that a logarithmic

term should be introduced.) The results derived below by making these approximations are compared in section 4 with the results of completely numerical solutions, and are found to be in error by a factor of ≤ 2 for β_n.

The simplified expression for β_n is

$$|\beta_n| \simeq \frac{9(\nu-1)\, r_e^{\,3}}{8\sqrt{15}\,\pi\, v_n^{\,2/3}\, \rho_e^{\,\frac{1}{2}}\, c_2} \left[\frac{(1+\bar{k}_2)\, M_2}{a^3}\, \mathscr{C}_n\right] \quad . \tag{3.35}$$

Substitution of this expression in relation (3.29) yields

$$A_+^{\,n} \simeq \frac{9(\nu-1)\, r_e^{\,5/2}\, \sigma^{\frac{1}{2}}}{8\sqrt{15}\,\pi^{3/2}\, v_n^{\,1/3}\, K_n^{\frac{1}{4}} c_2 \rho_e^{\frac{1}{2}}} \left[\frac{(1+\bar{k}_2)\, M_2}{a^3}\, \mathscr{C}_n\right] \tag{3.36}$$

for the amplitude of the WKB solution. The radial mechanical energy flux associated with the n^{th} mode is determined from this amplitude, via equation (2.52):

$$F_n(r,\theta) \simeq \frac{27(\nu-1)^2\, \sigma^3\, r_e^{\,5}}{640\,\pi^3\, v_n^{\,2/3}\, K_n c_2^{\,2} \rho_e} \left[\frac{(1+\bar{k}_2)\, M_2}{a^3}\, \mathscr{C}_n\right]^2 \frac{\Theta_n(\theta)^2}{r^2} \tag{3.37}$$

With the Hough function normalization of (2.30), the total rate of mechanical energy transport by this mode is

$$\dot{E}_n(r) = \int_0^{2\pi}\int_0^{\pi} F_n(r,\theta)\, r^2 \sin\theta\, d\theta\, d\varphi$$

$$\simeq \frac{27(\nu-1)^2\, \sigma^3 r_e^{\,5}}{320\,\pi^2\, v_n^{\,2/3}\, K_n c_2^{\,2} \rho_e} \left[\frac{(1+\bar{k}_2)\, M_2}{a^3}\, \mathscr{C}_n\right]^2 . \tag{3.38}$$

This result is, as already mentioned in the discussion of the WKB solutions in section 2e, independent of radius. The envelope is thus a region of transport, but not generation, of mechanical energy in the form of gravity waves. The generation of this energy by the tidal potential occurs in the convective core of the star, and its conversion into gravity waves takes place at the core-envelope boundary. The size of the core and the parameters of this boundary, r_e, ρ_e, and $v_n^2 \propto \left[r \frac{dN_V^2}{dr}\right]_{r_e}$, along with the amplitude of the n^{th} component of the tidal potential, thus determine the rate of energy generation. Note that $\dot{E}_n$ is not explicitly dependent on the stellar radius.

After being transported through the envelope to the surface of the star, this mechanical energy is either deposited as heat in the stellar atmosphere (due to viscous damping or shock formation at low pressure levels) or is radiated directly to space as a consequence of the mechanism of radiative damping. In either case, there is a loss of mechanical energy from the binary system which is attributable to the action of tidal forces on the primary. The rate of this energy loss, $\dot{E}$, determines the rate of synchronization, via equation (1.1).

For purposes of comparison with the results of numerical calculations, with Zahn's (1975) results, and with observational material, we rewrite the expression for $\dot{E}_n$ in terms of the binary orbital period, P (in days), and use equation (3.12) to substitute for the parameter v_n. The explicit dependence on the tidal frequency, σ, is also factored out, and expressed in terms of "σ_{-5}", i.e., in units of 10^{-5} sec^{-1}:

$$\dot{E}_n \equiv \mathscr{L}_n \, \sigma_{-5}^{11/3} \left[\frac{(1+\bar{k}_2)\ \mu\ \mathscr{C}_n}{P^2} \right]^2 \quad . \tag{3.39}$$

With the masses of primary and secondary denoted by M_1 and M_2 respectively, the constant $\mu \equiv M_2/(M_1+M_2)$. Our approximate analytic expression for $\mathscr{L}_n$ is then obtained from (3.38):

$$\mathscr{L}_n^{\,A} \simeq 6.07 \times 10^{32} \ \frac{(r_e/R_\odot)^5}{\left(r \frac{dN_v}{dr}^2 \right)^{1/3}_{r_e} \rho_e} \ (\nu-1)^2 \ K_n^{-4/3} \ \text{ergs/sec}, \tag{3.40}$$

where r_e has been expressed in units of the solar radius, $R_\odot$, and the remaining quantities are in CGS units.

In figure 5, $\mathscr{L}_n^{\,A}$ is presented as a function of the eigenvalue K_n for a primary of 5 solar masses. Stellar parameters used were taken from Table I. The curve is dashed for $K_n < 100$, to indicate the breakdown of some of the approximations made in simplifying expression (3.34) for β_n. For a different primary, only the constant coefficient of $\mathscr{L}_n^{\,A}$ is different; consequently, only the scale of the ordinate in figure 5 need be changed. To facilitate this change of scale, values of $\mathscr{L}_n^{\,A}$ for $K_n = 100$ are given in Table II for stars of 2,5,7, and 10 solar masses.

Zahn's (1975) result for the rate of energy transport by the dynamical tide may be cast in a similar form:

$$\dot{E}(\text{Zahn}) = \mathscr{L}^{Z} \, \sigma_{-5}^{11/3} \left(\frac{\mu}{P^2} \right)^2 \tag{3.41}$$

FIGURE 5: The variation of $\mathscr{L}_n$ with $K_n^{\frac{1}{2}}$ for a 5 $M_\odot$ star, as given by the approximate analytic expression (3.40). The dashed segment of the curve indicates the region where the approximation becomes poor. Zahn's (1975) result for the radial energy flux, expressed in terms of the quantity $\mathscr{L}^Z$ in equation (3.41), is represented by a single point at $K_n = 6$.

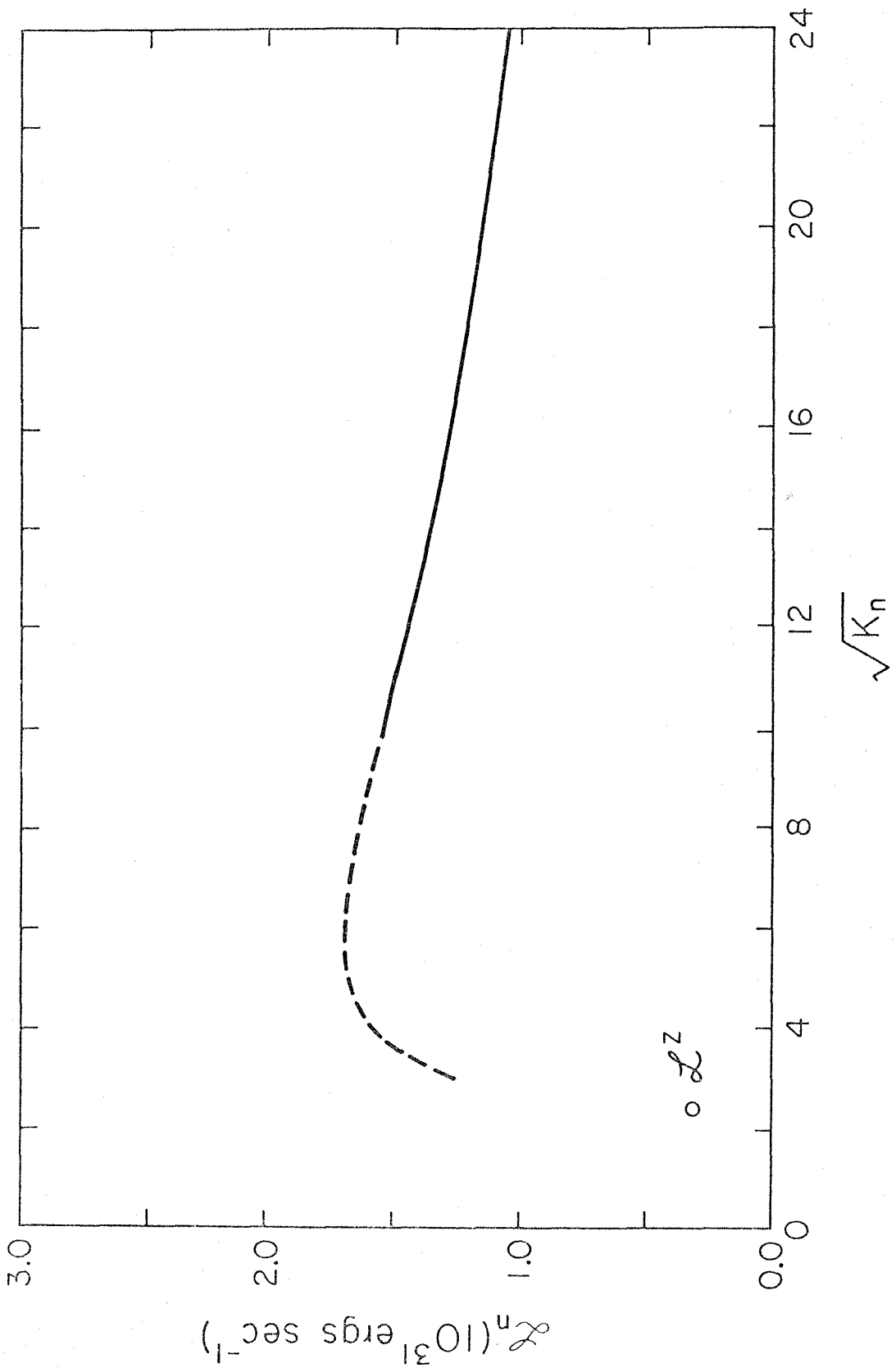
3.0
2.0
1.0
0.0
0
4
8
12
16
20
24
$\sqrt{K_n}$
$\mathscr{L}^z$ o
$\alpha_n(10^{31}$ ergs sec$^{-1})$

TABLE I

Parameters of Zero Age Main Sequence Stellar Models.

Mass ($M_\odot$)	2	5	7	10
Radius ($R_\odot$)	1.38	2.70	3.30	4.05
log ($L/L_\odot$)	1.36	2.71	3.22	3.74
log(T_{eff})	4.033	4.224	4.309	4.393
Approx. Spectral Type	A6	B6.5	B4.5	B3
Central Density, ρ_c ($g\ cm^{-3}$)	70.88	18.75	12.25	8.136
Central Pressure, p_c (10^{16} dynes cm^{-2})	21.09	6.68	4.77	3.50
Core radius ($R_\odot$)	0.200	0.483	0.650	0.900
$x_e \equiv \alpha\ r_e$	0.62	0.71	0.76	0.83
Boundary Γ	1.664	1.649	1.638	1.616
Boundary Density, ρ_e ($g\ cm^{-3}$)	47.8	11.2	6.85	4.25
$\left[r\left(dN_\nu^2/dr\right)\right]_{r_e}$ (10^{-6} sec^{-2})	8.4	3.0	1.8	1.2

All models have hydrogen mass fraction, X = 0.70. 2 $M_\odot$ model has "metal" mass fraction, Z = 0.01; other models have Z = 0.03.

TABLE II

Analytic results for the normalized mechanical energy transport rate, $\mathscr{L}_n^A$.

Mass ($M_\odot$)	2	5	7	10
$\dfrac{(r_e/R_\odot)^5}{\rho_e\left[r\left(dN_v^2/dr\right)\right]_{r_e}}$ ($g^{-1}cm^3sec^2$)	3.30×10^{-4}	0.163	1.39	13.1
$\mathscr{L}_n^A$ for $K_n^{\frac{1}{2}} = 10$	3.12×10^{28}	1.54×10^{31}	1.31×10^{32}	1.24×10^{33}
E_2 [1]	1.45×10^{-8}	1.53×10^{-7}	3.80×10^{-7}	1.02×10^{-6}
$\mathscr{L}_Z$ (ergs sec^{-1}) [2]	4.84×10^{27}	3.23×10^{30}	3.61×10^{31}	4.52×10^{32}
$\mathscr{L}_n^A(10)/\mathscr{L}^Z$	6.4	4.8	3.6	2.7

[1] Zahn (1975) Table I.

[2] Derived from E_2 via equation (3.42).

where
$$\mathscr{L}^Z = \frac{8.26 \times 10^{34} \, (R_1/R_\odot)^9}{(M_1/M_\odot)^{4/3}} \, E_2 \quad . \tag{3.42}$$

R_1 is the radius of the primary. E_2 is a constant which depends on the structure of the star, and which is tabulated by Zahn (1975). It depends particularly on r_e, $[r(dN_v^2/dr)]_{r_e}$, and $(1+\bar{k}_2)$, and appears to have hidden R_1 and M_1 dependences which cancel the anomalous explicit dependence on these two quantities exhibited by expression (3.42). Since the non-rotating case considered by Zahn corresponds, in our terminology, to $f = \infty$, Hough functions are replaced by associated Legendre functions (see section 2c[5]) and

$$\mathscr{C}_n = \delta_{2,n} \quad . \tag{3.43}$$

(See equation [2.34] for the definition of $\mathscr{C}_n$.) Thus, only the $n = 2$ mode contributes to $\dot{E}$, and the appropriate corresponding value of $K_n = n(n+1)$ is 6. The single point, $\mathscr{L}_n = \mathscr{L}^Z$ and $K_n = 6$, for a 5 solar mass star, is plotted on figure 5 for comparison with the present analytical results. Values of $\mathscr{L}^Z$ and E_2 for a range of primary masses are given in Table II. Note that $\mathscr{L}_n$ and $\mathscr{L}^Z$ are not exactly comparable quantities, inasmuch as the latter effectively includes the factor $(1+\bar{k}_2)^2$. In section 5a it is shown that $1+\bar{k}_2 \simeq 3.75$, so that we would expect to find $\mathscr{L}^Z \simeq 14 \; \mathscr{L}_n (K_n = 6)$. This is evidently not true, and we shall return to this point when the numerical results are discussed in section 4d.

Finally, we note an important feature of the present result for the rate of energy transport and loss, equation (3.39), which does not appear in Zahn's work:

$$\dot{E}_n \propto \mathscr{C}_n^2 \quad . \tag{3.44}$$

As the rotation of the primary approaches synchronization with the orbital motion, f decreases towards zero and $\mathscr{C}_n$ decreases rapidly for all n (see figure 3), thus greatly reducing $\dot{E}_n$ and the synchronization rate $|\frac{d\Omega}{dt}|$.

e) Summary

Analytic solutions are obtained to the differential equations (2.17), (2.18), and (2.23) governing the radial part of the dynamical tide. The convective core and the radiative envelope of the star are considered separately, and the solutions required to be continuous at the core-envelope boundary. Complete core solutions are given by (3.9) and (3.10), in terms of the dimensionless quantities $\Phi_i(x)$, $i = 1,2,3,4$. In the inner part of the envelope, where N_v^2 is given by the linear relation (3.12), complete solutions take the form of (3.24) and (3.25). At greater radii, the more general WKB solutions derived in section 2e describe the homogeneous part of the dynamical tide. The arbitrary WKB amplitudes $A_{\pm}^n$ are related to the inner envelope arbitrary constants η_n and β_n by (3.26).

These two constants, along with the constant ξ_n in the core solution, are determined by application of (1) the radiation condition to the envelope solution, and (2) the requirement of continuity for δp_n and h_n at the core-envelope boundary. The resulting exact expression for β_n is given as equation (3.34), and is simplified to produce the approximate expressions (3.35) and (3.36) for β_n and A_+^n.

The rate of radial transport of mechanical energy through the envelope by the n^{th} mode is calculated from the latter expression and equation (2.52), and is given in (3.38). An auxiliary quantity, $\mathscr{L}_n$, from which the explicit dependence on the tidal frequency and potential amplitude has been removed, is introduced and plotted in figure 5

as a function of the eigenvalue K_n for a 5 solar mass star. Table II indicates the way in which the results scale to other stars. The results of the analytic theory are compared with those of Zahn (1975), expressed in terms of the quantity $\mathscr{L}^Z$.

IV. NUMERICAL SOLUTIONS FOR A 5 SOLAR MASS STAR

There are several methods by which our estimate, (3.38), of the mechanical energy transport rate by the dynamical tide might be improved. The dimensionless quantities $\Phi_i(x_e)$ might be accurately computed by evaluating many of the coefficients of the corresponding power series (e.g. [3.5] and [3.6]), and substituting the results in expression (3.34) for β_n. Alternatively, the core solutions δp_{nP}, δp_{nH}, h_{nP}, and h_{nH} might be computed numerically, and subsequently matched to the analytic envelope solutions (3.24) and (3.25).

A third approach, and the one to be followed here, is to compute numerical solutions of the differential equations (2.17) and (2.18) spanning both the core and envelope of the star. It is then no longer necessary to match solutions at the core-envelope boundary, since each of the numerical solutions is already continuous at this point. Only the central boundary condition (δp_n must be bounded and h_n go to zero) and the radiation condition must be applied to these completely numerical solutions. The latter raises some problems, as we shall see in section 4c.

The numerical solutions to be presented here all apply to a main sequence star of 5 solar masses. In section 5, the analytic expressions derived in section 3d are used to scale these numerical results to other early main sequence stars.

a) The stellar model

The first requirement for a numerical solution is a realistic stellar model. Specifically, the variation of ρ_0, p_0, Γ, and N_v with radius throughout the stellar interior must be known. Since a detailed surface boundary condition has been replaced, for our purposes, by the simple radiation condition applied to the envelope solution, an accurate model of the stellar atmosphere is unnecessary.

A crude profile of the 5 solar mass zero-age-main-sequence stellar model used in the present calculations is given in Table III. This model is one of a set of four (2, 5, 7, and 10 solar masses) computed for the writer by C. Alcock, using a stellar evolution program developed by B. Paczynski. Parameters for all of these models are to be found in Table I, and are used in section 3d in the evaluation of the analytic expression for $\mathscr{L}_n$, equation (3.40), to produce figure 5 and Table II.

TABLE III

Profile of the $5M_{\odot}$ stellar model used in the numerical calculations (selected points only).

Radius* (10^{10} cm)	Mass ($M_{\odot}$)	Density (g cm^{-3})	Temperature (10^{7} K)	Pressure (10^{16} dynes cm^{-2})	Γ	N_v^2 (10^{-6} sec^{-2})
0.5034	0.005	18.55	2.583	6.554	1.641	0.0
1.014	0.040	17.92	2.527	6.196	1.642	0.0
1.513	0.128	16.92	2.439	5.641	1.643	0.0
2.043	0.300	15.52	2.313	4.901	1.644	0.0
2.495	0.518	14.12	2.183	4.202	1.646	0.0
3.048	0.871	12.26	2.000	3.340	1.648	0.0
3.368(r_e)	1.114	11.16	1.885	2.860	1.649	0.0
4.090	1.735	8.57	1.637	1.904	1.652	0.621
5.013	2.565	5.48	1.365	1.015	1.653	1.253
6.007	3.352	3.09	1.116	0.467	1.653	1.540
6.940	3.918	1.69	0.933	0.213	1.653	1.715
8.053	4.376	0.79	0.755	0.081	1.651	1.415

* Total radius = 18.792×10^{10} cm.

b) Boundary conditions

Equations (2.17) and (2.18) must be integrated outwards from the center of the star; a procedure dictated by the nature of the solutions near $r = 0$ and by the central boundary condition. It was pointed out in section 3a that the second homogeneous solution for δp_n is singular at $r = 0$, and the same holds for the corresponding solution for h_n. In fact,

$$\left.\begin{aligned} \delta p_{nH2} &\sim r^{-(\nu+1)} \quad , \\ \text{and} \qquad h_{nH2} &\sim r^{-(\nu+2)} \quad . \end{aligned}\right\} \tag{4.1}$$

Any attempt to numerically integrate the equations inwards would inevitably result in contamination by this rapidly growing singular solution, and the central boundary condition could not be satisfied. On the other hand, outward integration is stable inasmuch as the undesirable singular solution decreases rapidly outwards, while the regular homogeneous and particular integral solutions increase outwards. These latter two solutions automatically satisfy the central boundary condition, since both δp_n and h_n go to zero at $r = 0$.

In order to match the outer boundary condition, i.e., the radiation condition, it is necessary to compute both the regular homogeneous solution and a particular-integral solution. This boundary condition may be stated as follows, in a form suitable for use with the numerical solutions: the oscillatory component of the solution in the envelope must take the form

$$h_n = A_+^n \left[r^3 \rho_o(r) N_v(r) \right]^{-1/2} \exp i \left\{ K_n^{1/2} g(r) + \epsilon^n \right\}, \quad (4.2)$$

with $g(r)$ given by equation (2.44). A_+^n and ϵ^n are real constants to be determined by matching this expression to the final numerical solution.

Let us assume that, in the envelope of the star, the oscillatory parts of the particular-integral and regular homogeneous numerical solutions are given by the appropriate WKB expressions:

$$h_{nP} \simeq A_1 \left[r^3 \rho_o(r) N_v(r) \right]^{-1/2} \cos \left[K_n^{1/2} g(r) + \epsilon_1 \right], \quad (4.3)$$

and

$$h_{nH} \simeq A_2 \left[r^3 \rho_o(r) N_v(r) \right]^{-1/2} \cos \left[K_n^{1/2} g(r) + \epsilon_2 \right], \quad (4.4)$$

where A_1, A_2, ϵ_1, and ϵ_2 are adjusted to fit these solutions. (It will be shown presently that these WKB expressions do indeed accurately represent the oscillatory component of the numerical solutions.) Then we seek a complex constant B, such that the combined solution

$$h_n = h_{nP} + B\, h_{nH} \quad (4.5)$$

takes the form of expression (4.2). After a little manipulation, we obtain the result

$$B = - e^{i(\epsilon_2 - \epsilon_1)} \frac{A_1}{A_2} \quad (4.6)$$

and, for the parameters of the combined solution,

$$A_+^n = A_1 \sin (\epsilon_2 - \epsilon_1), \quad (4.7)$$

and

$$\epsilon^n = \epsilon_2 + \frac{\pi}{2}. \quad (4.8)$$

The outer boundary condition has now been satisfied, and the mechanical energy flux carried by the n^{th} component of the dynamical tide is calculated from A_+^n using expression (2.52):

$$F_n(r,\theta) = \frac{\sigma^2}{2r^2} K_n^{-\frac{1}{2}} (A_+^n)^2 \Theta_n(\theta)^2 \quad .$$

c) Numerical procedure

Equations (2.17) and (2.18) are integrated simultaneously by the numerical integration routine 'DIFSYS', to obtain the functions $\delta p_n(r)$ and $h_n(r)$. Necessary values of $\rho_0(r)$, $p_0(r)$, $\Gamma(r)$, and $N_v(r)$ are obtained by tabular interpolation. Since only the dynamical component of the tide is of interest in the present investigation, the righthand sides of (2.17) and (2.18) are replaced by (2.23).

The potential function, $\delta V_{2,n}$, given by equation (2.33), is set equal to $V_0 r^2$, where V_0 is a constant. We thus neglect the small (< 15%) variation of $k_2(r)$ through the core of the star (see figure 12). From (2.33),

$$V_0 = \frac{3GM_2}{\sqrt{15}\, a^3}\,(1+\bar{k}_2)\,\mathscr{C}_n \qquad (4.9)$$

$$= 4.096 \times 10^{-9}\left[\frac{(1+\bar{k}_2)\mu\,\mathscr{C}_n}{P^2}\right] .$$

All numerical solutions are computed for $V_0 = 10^{-11}$ sec^{-2}, but, as the equations are linear, the results may be scaled to any other value of V_o. Clearly, the functions δp_n and h_n (and therefore the amplitude A_+^n) scale linearly with V_0, while the energy flux scales quadratically.

The numerical integration procedure is started at a small radius in the core - usually at $r_0 = 1 \times 10^{10}$ cm $\simeq 0.14\ R_\odot$ - with initial values given by either : (1)

$$\left.\begin{aligned} \delta p_n(r_0) &= C\, r_0^{\nu} \\ \text{and}\qquad h_n(r_0) &= C\,\frac{\nu}{\sigma^2 \rho_c}\, r_0^{\nu-1} \end{aligned}\right\} \qquad (4.10)$$

for the regular homogeneous solution; or (2)

equations (3.5) and (3.7)

for the particular-integral solution. For $K_n^{1/2} \geq 12$, any small homogeneous component in the particular-integral solution grows so rapidly with r that it overwhelms the particular-integral component. In this situation, an initial radius of 2×10^{10} cm is used to reduce the range over which the homogeneous solution may grow.

Integration of the equations proceeds through the core, across the core-envelope boundary at $r \simeq 3.36 \times 10^{10}$ cm, and into the envelope, before being terminated at a radius of 7.5×10^{10} cm. This is still only half way to the surface of the star, but is well into the region of the envelope where the solutions may be represented by WKB formulae. Both regular homogeneous and particular-integral solutions are computed for each pair of parameters, σ and K_n.

To determine the WKB amplitude and phase, A_i and ϵ_i, for each of these two solutions, the function

$$(b + dr) + A \left[r^3 \rho_o(r) \, N_v(r) \right]^{-1/2} \cos \left(K_n^{1/2} g(r) + \epsilon \right) \qquad (4.11)$$

is least-squares fitted to a short radial segment of $h_n(r)$ by adjusting the parameters b, d, A, and ϵ. Parameters b and d serve to locally describe the non-oscillatory part of the particular-integral solution. The final composite solution which satisfies the outer boundary condition is given, in terms of these amplitudes and phases, by equations (4.5) and (4.6). The amplitude of this composite solution, from which the mechanical energy flux is computed, is given by (4.7).

In principle, the numerical solution of equations (2.17) and (2.18) is now complete. However, in most cases investigated, $\sin(\epsilon_2 - \epsilon_1) \simeq 0$, and the amplitude A_+^n is not well determined. In this situation a second particular-integral solution must be computed, from different initial conditions, which differs more in phase from the homogeneous solution. In practice, a satisfactory second particular-integral solution may be obtained by using the composite initial conditions:

$$\delta p_n(r_0) = \delta p_{nP}(r_0) + C' \, r_0^{\nu} \quad , \tag{4.12}$$

and

$$h_n(r_0) = h_{nP}(r_0) + C' \, \frac{\nu}{\sigma^2 \rho_c} \, r_0^{\nu-1} \quad ,$$

with the functions δp_{nP} and δh_{nP} given by equations (3.5) and (3.7) and the constant C' by

$$C' = -\frac{A_1}{A_2} C \cos(\epsilon_2 - \epsilon_1) \quad . \tag{4.13}$$

All numerical computations were performed on the IBM 370/158 at the Booth Computing Center, California Institute of Technology.

d) Results

Numerical solutions have been obtained for values of the tidal frequency in the range 2×10^{-5} sec$^{-1} \leq \sigma \leq 10^{-4}$ sec^{-1}, and for values of the Hough eigenvalue in the range $6 \leq K_n \leq 544$, or $2.45 \leq K_n^{1/2} \leq 23.33$. Corresponding values of the synchronization parameter f range from $^{\infty}$ down to 0.13 for the n = 2 Hough mode, and from $^{\infty}$ down to 0.30 for the n = 4 Hough mode (see figure 2). Table IV gives a complete list of the numerical solutions, with the following parameters for each solution:

σ , $K_n^{1/2}$, f (2^{nd} and 4^{th} modes) , WKB amplitude A_+^n (for $V_0 = 10^{-11}$ sec^{-2}) , phase difference $(\epsilon_2 - \epsilon_1)$ between the homogeneous and final particular-integral solutions, radial mechanical energy flux F_n (for $V_0 = 10^{-11}$ sec^{-2}) and normalized energy transport rate $\mathscr{L}_n$.

The final parameter, $\mathscr{L}_n$, is defined by equation (3.39):

$$\dot{E}_n \equiv \mathscr{L}_n \, \sigma_{-5}^{11/3} \left[\frac{(1+\bar{k}_2)\, \mu \, \mathscr{C}_n}{P^2} \right]^2 ,$$

and is independent of the strength of the tidal potential, V_0. In the approximate analytic theory of section 3, and in Zahn's (1975) work, $\mathscr{L}_n$ is also independent of σ. In terms of the numerical WKB amplitudes A_+^n, calculated for $V_0 = 10^{-11}$ sec^{-2},

$$\mathscr{L}_n = 5.27 \times 10^{-5} \, K_n^{-1/2} \, \sigma_{-5}^{-5/3} \, (A_+^n)^2 \quad . \tag{4.14}$$

In figure 6, $\mathscr{L}_n$ is displayed as a function of $K_n^{1/2}$ for each value of σ used in the numerical computations. The analytic expression

TABLE IV

Results of the numerical solutions for the 5 $M_\odot$ stellar model.

σ (10^{-5} sec^{-1})	$K_n^{1/2}$	f		A_+^n * (10^{18} $g^{1/2}cm\ sec^{-1/2}$)	$\epsilon_2 - \epsilon_1$ (reduced to the interval $[0°, 90°]$)	F_n * (10^4 ergs sec^{-1} cm^{-2})	$\mathscr{L}_n$ (10^{31} ergs sec^{-1})
		n = 2	n = 4				
2	2.45	∞	-	0.663	69°.5	0.807	0.262
	2.50	~8.	-	0.550	82°.2	0.620	0.201
	2.73	~2.3	-	0.299	85°.2	0.167	0.054
	3.00	1.3	-	0.0398	63°.8	0.0027	0.00088
	3.33	1.0	-	0.227	76°.8	0.079	0.026
	3.75	0.83	-	0.486	84°.0	0.322	0.104
	5.00	0.60	~1.85	1.10	89°.6	1.23	0.399
	7.50	0.40	0.86	1.78	83°.1	2.18	0.707
	15.00	0.20	0.47	2.64	72°.8	2.38	0.772
4	3.75	0.83	-	0.95	85°.8	4.91	0.125
	5.00	0.60	~1.85	2.08	90°.0	17.8	0.455
	7.50	0.40	0.86	3.33	89°.2	30.3	0.773
	8.75	0.34	0.76	3.74	88°.8	32.6	0.832
	11.67	0.26	0.59	4.45	40°.2	34.7	0.886
	15.00	0.20	0.47	4.96	81°.6	33.6	0.858

TABLE IV (continued)

σ	$K_n^{1/2}$	f		A_+^n *	$\epsilon_2 - \epsilon_1$	F_n *	$\mathscr{L}_n$
		n = 2	n = 4				
6	5.00	0.60	~1.85	3.05	25°.5	85.7	0.495
	7.50	0.40	0.86	4.90	88°.2	147.	0.850
	8.75	0.34	0.76	5.49	88°.7	159.	0.918
	11.67	0.26	0.59	6.46	72°.9	165.	0.950
	13.75	0.22	0.51	7.02	85°.1	165.	0.953
	15.00	0.20	0.47	7.26	89°.2	162.	0.933
	17.50	0.17	0.40	7.75	72°.4	158.	0.912
8	7.50	0.40	0.86	6.45	89°.3	454.	0.913
	11.67	0.26	0.59	8.58	71°.7	517.	1.040
	14.00	0.22	0.50	9.32	89°.4	508.	1.021
	15.00	0.20	0.47	9.61	86°.6	504.	1.013
	17.50	0.17	0.40	10.20	85°.9	487.	0.979
10	11.67	0.26	0.59	10.70	89°.7	1255.	1.113
	13.75	0.22	0.51	11.60	88°.0	1252.	1.111
	17.50	0.17	0.40	12.79	87°.8	1196.	1.061
	23.33	0.13	0.30	14.18	51°.4	1103.	0.979

* For tidal potential constant, $V_0 = 10^{-11}$ sec^{-2}.

FIGURE 6: Numerical results for $\mathcal{L}_n$ as a function of $K_n^{1/2}$, for different values of the tidal frequency σ, and calculated for a 5 $M_\odot$ star. Each curve is labeled by the appropriate value of σ, in units of 10^{-5} sec^{-1}. The uppermost curve is the analytic approximation of figure 5, plotted for comparison, and the circle again represents Zahn's (1975) result. Squares indicate the numerical solutions shown in figures 7-10. At the top of the figure, scales of the parameter f are given for n = 2, 4, and 6.

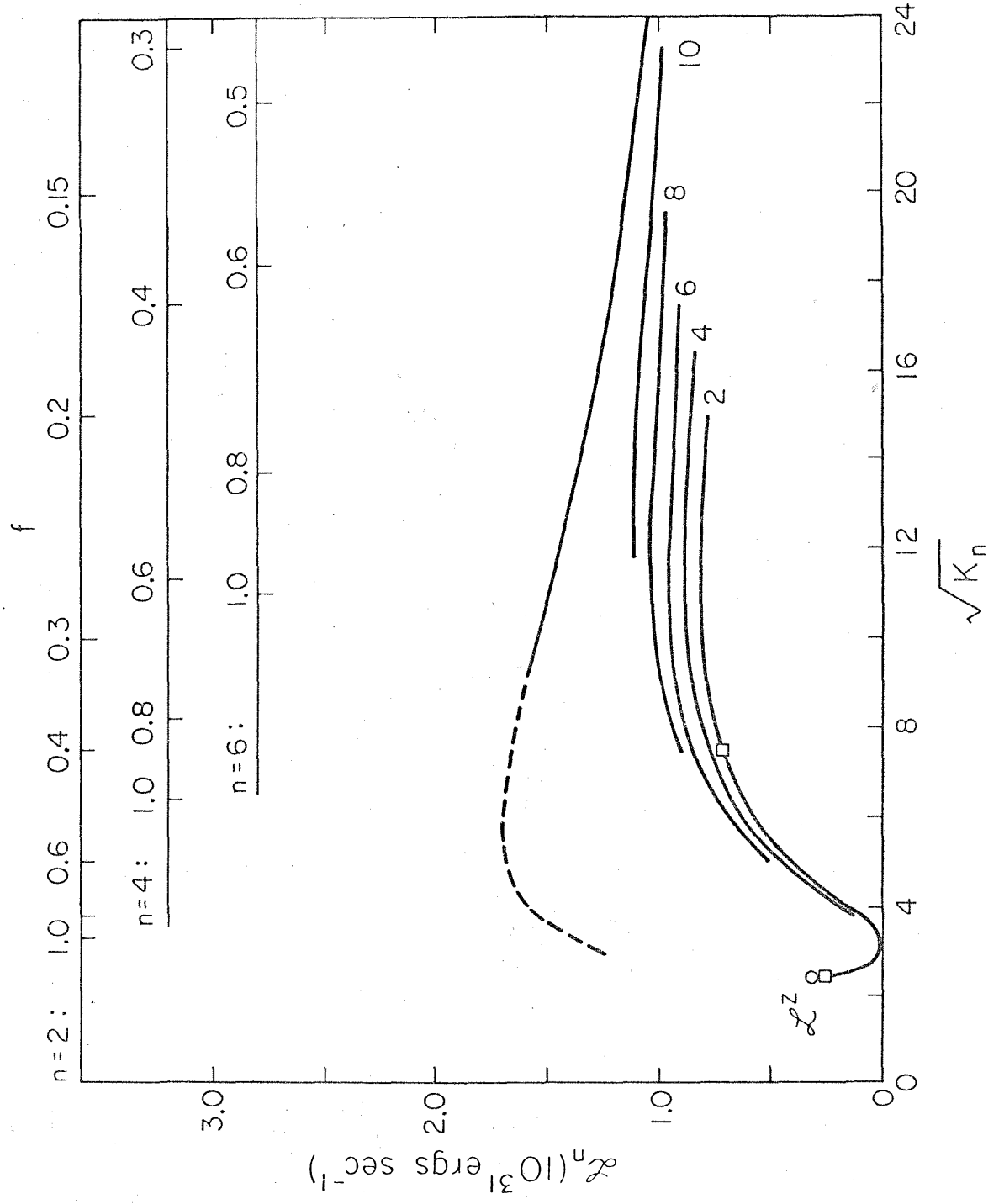
$\alpha_n(10^{31}$ ergs sec$^{-1})$
3.0
2.0
1.0
0
0
4
8
12
16
20
24
$\sqrt{K_n}$
f
n=2 : 1.0 0.6 0.4 0.3 0.2 0.15
n=4 : 1.0 0.8 0.6 0.4 0.3
n=6 : 1.0 0.8 0.6 0.5 0.4
2
4
6
8
10
α^z

for $\mathscr{L}_n$, from figure 5, is also shown. It is immediately apparent that, while $\mathscr{L}_n$ is not independent of σ, its dependence on this quantity is quite weak. In this respect, then, the analytic theory does rather well. However, the dependence of $\mathscr{L}_n$ on $K_n^{\frac{1}{2}}$ does not closely follow the analytic expression, especially for $K_n^{\frac{1}{2}} \leqslant 10$ where the analytic theory is expected to break down. In fact, the numerical $\mathscr{L}_n$ goes to zero for $K_n^{\frac{1}{2}} \simeq 3.05$, corresponding to $f \simeq 1.20$ for the 2^{nd} Hough mode.

For $K_n^{\frac{1}{2}} = 6^{\frac{1}{2}} \simeq 2.45$, corresponding to $f = \infty$ for the 2^{nd} mode, or, in other words, to a non-rotating star, the numerical value of $\mathscr{L}_n$ is in excellent agreement with the quantity $\mathscr{L}^Z$ obtained from Zahn's (1975) results (see equations [3.41] and [3.42]) and also plotted in figure 6. This agreement is rather puzzling since, as was pointed out in section 3d, $\mathscr{L}^Z$ effectively includes the factor $(1+\bar{k}_2)^2$, while $\mathscr{L}_n$ does not. For the 5 $M_\odot$ model used in the present calculations, $(1+\bar{k}_2)^2 \simeq 14$ (see section 5a). Zahn does not give a value for this parameter, but it is clearly included in his numerical calculation of the structure constant E_2. Either $1+\bar{k}_2$ is of order unity for the stellar model used by Zahn, which seems highly unlikely in view of the discussion in section 5a, or there is some other difference between the two numerical calculations which neatly cancels the factor of 14.

Some examples of the numerical solutions for $h_n(r)$ and $\delta p_n(r)$ are presented in figures 7 through 10. Figures 7 and 8 show the homogeneous and particular-integral solutions respectively for σ =

2×10^{-5} sec^{-1} and $K_n = 6$, i.e., for a non-rotating star. The phase difference between the two solutions in the envelope is $80^\circ.8$. Dashed curves show the envelopes of the WKB solutions (2.42) and (2.43), whose amplitude A is determined by a least-squares fit of the numerical solution from $r = 6 \times 10^{10}$ cm to 6.5×10^{10} cm, as described in section 4c. The agreement between the WKB envelopes and the envelopes of the numerical solutions, even quite close to the core, is both impressive and typical of all of the numerical solutions examined. In figure 8, a dot-dashed curve has been superimposed on the $\delta p_n(r)$ solution, which corresponds to the non-oscillatory part of the particular solution (3.25):

$$V_0 \frac{\sigma^2 \rho_0}{K_n} \frac{d}{dr} \left(\frac{r^4 \rho_0}{p'_0} \right) .$$

This aspect of the numerical solutions is also evidently in close agreement with the analytic theory. Finally, note that the non-oscillatory part of $h_n(r)$ in figure 8 is, as predicted, quite small.

Figures 9 and 10 show the homogeneous and particular-integral solutions respectively for $\sigma = 2 \times 10^{-5}$ sec^{-1} and $K_n = 56.25$, corresponding to $f = 0.40$ for the 2^{nd} mode or $f = 0.86$ for the 4^{th} mode. The phase difference between the solutions is $77^\circ.0$.

FIGURES 7 and 8: Numerical solutions for $h_n(r)$ and $\delta p_n(r)$ for a 5 $M_\odot$ star, and for the parameters $\sigma = 2 \times 10^{-5}$ sec^{-1} and $K_n = 6$. Figures 7 and 8 display the homogeneous and particular-integral solutions respectively. Dashed curves indicate the envelopes of the WKB solutions, whose arbitrary amplitudes were determined by least-squares fits to $h_n(r)$ for 6.0×10^{10} cm $\leq r \leq 6.5 \times 10^{10}$ cm. The dot-dashed curve in figure 8 represents the non-oscillatory part of δp_n, as predicted by the analytic theory of section 3. The non-oscillatory part of h_n in figure 8 is also apparent for large r, but is small.

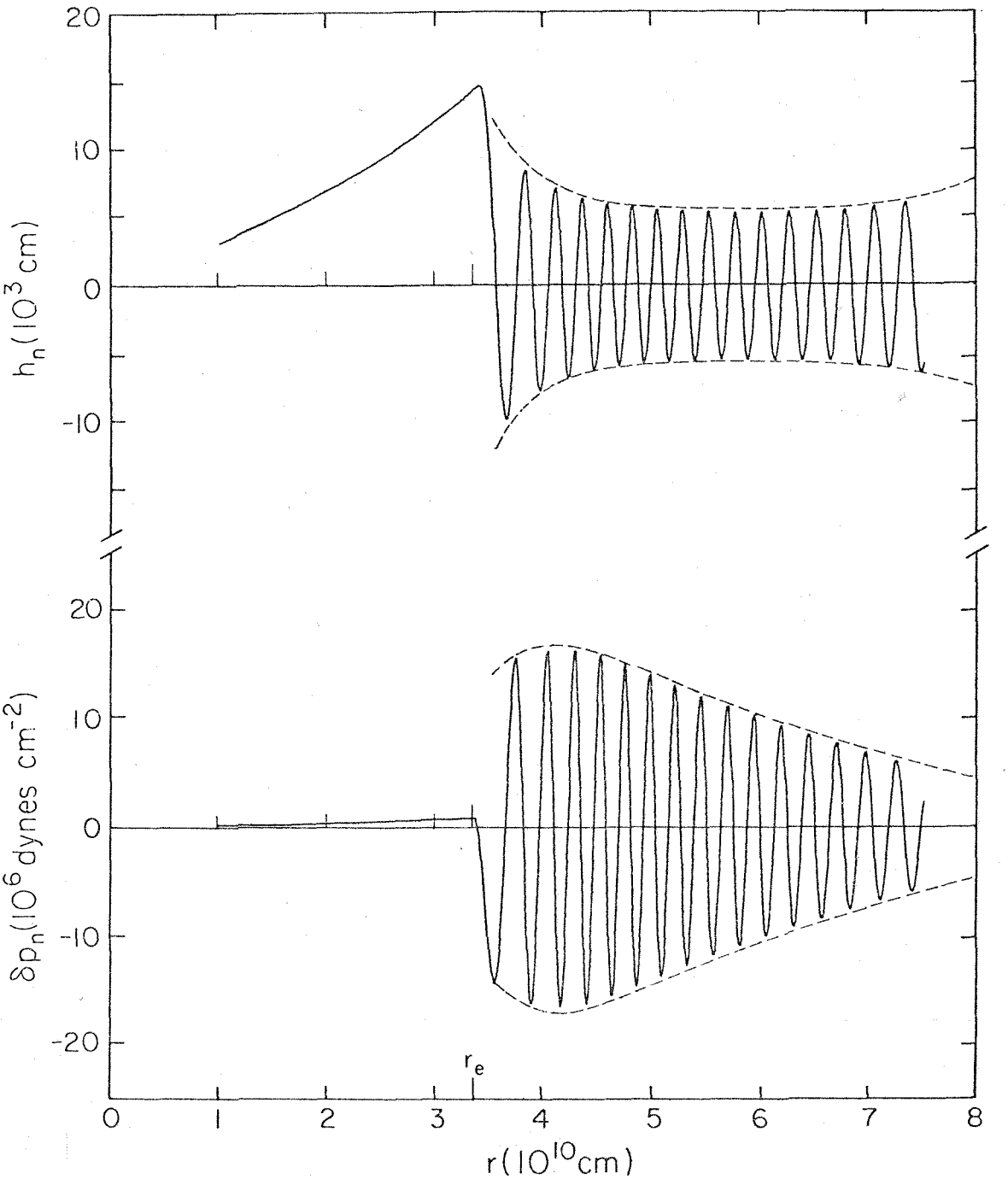
20
10
0
-10
$h_n(10^3 cm)$
20
10
0
-10
-20
$\delta p_n(10^6 dynes\ cm^{-2})$
r_e
0
1
2
3
4
5
6
7
8
$r(10^{10} cm)$

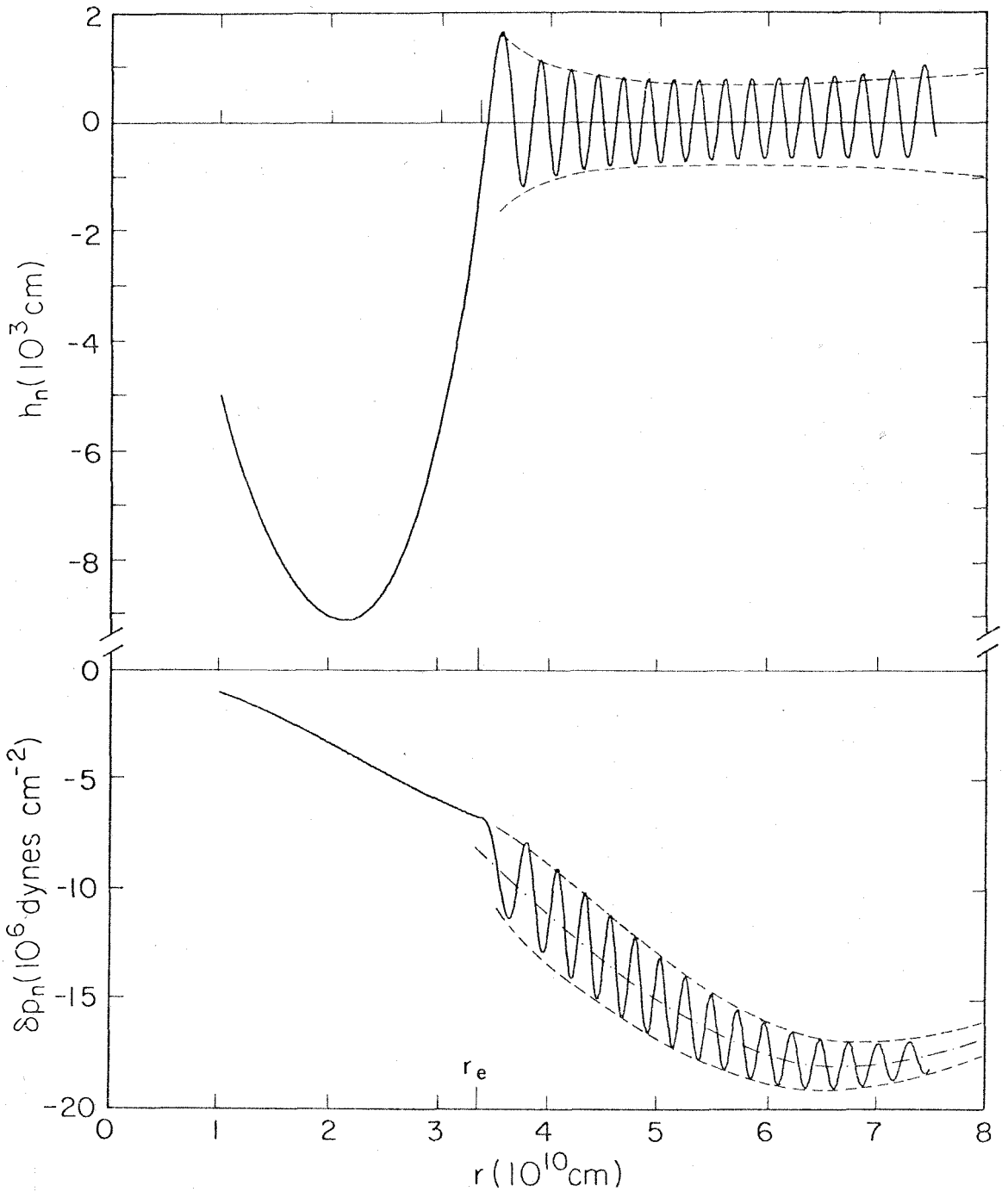
2
0
-2
-4
-6
-8
$h_n(10^3 cm)$
0
-5
-10
-15
-20
$\delta p_n(10^6 dynes\ cm^{-2})$
r_e
0
1
2
3
4
5
6
7
8
$r(10^{10} cm)$

FIGURES 9 and 10: Same as figures 7 and 8, but for $\sigma = 2 \times 10^{-5}$ sec^{-1} and $K_n = 56.25$. WKB envelopes are not shown, but the non-oscillatory part of δp_n is again indicated in figure 10.

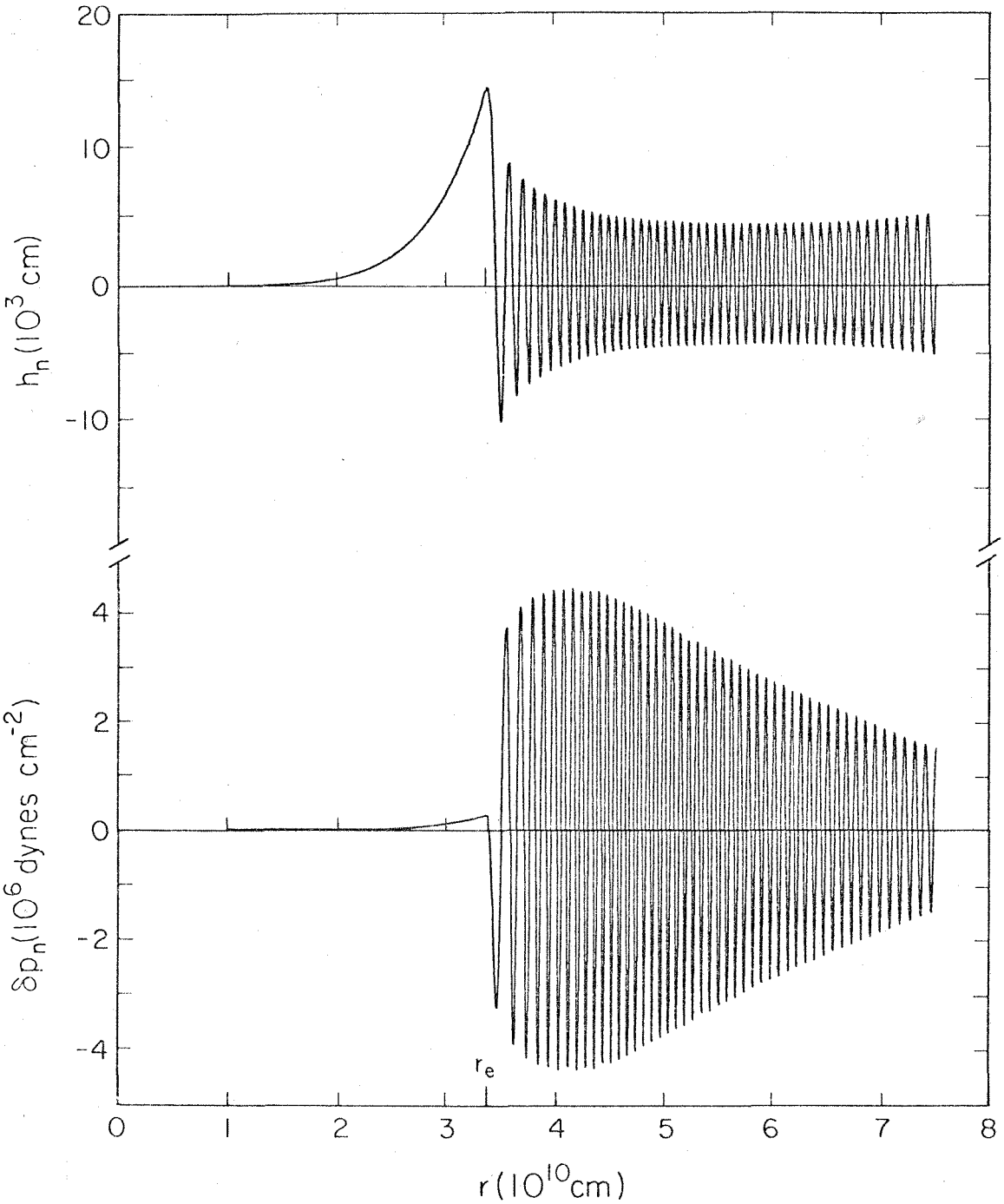
20
10
0
-10
$h_n(10^3 cm)$
4
2
0
-2
-4
$\delta p_n(10^6 dynes\ cm^{-2})$
r_e
0
1
2
3
4
5
6
7
8
$r(10^{10} cm)$

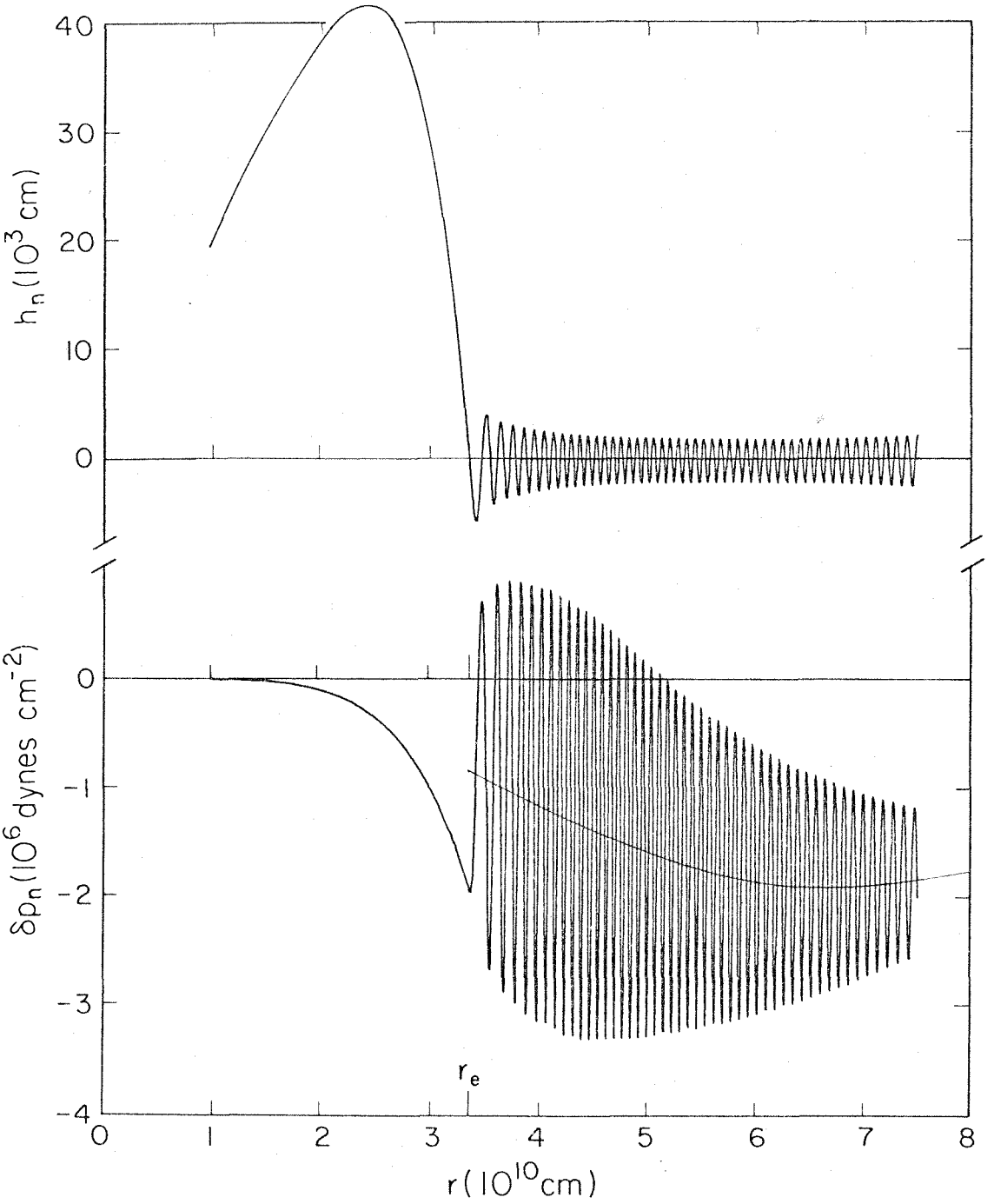
40
30
20
10
0
$h_n(10^3\,cm)$
0
-1
-2
-3
-4
$\delta p_n(10^6\,dynes\,cm^{-2})$
r_e
0
1
2
3
4
5
6
7
8
$r(10^{10}cm)$

e) Atmospheric propagation

All numerical solutions presented in this section have been computed with the radiation condition ($A_-^n = 0$) as the outer boundary condition. It was stated in section 2f that this condition is only rigorously applicable when the gravity waves constituting the n^{th} Hough mode can propagate through the region of minimum temperature in the stellar atmosphere. This propagation condition is expressed by equation (2.50):

$$\sigma f < \frac{2(2n-1)}{R_1} \left[\frac{(\Gamma - 1)\, g\, H_{min}}{\Gamma}\right]^{\frac{1}{2}} ,$$

in terms of the surface gravity, g, and the minimum scale height, H_{min}. When this condition is not satisfied for a particular mode, application of the radiation condition amounts to an assumption that the damping constant $\gamma \gtrsim 0.5$.

For the 5 $M_\odot$ stellar model used in the present calculations, the effective temperature, T_{eff}, is 16,750° K (see Table I). The minimum temperature of the optically thin region above the photosphere must be $\geq T_{eff}/2^{1/4} = 14{,}100°$ K, based on simple concepts of radiative equilibrium. Therefore,

$$gH_{min} = \frac{k\, T_{min}}{\bar{\mu}\, M_H} \geq \frac{k\, T_{eff}}{2^{\frac{1}{4}}\, \bar{\mu} M_H} , \qquad (4.15)$$

where k is Boltzmann's constant, M_H is one atomic mass unit, and $\bar{\mu}$ is the mean atomic weight of the gas. In terms of the standard stellar abundances X and Y, and the hydrogen ionization fraction x,

$$\bar{\mu} \simeq \left[(1+x)\ X + Y/4\right]^{-1} \qquad (4.16)$$

$$\simeq 0.96 \quad ,$$

where we have substituted X = 0.70 and Y = 0.27 from Table I and obtained x from Allen (1973).

A conservative propagation condition for the 5 $M_\odot$ stellar model is thus

$$\sigma f < 0.74 \times 10^{-5}\ (2n-1)\ \text{sec}^{-1} \quad . \qquad (4.17)$$

The precise value of the numerical constant in this expression is rather dependent on the stellar model employed. Using parameters for a 5 $M_\odot$ main sequence star from Allen (1973) and Cox and Giuli (1968) we obtain 0.54×10^{-5} sec^{-1} and 0.97×10^{-5} sec^{-1} respectively.

In figure 11 tidal evolutionary tracks of binary systems in the f, σ plane are displayed for orbital periods of 1, 2, 4, and 8 days. This evolution is discussed in detail in section 5b. Also shown are the regions where (4.17) is satisfied for n = 2, 4, and 6. Taking as an example a binary with a period of 4 days, we see that, for $f > 0.75$, only the 8th and higher Hough modes can propagate through the stellar atmosphere. As f decreases below 0.75, and then below 0.68, the 6^{th} and 4^{th} modes, respectively, begin to propagate. Finally, for $f < 0.54$, the 2^{nd} (and lowest) mode may propagate, as well as all higher order modes.

If radiative or viscous damping of non-propagating modes should prove, upon detailed examination, to be insignificant (i.e., $\gamma \ll 1$), then only propagating modes contribute to the net transport of mechanical energy through the stellar envelope. In this situation,

it is apparent from figure 11 and from the decrease of the projection coefficients $\mathcal{C}_n$ with increasing n that the energy dissipation rate is greatly reduced in the early stages of synchronization.

However, for the calculations of synchronization rates in the next section, we shall assume that the radiation condition is applicable for all values of σ and f.

FIGURE 11: Variation of σ (in units of 10^{-5} sec^{-1}) and f during the process of tidal synchronization, for binaries with orbital periods of 1, 2, 4, and 8 days. Arrows indicate the direction of rotational evolution. Dashed lines separate the $f\sigma$ plane into regions where the propagation condition (4.17) [applicable to a 5 $M_\odot$ star] is satisfied for the indicated Hough modes. See text for further interpretation.

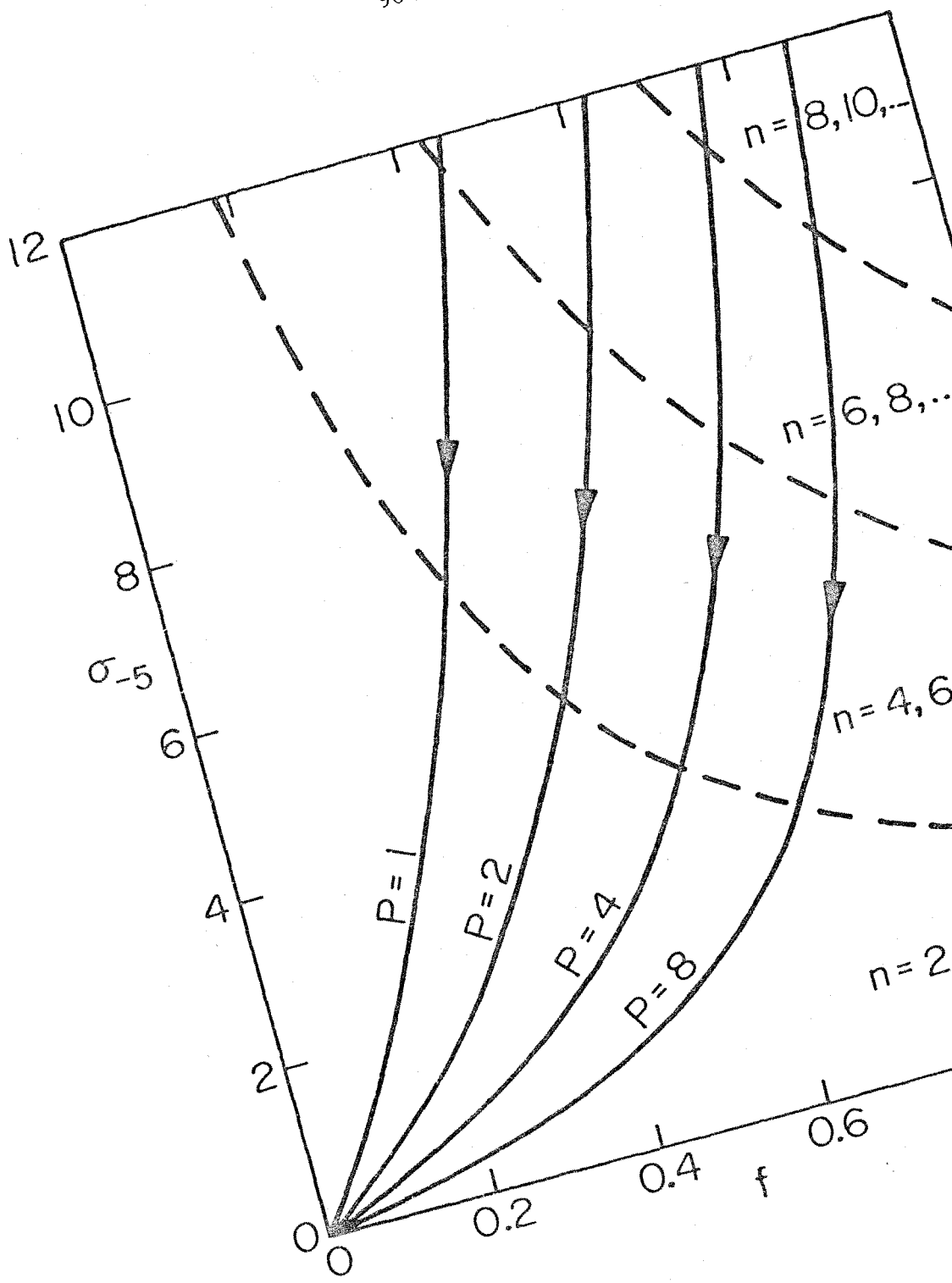
n = 8,10,..
n = 6,8,..
n = 4,6
n = 2
P=1
P=2
P=4
P=8
σ-5
f
0
2
4
6
8
10
12
0.2
0.4
0.6

f) Extrapolation to other stars

To the extent that the numerical results for the 5 solar mass star agree with the analytic theory developed in section 3, one may be justified in scaling the present numerical results to other early-type main sequence stars, using the analytic expressions as a guide. The weak dependence of $\mathscr{L}_n$ on σ, and the reasonable agreement between $\mathscr{L}_n$ (analytic) and $\mathscr{L}_n$ (numerical) for $K_n^{\frac{1}{2}} > 10$ are two such points of agreement which can probably be extrapolated safely. On the other hand, the dependence of $\mathscr{L}_n$ on $K_n^{\frac{1}{2}}$ for $K_n^{\frac{1}{2}} \leq 10$, which is not well predicted, at least by the approximate analytic expression (3.40), may vary considerably for different stellar models. In particular, there seems to be nothing fundamental about the value of K_n for which $\mathscr{L}_n = 0$, and this value might well be different for other models.

However, in the interests of simplicity, it will be assumed in the next section that the form of the function $\mathscr{L}_n(K_n^{\frac{1}{2}})$ is approximately the same for all early-type main sequence stars, and that its absolute value may be scaled according to expression (3.40).

V. SYNCHRONIZATION TIMESCALES

Using the numerical results of section 4, we describe here the process of tidal synchronization of the rotation of a 5 $M_\odot$ star. The time scale for synchronization is given as a function of the binary orbital period P, and the secondary mass fraction μ. These results are extrapolated to other early-type stars with the aid of the analytic expressions derived in section 3.

Observations of synchronization in close binaries are summarized, and compared with the theoretical predictions.

a) The Love function

To apply the formulas of sections 3 or 4 for $\dot{E}$, the energy dissipation rate due to the dynamical tide, we must estimate the effective average value of the Love function, $k_2(r)$, in the stellar core. This quantity is obtained by integrating Poisson's equation (2.11), with the density perturbation corresponding to the equilibrium tidal perturbations given by (2.21). The integration is carried to the surface of the star, where appropriate boundary conditions are applied.

Because the stellar model used for the numerical calculations in section 4 was computed for only the inner 50% of the radius of the star (including, however, 90% of the mass), the integration of Poisson's equation cannot be carried to the surface. In consequence, the function $1 + k_2(r)$ may be computed for the interior, but it contains an arbitrary multiplicative constant. However, the structure of a star which is largely in radiative equilibrium, such as an early-type

main sequence star, is given to a reasonable approximation by that of a polytrope of index 3 (cf. Eddington's 'Standard Model').

Chandrasekhar (1933) has calculated the internal potential in tidally distorted polytropic models; these results have been converted to our function $1 + k_2(r)$, and plotted in figure 12 for polytropes of index 2, 3, and 4 with radii scaled to the radius of the 5 solar mass model. Also plotted is $1 + k_2(r)$ for this model, with the arbitrary constant chosen by matching the form of the function to the forms exhibited by the polytropic sequence. As expected, the index 3 polytrope provides an excellent representation of the Love function of the "real" stellar model.

Since the particular-integral solutions for the dynamical tide in the core, equations (3.5) and (3.7), are increasing functions of radius, the effective average value of $k_2(r)$ should be weighted towards the outer part of the core. We adopt the value

$$1 + \bar{k}_2 = 3.75 \quad . \tag{5.1}$$

This value is essentially a characteristic of the index 3 polytrope, so it will subsequently be used for stars of 2, 7, and 10 $M_\odot$ also.

FIGURE 12: The dimensionless function $1 + k_2(r)$ for polytropic models of index 2, 3, and 4 (scaled to a radius of 18.79×10^{10} cm) and for the 5 $M_\odot$ stellar model. The radius of the core is indicated by r_e.

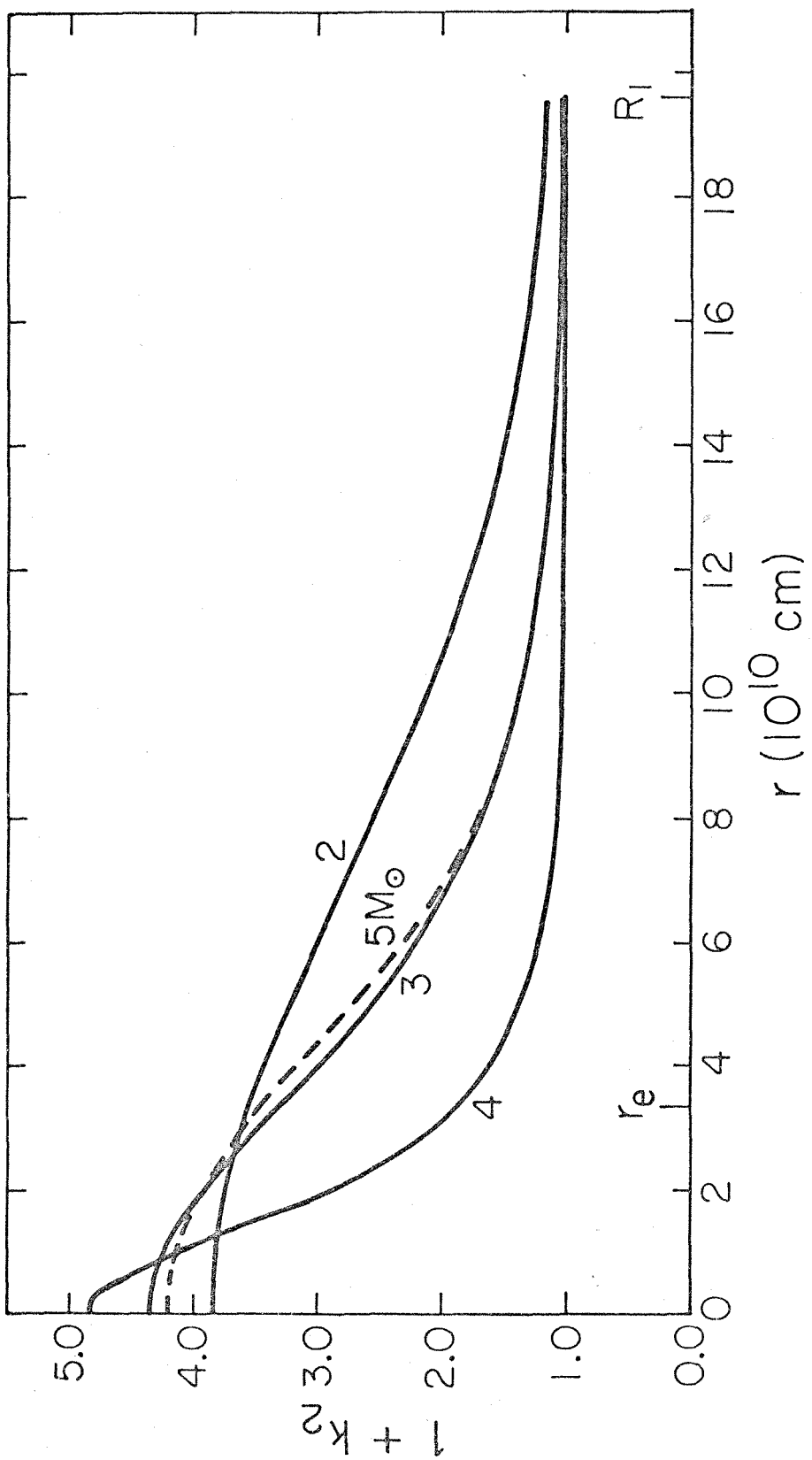
5.0
4.0
3.0
2.0
1.0
0.0
1 + k2
0
2
4
6
8
10
12
14
16
18
r (10^10 cm)
Re
RI
2
5M⊙
3
4

b) Tidal synchronization

Consider a binary system in which the components (1) move in circular orbits about their common center of mass, and (2) rotate about axes perpendicular to the orbital plane. For simplicity, we neglect the rotational energy and angular momentum of the secondary and concentrate attention on the primary. Denoting the center-to-center distance between the two stars by a, the orbital angular velocity by ω, the primary's rotational angular velocity by Ω, the masses of primary and secondary by M_1 and M_2 respectively, and the moment of inertia of the primary by I, we obtain the following expressions for the total angular momentum of the system about its center of mass, and for the total mechanical energy of the system:

$$L = \frac{G^{2/3} M_1 M_2}{(M_1 + M_2)^{1/3}} \omega^{-1/3} + I\Omega \quad , \tag{5.2}$$

$$E = -\frac{G^{2/3} M_1 M_2}{2(M_1 + M_2)^{1/3}} \omega^{2/3} + \tfrac{1}{2} I\Omega^2 \quad . \tag{5.3}$$

Kepler's third law

$$\omega^2 a^3 = G(M_1 + M_2) \tag{5.4}$$

has been used to eliminate a, and ω is assumed to be positive. There is no restriction on the sign of Ω.

Tidal interactions between the two components cannot change the total angular momentum, L, but do change both ω and Ω. In consequence, the total mechanical energy must also change. Applying this constraint

on L, and denoting the rate of *decrease* of total mechanical energy by $\dot{E}$, we obtain

$$\dot{\Omega} = -\frac{\dot{E}}{I(\Omega - \omega)} \tag{5.5}$$

$$\equiv -\frac{2\dot{E}}{I\sigma_2} \quad , \tag{5.6}$$

and

$$\dot{\omega} = \frac{3(M_1 + M_2)^{1/3}\, I}{G^{2/3} M_1 M_2}\, \omega^{4/3}\, \dot{\Omega} \tag{5.7}$$

$$= \frac{3I}{I_{orb}}\, \dot{\Omega} \quad . \tag{5.8}$$

In the latter expression for $\dot{\omega}$, I_{orb} is the orbital moment of inertia of the system about its center of mass:

$$I_{orb} = \frac{M_1 M_2}{M_1 + M_2}\, a^2 \quad . \tag{5.9}$$

Since $I \sim 0.06\, M_1 R_1^{\,2}$, where R_1 is the radius of the primary, and $(R_1/a)^2 \ll 1$ generally, we have

$$I \ll I_{orb} \quad , \tag{5.10}$$

and consequently

$$|\dot{\omega}| \ll |\dot{\Omega}| \quad . \tag{5.11}$$

From equation (5.5), we see that dissipation of mechanical energy by tidal interactions (e.g., by the driving and ultimate dissipation of gravity waves, as we have considered) causes Ω to approach ω, i.e., causes synchronization of rotation and orbital motions. If $\Omega > \omega$, then $\dot{\Omega} < 0$, while if $\Omega < \omega$ (including negative Ω),

$\dot{\Omega} > 0$. At the same time, ω is also changing, and, by (5.8), in the same direction as Ω. However, as long as $I_{orb} > 3I$, which is always the case in real binary star systems, ω changes more slowly than Ω, and the system evolves towards a stable state of synchronous rotation and orbital motion.

From equation (5.6), the evolution of the tidal frequency σ_2 (hereafter denoted by σ) is given by

$$\dot{\sigma} \equiv 2(\dot{\Omega} - \dot{\omega}) \simeq - \frac{4\dot{E}}{I\sigma} \quad , \tag{5.12}$$

where we have neglected $\dot{\omega}$ in comparison with $\dot{\Omega}$. As $\Omega \to \omega$, $\sigma \to 0$. The synchronization parameter f, of Laplace's tidal equation (2.19), also evolves:

$$\dot{f} = f(1 - f) \frac{\dot{\sigma}}{\sigma} \quad . \tag{5.13}$$

As $\Omega \to \omega$, $f \to 0$ also. Figure 13 shows $\sigma/2\omega$ and Ω/ω as functions of f. This figure is a modification of figure 11, in which the different evolutionary tracks have been combined into a single track by plotting $\sigma/2\omega$ rather than σ. A tidally evolving binary system must follow this track towards $f = 0$, $\sigma = 0$, and $\Omega = \omega$, at a rate determined by the energy dissipation rate $\dot{E}$ via equation (5.12).

Thus far, the discussion of tidal synchronization has been deliberately general in nature. Let us now consider the specifics of synchronization due to eventual dissipation of the mechanical energy generated and transported outwards through the primary by the dynamical tide. Since $\dot{E}$ depends in a complex fashion on f, via the eigenvalues

FIGURE 13: The relation between $\sigma/2\omega$, Ω/ω, and f for $\Omega \geq \omega$. The decrease of σ and f accompanying the process of synchronization is indicated by the arrow. Since the orbital mean motion ω does not change significantly during synchronization, the f-σ evolution curves of figure 11 are essentially this curve, scaled to different values of ω.

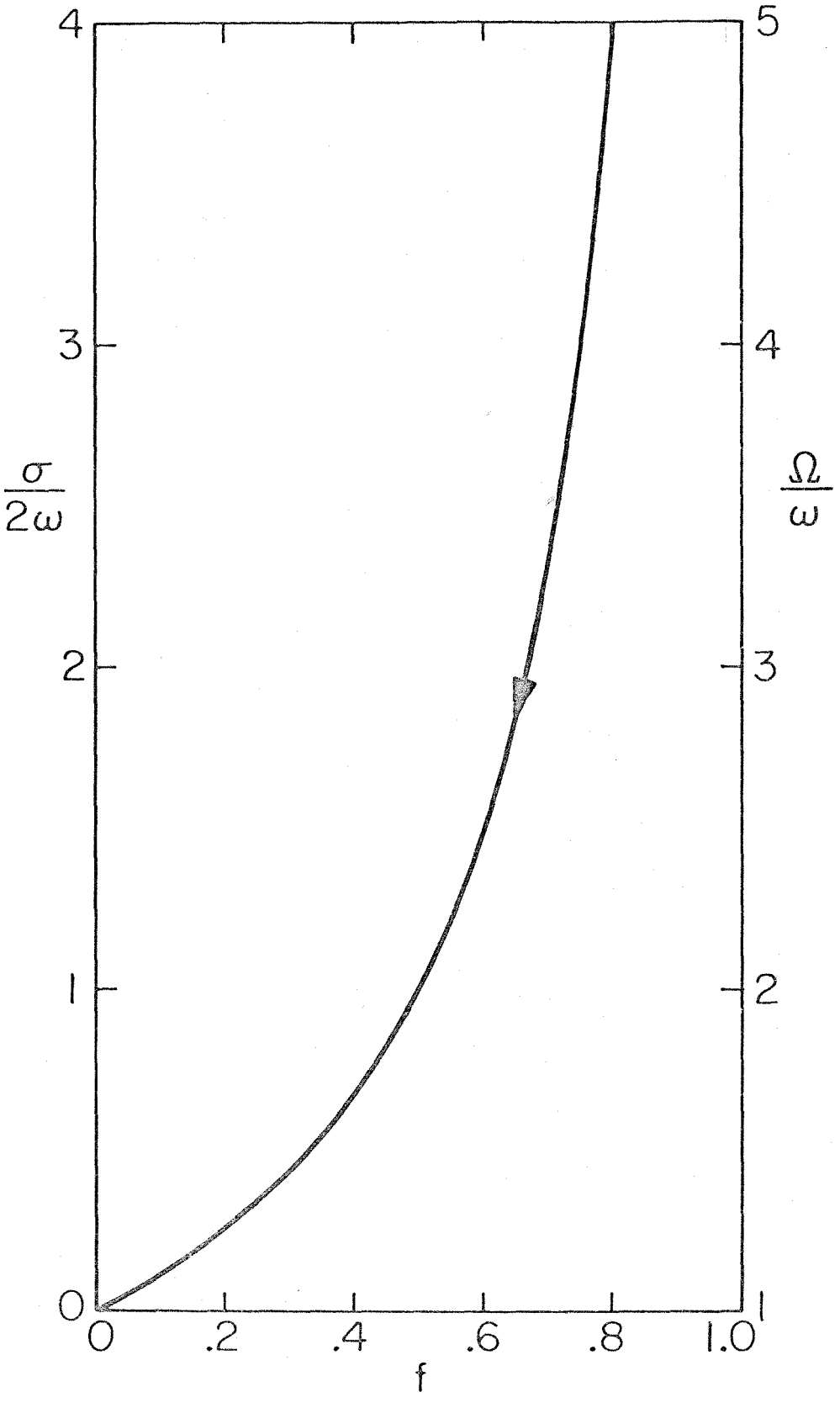
4
3
2
1
0
5
4
3
2
1
σ/2ω
Ω/ω
0
.2
.4
.6
.8
1.0
f

$K_n(f)$, the evolution of the system is best examined in terms of this parameter, rather than in terms of σ or Ω.

Combining equations (5.12) and (5.13), substituting expression (3.39) for $\dot{E}_n$, and eliminating σ in terms of f and the orbital period, P (in days), we obtain the equation governing the evolution of f:

$$\dot{f} = -\frac{1}{\tau}\frac{f^{8/3}}{(1-f)^{2/3}}\sum_{n=2}^{\infty}\left(\mathscr{L}_n(f,\sigma)\left[\mathscr{L}^{10}(\sigma)\right]^{-1}\mathscr{C}_n(f)^2\right) . \qquad (5.14)$$

$\mathscr{L}^{10}(\sigma)$ represents the value of $\mathscr{L}_n(f,\sigma)$ corresponding to $K_n^{\frac{1}{2}} = 10$, and is a convenient normalization for $\mathscr{L}_n(f,\sigma)$. The analytic approximation for $\mathscr{L}^{10}$, which is independent of σ, has been given in Table II for stars of 2, 5, 7, and 10 $M_\odot$. The time constant τ is a function of P, μ, and the structure of the primary:

$$\tau = 9.141 \times 10^{-21}\left[\frac{I\,P^{17/3}}{(1+\bar{k}_2)^2\,\mu^2\,\mathscr{L}^{10}(\sigma)}\right] \text{ yr} \qquad (5.15)$$

$$\equiv \tau_0\frac{P^{17/3}}{\mu^2} , \qquad (5.16)$$

where τ_0 is a function only of the primary's structure.

To integrate equation (5.14), we retain only the n = 2 and n = 4 terms in the sum over Hough modes. The numerical solution for $\mathscr{L}_n(f,\sigma)$ for a 5 $M_\odot$ star is given in figure 6. We neglect the slight dependence of $\mathscr{L}_n$ on σ, and adopt the curve $\mathscr{L}_n(f)$ for $\sigma = 6 \times 10^{-5}\,\text{sec}^{-1}$ as a representative average. With projection coefficients $\mathscr{C}_2(f)$ and $\mathscr{C}_4(f)$ as shown in figure 3, the sum in equation (5.14) is evaluated

and displayed as a function of f in figure 14. The increase of this sum as f decreases from 1.0 to $\sim$ 0.6 is due to the growth of $\mathscr{L}_2(f)$ in this range, while the decrease for $f \leqslant 0.6$ is due to the rapid diminishing of $\mathscr{C}_2(f)$ and $\mathscr{C}_4(f)$ as f becomes small.

Equation (5.14) may now be numerically integrated, starting with f = 1.0 at t = 0, to yield $f(t/\tau)$, as shown in figure 15. Not surprisingly, the rate of evolution of f decreases considerably as f decreases below 0.5. Thus the time scale for synchronization, τ_{syn}, depends critically on the adopted practical criterion for a system to be considered synchronous. On the other hand, this time scale is relatively independent of the initial value of f, as long as this is not too small. Referring to both figures 15 and 13, we note the following values of τ_{syn} for various synchronization criteria:

$$\left.\begin{aligned} f_{syn} &= 2/3 \text{ or } \Omega = 3\omega \quad , \quad \tau_{syn} = \tau \quad ; \\ f_{syn} &= 1/2 \text{ or } \Omega = 2\omega \quad , \quad \tau_{syn} = 2.4\,\tau \quad ; \\ f_{syn} &= 1/3 \text{ or } \Omega = 1.5\omega \quad , \quad \tau_{syn} = 12.0\,\tau \quad ; \end{aligned}\right\} \qquad (5.17)$$

Note that the function $f(t/\tau)$ and the results above strictly refer only to a 5 $M_\odot$ primary, for which $\mathscr{L}_n(\sigma,f)$ is given in figure 6. However, if it is assumed that the form of the function $\mathscr{L}_n(\sigma,f)$ is approximately the same for all early-type stars, and that only the amplitude (specified by $\mathscr{L}^{10}$) changes, then these results may be applied to other early-type stars, with appropriate values of τ_0.

FIGURE 14: The numerical results for $\mathscr{L}_2(\sigma,f)$ and $\mathscr{L}_4(\sigma,f)$ for a 5 $M_\odot$ star, plotted as a function of f for $\sigma = 6 \times 10^{-5}$ sec^{-1}, and derived from figure 6. Also shown is the sum $\sum_{n=2}^{4} \mathscr{L}_n \mathscr{C}_n^2$, which appears in equation (5.14). The parameter $\mathscr{L}^Z$, derived from Zahn's work, is independent of f.

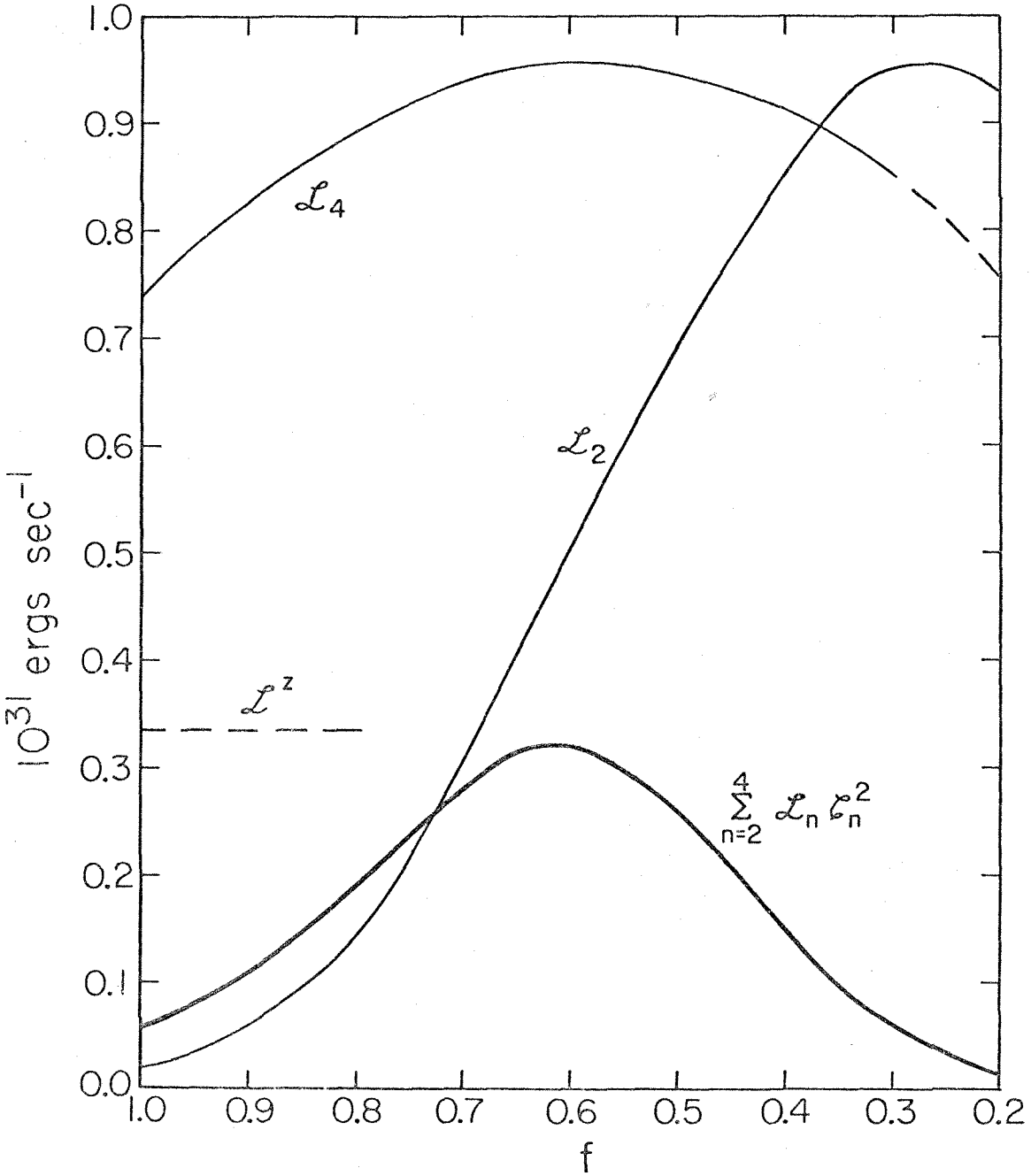
1.0
0.9
0.8
0.7
0.6
0.5
0.4
0.3
0.2
0.1
0.0
10^{31} ergs sec^{-1}
$\mathcal{L}_4$
$\mathcal{L}_2$
$\mathcal{L}^z$
$\sum_{n=2}^{4} \mathcal{L}_n \mathcal{C}_n^2$
1.0
0.9
0.8
0.7
0.6
0.5
0.4
0.3
0.2
f

FIGURE 15: Evolution of the synchronization parameter f, as a function of the dimensionless time variable t/τ, for a 5 $M_\odot$ star. This curve was obtained by the numerical integration of equation (5.14), and represents the contributions by the 2nd and 4th Hough modes to the dynamical tide, as shown in figure 14.

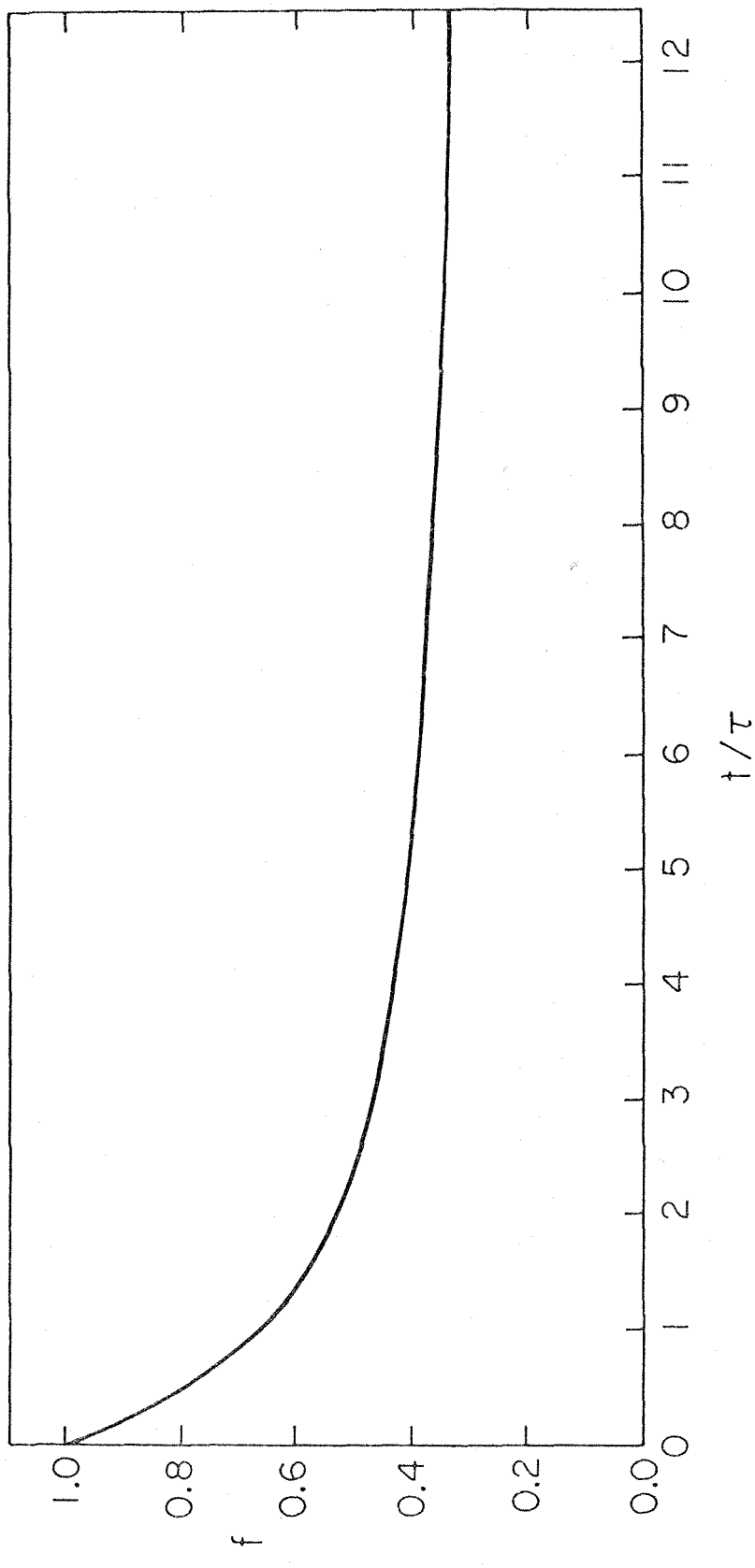
1.0
0.8
0.6
0.4
0.2
0.0
f
0
1
2
3
4
5
6
7
8
9
10
11
12
t/τ

c) Synchronization times and critical periods

For the 5 $M_\odot$ stellar model, $\mathscr{L}^{10}$ is obtained from the numerical results displayed in figure 6:

$$\mathscr{L}^{10} \simeq 0.95 \times 10^{31} \text{ ergs sec}^{-1} \quad . \tag{5.18}$$

The moment of inertia, I, is calculated from the density profile of the model: $I = (2.2 \pm 0.3) \times 10^{55}$ g cm^2. With $1 + \bar{k}_2 = 3.75$ (see section 5a), the parameter τ_0 of equation (5.16) is

$$\tau_0 = 1500 \text{ yr} \quad . \tag{5.19}$$

To estimate τ_0 for other early-type stars, recall the approximate analytic expression for $\mathscr{L}_n$, equation (3.40):

$$\mathscr{L}_n \propto \frac{r_e^5}{\left[r(dN_v^2/dr)\right]_{r_e}^{1/3} \rho_e} \quad .$$

With stellar parameters from Table I, this expression has previously been evaluated for $K_n^{\frac{1}{2}} = 10$, and the results listed in Table II. For the 5 $M_\odot$ model we obtained

$$\mathscr{L}^{10}(\text{analytic}) = 1.54 \times 10^{31} \text{ ergs sec}^{-1} \quad . \tag{5.20}$$

A comparison of this result with the more accurate numerical result (5.18), reveals that the analytic estimates of $\mathscr{L}^{10}$ should be reduced by a factor of 0.62. The moment of inertia factor, $I/M_1R_1^2$, is assumed to be the same for all stars in the mass range 2 to 10 $M_\odot$ (see e.g., Zahn, 1975 Table I), and to take the value 0.063, derived for the 5 $M_\odot$ model. Finally, as intimated in section 5a, the constant $1 + \bar{k}_2$ is taken to be 3.75 for all early-type stars.

We thus obtain the following estimates for τ_0:

$$\left.\begin{aligned} \tau_0 &= 78{,}000 \text{ yr} \qquad (M_1 = 2\ M_\odot) \quad , \\ \tau_0 &= 370 \text{ yr} \qquad (M_1 = 7\ M_\odot) \quad , \\ \tau_0 &= 84 \text{ yr} \qquad (M_1 = 10\ M_\odot) \quad . \end{aligned}\right\} \tag{5.21}$$

A convenient power-law representation of τ_0 as a function of primary mass is

$$\tau_0 \simeq 1.5 \times 10^6 \ (M_1/M_\odot)^{-4.25} \text{ yr} \quad , \tag{5.22}$$

which yields the following approximate form of equation (5.16):

$$\tau \simeq 1.5 \times 10^6 \left(\frac{M_1}{M_\odot}\right)^{-4.25} \frac{P^{17/3}}{\mu^2} \text{ yr.} \tag{5.23}$$

In order to compare these results with observational material, we ask the following question: What is the critical value of the orbital period, P_{crit}, such that most observed close binaries with $P \leq P_{crit}$ should exhibit essentially synchronous rotational velocities? The answer depends somewhat on "most", since not all observed binaries are the same age, and on the criterion for synchronization, as was discussed in section 5b. Following Zahn (1977), we require the synchronization time, τ_{syn}, to be no more than ¼ of the main sequence lifetime, τ_{MS}, of the primary. The critical period is then given by

$$P_{crit} = \left[\frac{\mu^2 \tau_{MS}}{4\ \tau_0 (\tau_{syn}/\tau)}\right]^{3/17} \tag{5.24}$$

where the ratio (τ_{syn}/τ) depends on the adopted criterion for synchronization. For example, from (5.17) we have $\tau_{syn}/\tau = 2.4$ for $f_{syn} = \frac{1}{2}$.

Table V gives the critical periods for stars of 2, 5, 7, and 10 $M_\odot$, evaluated for $\mu = \frac{1}{2}$ and $f_{syn} = \frac{1}{2}$ and 1/3. These results may be easily scaled to different values of μ or f_{syn} by reference to equation (5.24) and figure 15. The main-sequence lifetimes in the table were obtained by adopting the value 7×10^7 yr for the 5 $M_\odot$ model (Cox and Giuli, 1968 , vol. 2, p. 988), and then scaling this according to mass/luminosity (see Table I) for the other stellar models. An excellent approximation is

$$\tau_{MS} \simeq 3.2 \times 10^9 \ (M/M_\odot)^{-2.38} \quad \text{yr.} \qquad (5.25)$$

TABLE V

Critical orbital periods for the synchronization of close binaries.

Mass ($M_\odot$)		2	5	7	10
τ_{MS} (yr)		6×10^8	7×10^7	3×10^7	1.3×10^7
τ_0 (yr)		7.8×10^4	1.5×10^3	3.7×10^2	8.4×10^1
P_{crit}(days) for $\mu = 0.5$	$f_{syn} = \frac{1}{3}$	1.92	2.63	2.91	3.26
	$f_{syn} = \frac{1}{2}$	2.55	3.50	3.86	4.33
P_{crit} (days) (Zahn [1977])		1.59	2.19	2.69	3.30

An approximate expression for the critical period may be derived from expressions (5.22) for τ_0 and (5.25) for τ_{MS}:

$$P_{crit} \simeq 3.03 \left[\frac{\mu^2}{\tau_{syn}/\tau}\right]^{3/17} (M_1/M_\odot)^{0.33} \quad , \qquad (5.26)$$

$$\text{for} \quad 2M_\odot \leq M_1 \leq 10M_\odot \quad .$$

The last line in Table V gives the critical periods for synchronization calculated by Zahn (1977). Zahn has adopted a slightly different definition of the synchronization time τ_{syn}:

$$\frac{1}{\tau_{syn}^{Z}} \equiv \frac{d}{dt}\left(\frac{\sigma}{2\omega}\right)^{-5/3} \quad , \qquad (5.27)$$

which reflects the fact that $\mathscr{L}_n$ and $\mathscr{C}_n$ are independent of f when the rotation of the star is neglected. Evidently, τ_{syn}^{Z} is the time taken for the system to evolve from f = 1.0 ($\sigma/2\omega = \omega$) to f = 0.5 ($\sigma/2\omega = 1$). Zahn's values for the critical periods should thus be compared with the present values of P_{crit} for $f_{syn} = \frac{1}{2}$.

In terms of Zahn's dimensionless parameter E_2 (see Table II),

$$\tau_{syn}^{Z} = \frac{6.64 \times 10^{-56} (M_1/M_\odot)^{4/3}}{E_2 (R_1/R_\odot)^9} \left[\frac{IP^{17/3}}{\mu^2}\right] \text{yr} \quad . \qquad (5.28)$$

Comparing this expression with equation (5.15) for τ, and substituting for E_2 in terms of $\mathscr{L}^Z$ (see equation [3.42]), we find

$$\tau_{syn}^{Z} = \frac{3}{5} \frac{(1+\bar{k}_2)^2 \mathscr{L}^{10}}{\mathscr{L}^Z} \tau \quad . \qquad (5.29)$$

For a primary of 5 $M_\odot$, $\tau_{syn}^{Z} \simeq 24.8\ \tau$, or about 10 times longer than

our $f_{syn} = \frac{1}{2}$ synchronization time of 2.4 τ. This factor of 10 difference in predicted synchronization times results in the factor of $\sim 10^{-3/17} \simeq 2/3$ difference between Zahn's critical periods and those obtained in the present study. We shall presently see that the shorter synchronization times and correspondingly greater critical periods are in closer agreement with the observational evidence.

Before turning to a discussion of the observations pertaining to synchronization, we digress briefly to consider a point of interpretation raised by Zahn (1977).

The rate of dissipation of mechanical energy associated with the dynamical tide, and hence the time scale for synchronization, depends basically on three things: (1) the strength of the tidal potential; (2) the tidal frequency σ; and (3) the structure of the core and inner envelope of the primary. Concentrating on the first of these parameters, we have

$$\dot{E} \propto \left(\frac{M_2}{a^3}\right)^2 \equiv \left(\frac{\mu(M_1+M_2)}{a^3}\right)^2 \propto \left(\frac{\mu}{P^2}\right)^2 \quad . \tag{5.30}$$

Since σ also depends on P, it is apparent that P is indeed a fundamental parameter of the process of tidal synchronization. Zahn, however, recommends the use of the fractional radius, R_1/a, in place of P in the analysis of observational material and in comparisons of these data with theory. This parameter, as well as P, may be obtained directly from an analysis of the light curves of eclipsing binaries.

This recommendation is ill-advised, inasmuch as the primary's radius R_1 does not directly enter into the calculation of the dynamical tide. This seems at odds with equation (5.28), but in fact E_2 depends strongly on R_1^{-1} through Zahn's practice of normalizing the radius variable by R_1 and the tidal frequency by $(GM_1/R_1^3)^{\frac{1}{2}}$. In the present work this apparent dependence on R_1 has been removed by avoiding such normalizations.

The significance of this distinction between the use of the parameters P and R_1/a lies in the fact that the radii of stellar models are quite uncertain. For example, for a 5 solar mass zero-age main sequence star, we find the following radii in use: 2.24 $R_\odot$ (Cox and Giuli, 1968 , vol. 2, p. 982), 2.35 $R_\odot$ (Zahn, 1975, 1977), 2.70 $R_\odot$ (present calculations), and 3.31 $R_\odot$ (Allen, 1973). Referring to equation (5.15) for the tidal synchronization time scale, we have $\tau \propto \tau_0 P^{17/3}$. If this equation is rewritten in terms of the fractional radius, it becomes

$$\tau \propto \tau_0' \left(\frac{a}{R_1}\right)^{17/2} , \qquad (5.31)$$

but the new constant $\tau_0' \propto \tau_0 R_1^{17/3}$ and is consequently quite uncertain.

d) Comparison with observations

Rotational velocities have been measured for ~ 100 early type (O-F) stars in close binary systems, by modeling the rotational doppler broadening of sharp spectral lines. Unfortunately there are two serious problems connected with the interpretation of these data. First, only the radial component of the rotational velocity is measured i.e., $v_R \sin i$, where i is the inclination of the star's equatorial plane to the plane of the sky. Second, to compute the rotational angular velocity Ω, or, equivalently, the expected "synchronous rotational velocity" v_s, the radius of the star must be known.

1) Eclipsing binaries

Both of these problems may be solved for one class of close binaries - the eclipsing binaries. These systems are seen, by definition, almost edge-on, so that, with the assumption that the stellar equatorial plane is coincident with the orbit plane, $\sin i \simeq 1$. From the analysis of the light curve of an eclipsing binary, the inclination and one or both fractional stellar radii, R_1/a and R_2/a, may often be obtained. If the radial velocity curves for both primary and secondary are measurable, the total mass $(M_1 + M_2)$ and the semi-major axis 'a' may be computed, thus yielding absolute radii. Alternatively, the absolute radii may be estimated from the apparent magnitudes of the stars, if the distance to the binary is known.

Koch, Olson, and Yoss (1965) and Olson (1968) have measured the rotational velocities v_R of 40 early type stars in 29 close-binary

systems, most of which are eclipsing, and compared these velocities with the "synchronous velocities" v_s. These data have been carefully discussed, and four more systems added, by Plavec (1970).

The simplest and most obvious conclusion to be drawn from the data on eclipsing binaries is that, for each spectral type, the average rotational velocities are about one-half of the typical field star rotational velocities (see Plavec, Fig. 1). Either the components of binaries are formed with comparatively low rotation rates, which is quite plausible since most of the angular momentum of these systems resides in their orbital motion, or some process of synchronization is at work. An examination of Olson's (1968) plot of v_R against v_s (Olson, Fig. 2; Plavec, Fig. 2) led Plavec to draw the following conclusions:

> "(1) No case is known of a component rotating considerably more slowly than required by synchronism.
> (2) As a rule, the rotation is synchronized with orbital motion, or may be somewhat faster.
> (3) A few stars rotate considerably more rapidly than they should if synchronism applied to them."
>
> (Plavec, 1970, p. 137)

Most of the "synchronously" rotating ($\Omega \leqslant 1.5\,\omega$) stars discussed by the above writers have orbital periods $\leqslant$ 4 days, and fractional radii $\geqslant 0.15$, while most of the definitely non-synchronous rotators do not satisfy these inequalities. There are, however, exceptions in both cases, e.g., the primary of V380 Cyg, which rotates synchronously with a period of 12.4 days; and the primary of U Cep, which has an orbital period of 2.5 days but rotates 5.25 times faster than

synchronism requires. Moreover, most of the systems studied have periods less than 6 days. Plavec concludes that "...nothing statistically meaningful can be said about periods longer than 4 days."

The 33 systems considered in the above studies are used here in an observational test of the theory of synchronization by the action of dynamical tides. The component stars range in spectral type from F0($M \sim 1.6\ M_\odot$) to O8.5 ($M \sim 23\ M_\odot$), most falling within the mass range $2\ M_\odot - 10\ M_\odot$ covered by our theoretical analysis. We have seen already that the predicted critical period for synchronization (Table V) is 2-3 days for $f_{syn} = \frac{1}{3}$ ($\Omega = 1.5\omega$), or 3-4 days for $f_{syn} = \frac{1}{2}(\Omega = 2\omega)$. These periods are of the same order as, but perhaps somewhat shorter than, the critical period of $\gtrsim 4$ days suggested by the observational data.

A more detailed test may be performed by calculating the tidal synchronization time constant, τ, for each binary component whose rotation has been measured, and comparing this with the star's main-sequence lifetime, τ_{MS}. Equations (5.23) and (5.25), extrapolated to $M_1 > 10\ M_\odot$ when necessary, are used to obtain τ and τ_{MS}, respectively. The primary mass M_1, and the secondary mass fraction μ are obtained by reference to Batten's (1967) Sixth Catalogue. When both primary and secondary radial velocity curves have been measured for a system, and the inclination estimated, both masses are known. For systems with only one measured radial velocity curve, the primary's mass has been estimated from its spectral type (with the calibration from Allen [1973]), and μ has been set equal to 0.5.

Table VI gives the resulting values of τ/τ_{MS}, along with measured v_R/v_S, for 44 components in 34 close binaries. These results are also plotted in figure 16, in the form of $\log(v_r/v_s) \equiv \log(\Omega/\omega)$ against τ/τ_{MS}. Recall (equation [5.17]) that the time for a star to spin down from an initially rapid rate to $\Omega = 1.5\omega$ is $\sim 12\tau$. We thus expect to find $\Omega/\omega \leqslant 1.5$ for most stars with $\tau/\tau_{MS} < 0.02$, and for very few stars with $\tau/\tau_{MS} > 0.08$. On the other hand, if the looser synchronization criterion of $\Omega \leqslant 2\omega$ is adopted, these limits become $\tau/\tau_M < 0.1$ and $\tau/\tau_{MS} > 0.4$, respectively.

Disregarding certain obvious exceptions, figure 16 reveals that most stars with $\tau/\tau_{MS} < 1$ satisfy the tighter criterion $\Omega/\omega < 1.5$. For $\tau/\tau_{MS} > 1$, the distribution of Ω/ω appears, at present, to be random. (Because of the strong dependence of τ on the period P, figure 16 is not greatly different in the distribution of data points from Plavec's plot of $\log(v_r/v_s)$ against P.) The theory is thus qualitatively successful in ranking most binaries according to their synchronization time scales. Quantitatively, however, the predicted times for spin-down to $\Omega/\omega = 1.5$ are about one order of magnitude too long to explain many observed cases of "tight" synchronism, although the times predicted for spin down to $\Omega/\omega = 2$ ("loose" synchronism) are compatible with the observations.

It appears, therefore, that the problems of the dynamical tide model of synchronization lie not with the basic time constant τ, but with the long "tail" exhibited by figure 15. For values of $f < 0.5$, or $\Omega/\omega < 2$, the predicted rate of synchronization decreases rapidly,

TABLE VI

Rotational velocities and synchronization time constants for 44 components of 34 close binaries. Systems denoted by asterisks are eclipsing - others are single- or double-line spectroscopic binaries. Values of v_R/v_S from Olson (1968) and Plavec (1970); all other data from Batten (1967). Values of τ/τ_{MS} calculated with a mass inferred from the spectral type are indicated by a †.

System	Orbital Period (days)	Spectral Type	v_R/v_S	τ/τ_{MS}
γ And B	2.67	B9.5 V	1.22:	0.03†
σ Aql*	1.95	B3	1.11	0.003
		B3	1.61	0.003
β Aur*	3.96	A2 IV	1.16	0.97
		A2 IV	1.14	0.97
WW Aur*	2.53	A7	1.08	0.12
		A7	1.03	0.12
R CMa*	1.14	F0	1.26	0.0014†
δ Cap*	1.02	Am	0.83:	~ 0.0006†
AO Cas*	3.52	O8.5n	0.80	~ 0.01†
		O8.5n	0.97	~ 0.01†
AR Cas*	6.07	B3	4.06	0.9†
RZ Cas*	1.20	A2	1.30	0.0008†
YZ Cas*	4.47	A2	0.97	1.4†
AH Cep*	1.77	B0n	1.21	~ 0.0004
		B0n	1.13	~ 0.0003
U Cep*	2.49	B8	5.25	0.02†
α CrB*	17.4	A0	14	~ 100†
V380 Cyg*	12.42	B1.5	0.98	~ 42
Y Cyg*	3.00	O9.5n	1.46	~ 0.005
		O9.5n	1.41	~ 0.005
AI Dra*	1.20	A0	1.15	0.0006†
66 Eri	5.52	B9	0.70:	2.6†

TABLE VI (Continued)

System	Orbital Period (days)	Spectral Type	v_R/v_S	τ/τ_{MS}
68 Her*	2.05	B3	1.01	0.0016†
RX Her*	1.78	B9.5	1.15	0.008
		A1	1.19	0.008
δ Lib*	2.33	A0 V	1.03	0.024†
δ Ori A*	5.73	B1	0.94	~ 0.3†
VV Ori*	1.49	B2	0.62:	0.007
U Oph*	1.68	B4	1.05	0.002
		B5	0.94	0.002
AW Peg*	10.62	A5e	6	4500
EE Peg*	2.63	A4 IV	1.13	0.1†
AG Per*[1]	2.03	B3	0.99	0.006
		-	1.11	0.006
b Per	1.53	A2	0.91:	0.003†
o Per	4.42	B1 III	0.98:	0.06[2]
		-	1.22:	0.06
RY Per*	6.86	B4	10	~ 2†
U Sge*	3.38	B9n	0.86	0.16†
RZ Sct*	15.19	B2	4	~ 100†
λ Tau*	3.95	B3 V	0.97	0.8
RS Vul*	4.48	B5	1.96	2.4
HD 98088	5.91	A2p	1.00[3]	~ 12

1) Probable member of II Persei association, which has a kinematic age of ~ 1.6×10^6 yr.

2) τ/τ_{MS} probably invalid, since primary is not on the main sequence.

3) Synchronism based on spectrum and magnetic variations, not on rotational velocity.

FIGURE 16: Plot of lot (v_R/v_S) against τ/τ_{MS} for components of the binary systems listed in Table VI. Open circles represent systems for which the masses of both primary and secondary are given by Batten (1967). For the systems indicated by filled circles, the primary mass was estimated from the spectral type and the mass fraction μ set equal to 0.5. Perfect synchronism is indicated by the solid line, and the "tight" synchronization criterion by the dashed line. Unusual or non-synchronous systems are identified for convenient reference.

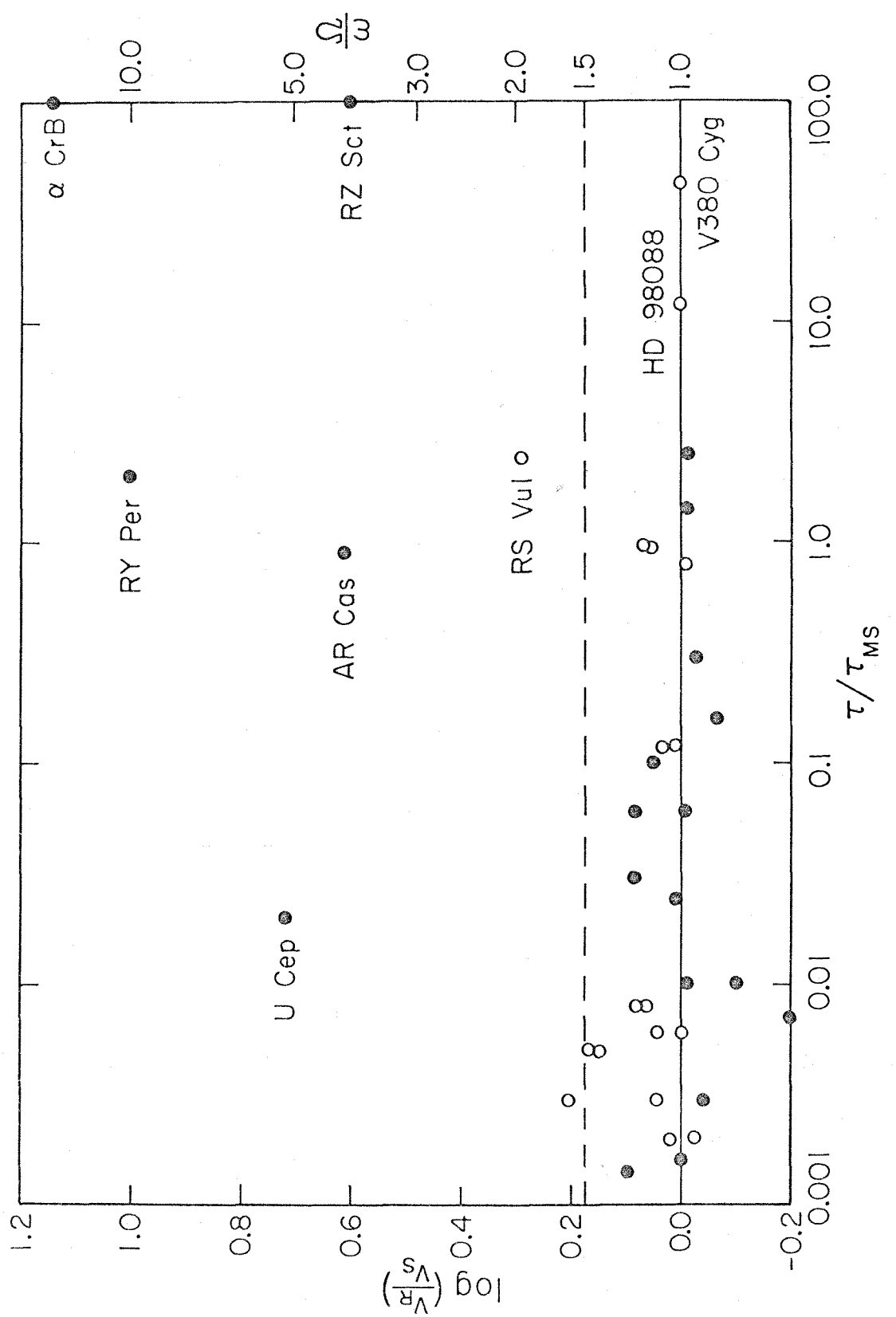
α CrB
RY Per
AR Cas
U Cep
RZ Sct
RS Vul
HD 98088
V380 Cyg
10.0
5.0
3.0
2.0
1.5
1.0
Ω/ω
1.2
1.0
0.8
0.6
0.4
0.2
0.0
-0.2
log (V_R/V_S)
100.0
10.0
1.0
0.1
0.01
0.001
τ/τ_MS

due to the decrease of the projection coefficients $\mathscr{C}_n$. The theory thus predicts that a large number of systems with $0.01 \leqslant \tau/\tau_{MS} \leqslant 1$ should exhibit values of Ω/ω in the neighborhood of, or somewhat less than, 2. Further reduction of Ω/ω (to 1.5 or less) should only have occurred for those systems with $\tau/\tau_{MS} \leqslant 0.02$, a prediction which is clearly at odds with the observations.

One process which might be responsible for the subsequent reduction of Ω/ω from ~ 2 to ~ 1, and also for the several values of $\Omega/\omega < 1$ shown in figure 16, is the slow evolutionary expansion of early type main sequence stars. In order to conserve angular momentum, the star's rotation rate must decrease as the star expands - even below the synchronous rate, if the tidal interactions are too weak to transfer sufficient angular momentum from the orbital motion to compensate. Olson (1968) has already speculated that this effect might be operating, based on a correlation between values of $\Omega/\omega < 1$ and low stellar surface gravities. Zahn (1977, fig. 3) included this expansion in a calculation of the rotational evolution of a 15 $M_\odot$ star, and showed it to be quite important, especially in the latter stages of the star's main sequence lifetime. We shall have cause to return to this matter presently.

Besides the inevitable processes of tidal interaction and evolutionary expansion, other factors may control the rotational evolution of the components of some close binaries. About 40% of the systems listed in Table VI are classified as semi-detached binaries, i.e., systems in which one component (usually the secondary, dimmer star)

fills its Roche lobe and is transferring mass to the other component (usually a main sequence star). This transfer of mass must be associated with a transfer of angular momentum, which probably serves to spin-up at least the surface layers of the mass-gaining component (Plavec, 1970). This latter component is usually the more massive and the brighter of the two stars, and is the one whose rotational velocity is most commonly measured.

Of the 6 clearly non-synchronous stars shown in figure 16, RZ Sct, RS Vul, RY Per, and U Cep all represent the primaries of such semi-detached systems. The same is true of AW Peg, for which $\tau/\tau_{MS} \simeq 4500$, and which consequently does not appear in figure 16. U Cep, in particular, is well known for the spectroscopic effects which accompany the transfer of mass, and, in light of its period of only 2.49 days and its value of $\tau/\tau_{MS} \simeq 0.02$, is a likely candidate for spin-up due to mass transfer.

The other two stars shown in figure 16 which are clearly non-synchronous, α Cr B and AR Cas, represent the primaries of ordinary detached binaries. The long period (17.4 days) of the former is responsible for the large value of $\tau/\tau_{MS} \simeq 100$ and, as pointed out by Plavec, it is not surprising that it is still in a state of rapid rotation. The primary of AR Cas, on the other hand, has a period of 6.07 days and $\tau/\tau_{MS} \simeq 0.9$ - both comparable to some other synchronous stars, although longer than most. It is quite possible that this is simply a young star whose rotation has not yet been greatly affected by tidal interactions with its small companion.

Finally, we consider the last entry in Table VI, HD 98088, which suggests still another possible influence on rotation rates in certain close binaries. The primary in this system is an A_p star, a member of a group of stars which is very poorly represented in close binaries, but is characterized by slow rotation rates (among other things). The rotational velocity of the star has not been directly measured, but it exhibits spectrum variations which are perfectly synchronous with the orbital period of 5.91 days (Abt, et al [1968]). A stellar magnetic field has been identified (another common property of A_p stars), and its observed strength also varies synchronously with the orbital period. Dynamical tides cannot possibly explain the precise synchronism exhibited by this system. The obvious candidate for a synchronization mechanism in such a system is some form of magnetic braking, which may conceivably act only on the surface layers of the star.

(2) Other binaries

A separate analysis of observational material pertaining to synchronization in binaries has been carried out by Levato (1976), who considered all binary systems with measured stellar rotational velocities, $v_R \sin i$, and $u v b y \beta$ spectral parameters. Since most of the 122 systems considered are not eclipsing, the inclinations and fractional stellar radii are unknown. The measured stars were divided into eight spectral categories, corresponding to the average spectral types B2, B7, A5, and F5 ($\sim$ 11, 5, 2, and 1.3 $M_\odot$, respectively), and, for each spectral type, to "non-evolved" and "evolved" main sequence stars. The boundary between non-evolved and evolved stars was drawn

such as to place approximately equal numbers of stars in each of these two classes. Standard radii were adopted for each category and used, with the orbital period, to calculate the "synchronized velocity" v_s.

Using a loose synchronization criterion of $\Omega/\omega \leq 2$, Levato established a critical period *range* for synchronization for each category. His results are given in Table VII.

TABLE VII

Critical period ranges for synchronization of close binaries (Levato, 1976).

Average spectral type	Critical period range (days)	
	Non-evolved stars	Evolved stars
B2 ($\sim$ 11 $M_\odot$)	4 -7.5	9.5-12.5
B7 ($\sim$ 5 $M_\odot$)	3.5-4.5	4 - 6.5
A5 ($\sim$ 2 $M_\odot$)	2	3 - 4.5
F5 ($\sim$ 1.3 $M_\odot$)	10.5-14.5	9.5-17.5

Comparison of the critical periods for "non-evolved" stars with the theoretical predictions of Table V for $f_{syn} = \frac{1}{2}$ reveals excellent agreement for the first three average spectral types. Stars of mass $\leqslant 1.6\ M_\odot$ (e.g., F5 stars) possess extensive convective envelopes. Zahn (1966, 1977) has shown that tidal energy dissipation by turbulent viscosity in the envelopes of such stars is quite efficient and leads to rapid synchronization, even for orbital periods of the order

of 10 days. The dynamical tide model of synchronization is thus again shown to successfully predict the occurrence of "loose" synchronization (i.e., $\Omega/\omega \leq 2$) in early-type stars which have not yet evolved significantly from their zero age main sequence configurations.

However, when Levato's results for "evolved" main sequence stars are compared with the predictions of Table V, it is apparent that some much more efficient synchronization mechanism is at work. From equation (5.15), we see that an increase of a factor of 2 in the orbital period implies an increase of a factor of 50 in the required synchronization time, all else being equal. Thus the greater average age of the evolved stars does not, by itself, seem to account for the considerably greater critical periods. An obvious candidate for the synchronization mechanism which seems to be so effective in evolved stars is the expansion which accompanies evolution. We have already discussed this expansion in connection with the observations of "tight" synchronization ($\Omega/\omega < 1.5$) and sub-synchronous rotation ($\Omega/\omega < 1$) in eclipsing binaries.

VI. CONCLUSIONS

(1) The investigation of the dynamical tide generated in an early type main sequence component of a close binary, first carried out by Zahn (1975), has been successfully extended to include the most important effects of the stellar rotation. These effects enter through the coriolis term in the equations of motion of the fluid in the stellar interior, and have previously been neglected.

By retaining only the radial component of the rotational angular velocity of the star in the evaluation of this term, it has proved possible to separate the linearized fluid equations in spherical polar co-ordinates, thus considerably simplifying the analysis. The validity of this approximation in the radiative envelope of the star has been demonstrated, but when applied in the convective core, it must introduce some error in the calculated amplitude of the dynamical tide.

(2) The functions which describe the angular dependence of the separated solutions are of the form $\Theta_{mn}(\theta)\, e^{im\varphi}$, where Θ_{mn} is a solution of Laplace's tidal equation. These functions replace the spherical harmonics $P_\ell^m(\theta)\, e^{im\varphi}$, which arise when the coriolis term is completely neglected, and have been previously encountered in the study of oceanic and atmospheric oscillations on rotating planets. The equations governing the radial dependence of the dynamical tide are unchanged by the inclusion of the coriolis term, except for the appearance of an eigenvalue K_{mn} which replaces the constant $\ell(\ell+1)$.

(3) Each temporal Fourier component of the tidal potential, $U_{\ell}^{m}(r,\theta)e^{i(m\varphi+\sigma_m t)}$, excites a response which is composed of many different modes of oscillation, corresponding to $n = \pm m, \pm(m+1), \pm(m+2), \ldots$. The amplitudes of these excited modes are controlled by the projection coefficients $\mathscr{C}_n$, the most important modes corresponding to small, positive, even values of n. A rapid decrease of these coefficients as the rotation of the star approaches the synchronous state causes a decrease in the energy dissipation rate and, consequently, in the rate of synchronization. This result implies that, in most cases, dynamical tides are incapable of reducing the rotation rate Ω to much less than twice the orbital mean motion ω in the lifetime of the star.

(4) An approximate analytic solution for the radial dependence of the dynamical tide's various modes has been obtained. It is apparent from this solution that the mechanical energy transported by the dynamical tide is generated by the tidal forces acting on the convective core of the star. The radiative envelope is a region of transport through which this energy is carried to the stellar surface in the form of gravity waves. Subject to the validity of the radiation condition applied to this solution, the energy generation and transport rate for the n^{th} mode is given by equations (3.39) and (3.40):

$$\dot{E}_n = \mathscr{L}_n \sigma_{-5}^{11/3} \left[\frac{(1+\bar{k}_2)\mu \mathscr{C}_n}{P^2} \right]^2$$

with

$$\mathscr{L}_n \propto r_e^{5}\, \rho_e^{-1} \left[r(d N_V^2/dr) \right]_{r_e}^{-1/3}$$

The strong dependence of $\mathscr{L}_n$ on r_e, the radius of the core, is a noteworthy feature of this result, and one to which Zahn (1977) has also drawn attention.

(5) Zahn's zero-temperature surface boundary condition has been replaced by a finite temperature stellar atmosphere with $T \geq 2^{-\frac{1}{4}} T_{eff}$. A consequence of this improvement is the result that the gravity waves corresponding to certain of the modes of tidal oscillation are not reflected at the surface of the star, but may propagate outwards until they become non-linear and are damped. The eventual dissipation of the mechanical energy transported outwards by these modes is thus ensured, and is not dependent on the efficiency of radiative damping, as was stated by Zahn (1975, 1977).

(6) An extensive series of numerical solutions for a 5 $M_\odot$ star have been carried out to complement and check the validity of the analytic solution. The analytic expression for $\mathscr{L}_n$ is found to be accurate to better than a factor of 2, except for small values of the eigenvalue K_{mn}. As predicted, $\mathscr{L}_n$ is almost independent of the tidal frequency σ.

(7) These numerical results have been used to investigate the rotational evolution of a 5 $M_\odot$ star in a close binary system, and to determine the time constant τ for the synchronization process. With the aid of the analytic expression for the parameter $\mathscr{L}_n$, the results have been extrapolated to other early type stars to give (equation

[5.23])

$$\tau \simeq 1.5 \times 10^{6} \left(\frac{M_1}{M_\odot}\right)^{-4.25} P^{17/3} \mu^{-2} \text{ yr.}$$

This expression is valid over the stellar mass range $2M_\odot \leq M_1 \leq 10\ M_\odot$, and possibly for larger masses. Predicted synchronization times are strongly dependent on the adopted criterion for synchronization, but for spin-down from $\Omega/\omega = \infty$ to $\Omega/\omega = 2$ are about a factor of 10 shorter than those calculated by Zahn (1977).

(8) The strong dependence of τ on the orbital period P suggests the existence of well-defined "critical orbital periods", P_{crit}, such that the components of most binaries satisfying $P < P_{crit}$ exhibit synchronous rotation. For the synchronization criterion $\Omega/\omega \leq 2$, the predicted critical periods range from 2.5 days (2 $M_\odot$ primary) to 4.3 days (10 $M_\odot$ primary). Tighter synchronization criteria (e.g., $\Omega/\omega \leq 1.5$) imply considerably longer synchronization times and correspondingly smaller critical periods.

Observations of the rotational velocities of early type components of eclipsing binaries are in general agreement with the predicted synchronization times and critical periods for the criterion $\Omega/\omega \leqslant 2$, but in many cases the observed synchronism between rotational and orbital periods is considerably better than expected. More extensive data concerning the projected rotational velocities of spectroscopic binaries, although somewhat corrupted by the inclination effect and by uncertain stellar radii, suggest critical periods for unevolved early type main sequence stars which agree quite well

with the predicted values (again for the criterion $\Omega/\omega \leqslant 2$). However, for somewhat evolved early type main sequence stars, the same study indicates much greater critical periods.

Considerable support for the basic hypothesis of some sort of tidal mechanism for rotational synchronization in close binaries is provided by the very existence of such critical periods. This follows from the strong dependence of the tidal potential on the period: $U \sim a^{-3} \sim P^{-2}$. The present specific model of tidal synchronization for early type stars, *viz.*, the dissipation of mechanical energy transported through a star by the dynamical tide, does successfully predict the time scales, and the corresponding critical periods, for spin-down from a state of rapid rotation to a state in which $\Omega/\omega \sim 2$.

Further reduction in the rotational angular velocity due to the dynamical tide proceeds very slowly because of the rapidly diminishing values of the projection coefficients (see [3] above). It is concluded, therefore, that while the dynamical tide model adequately describes the initial stages of synchronization, an additional mechanism is required to explain both the prevalence of "tight" synchronism ($\Omega \leqslant 1.5\omega$) amongst eclipsing binaries and the much greater critical periods associated with "evolved" main sequence stars. Slow stellar expansion, especially in the later stages of main sequence evolution, may provide this mechanism.

APPENDIX 1

The coriolis force approximation

With the aid of the analytic solutions developed in section 3, and of the WKB solutions of section 2, the validity of approximation (2) made in section 2b is examined. This approximation involved the neglect of the non-radial (or "horizontal") component of the rotational angular velocity in calculating the coriolis force.

We return to the linearized equations of motion (2.8), (2.9), and (2.10), and rewrite them in a schematic form so that the relative sizes of the terms may be ascertained. Vectors $\underset{\sim}{v}$, $\underset{\sim}{\Omega}$, and ∇ are separated into radial (v_r, $\Omega_r = \Omega \cos\theta$, ∇_r) and horizontal (v_H, $\Omega_H = \Omega \sin\theta$, ∇_H) components, as is the momentum equation (2.8). Introducing the characteristic radial and horizontal scales of the perturbed quantities, L_r and L_H, we make the following schematic substitutions:

$$\left.\begin{aligned} \nabla_r(\delta x) &\sim \frac{\delta x}{L_r} \quad , \\ \nabla_H(\delta x) &\sim \frac{\delta x}{L_H} \quad , \\ \frac{\partial}{\partial t}(\delta x) &= i\sigma\,\delta x \quad , \end{aligned}\right\} \qquad \delta x = \delta p,\ \delta\rho, \text{ or } \underset{\sim}{v} \tag{A1.1}$$

and

$$\nabla_r V_0 = g = -\frac{1}{\rho_0}\frac{dp_0}{dr} \sim \frac{p_0}{r\rho_0} \quad , \tag{A1.2}$$

where g is the gravitational acceleration. The momentum equation becomes:

$$\sigma \rho_0 v_r + \frac{\delta p}{L_r} + \frac{p_0 \delta\rho}{r\rho_0} + 2\rho_0 \Omega_H v_H = 0 \quad , \tag{2.8'}$$

and

$$\sigma \rho_0 v_H + \frac{\delta p}{L_H} + 2\rho_0(\Omega_r v_H + \Omega_H v_r) = 0 \quad , \tag{2.8''}$$

where we have dropped the forcing term $\nabla\delta V$. The continuity equation (2.9) takes the form:

$$\sigma \delta\rho + \frac{\rho_0}{r} v_r + \rho_0 \left(\frac{v_r}{L_r} + \frac{v_H}{L_H} \right) = 0 \quad . \tag{2.9'}$$

More care is required with the adiabatic condition (2.10). Noting that

$$\frac{1}{p_0} \frac{dp_0}{dr} - \frac{\Gamma}{\rho_0} \frac{d\rho_0}{dr} \equiv \frac{\Gamma N_v^2}{g} \quad , \tag{A1.3}$$

(2.10) is rewritten schematically as

$$\sigma \left(\frac{\delta\rho}{\rho_0} + \frac{\delta p}{p_0} \right) + \frac{N_v^2}{g} v_r = 0 \quad . \tag{2.10'}$$

In the convective core, $N_v^2 = 0$, and we have

$$\frac{\delta\rho}{\rho_0} \sim \frac{\delta p}{p_0} \quad , \tag{2.10''}$$

but in the envelope $N_v^2/g \sim 1/r$ and this term may not be neglected.

Our objective is to determine whether or not the Ω_H terms in (2.8') and (2.8'') may be safely neglected. To make this decision, it is necessary to use (2.9') and (2.10') to estimate the magnitudes of $\delta\rho$ and v_r in terms of δp and v_H. We consider the envelope and core solutions separately.

a) Envelope scaling

Substituting the WKB solutions for δp and v_r into equation (2.10'), we find

$$\sigma \frac{\delta p}{p_0} \sim \frac{\sigma}{N_v} K_n^{-\frac{1}{2}} \left(\frac{N_v^2}{g} v_r \right) \quad . \tag{A1.4}$$

Since $\sigma/N_v \sim 10^{-2}$ in the envelope, and $K_n > 1$, evidently the $\delta p/p_0$ term is unimportant and (2.10') becomes

$$\frac{\delta \rho}{\rho_0} \sim \frac{N_v^2}{\sigma g} v_r \sim \frac{v_r}{\sigma r} \quad . \tag{2.10'''}$$

Turning now to the continuity equation (2.9'), we observe that the first two terms are comparable and may be combined as one. To extract more information from this equation, we note that

$$L_H \sim K_n^{-\frac{1}{2}} r \leqslant r \tag{A1.5}$$

(from the latitudinal range of the Hough functions: $-f \leqslant \mu \leqslant f$), and that L_r is given by the WKB wavelength (2.45):

$$L_r \sim K_n^{-\frac{1}{2}} \frac{\sigma}{N_v} r \sim 10^{-2} L_H \quad . \tag{A1.6}$$

Consequently $v_r/r \ll v_r/L_r$ and (2.9') becomes

$$v_r \sim \frac{L_r}{L_H} v_H \sim 10^{-2} v_H \quad ; \tag{A1.7}$$

i.e., the two velocity components scale linearly with the corresponding characteristic length scales.

Armed with this result, we see immediately that the Ω_H term in the horizontal momentum equation (2.8") may indeed be neglected in

comparison with both the Ω_r coriolis term (except for $\theta \simeq \pi/2$) and the inertial term $\sigma\ \rho_0\ v_H$. The latter follows from the fact that, for tidally induced oscillations, $\sigma \sim \Omega$. It is thus apparent that these two comparable large terms must be balanced by the pressure term $\delta p/L_H$:

$$\delta p \sim \sigma\ L_H\ \rho_0\ v_H \quad . \tag{A1.8}$$

We are now equipped to analyze the radial momentum equation (2.8'), which takes the following form when expressions (2.10"'), (A1.7), and (A1.8) are substituted for $\delta\rho$, v_r, and δp:

$$\sigma\ \rho_0\ v_H \left[\frac{L_r}{L_H} + \frac{L_H}{L_r} + \left(\frac{p_0}{\sigma^2 \rho_0 r^2}\right)\ \frac{L_r}{L_H} + \frac{2\Omega_H}{\sigma}\right] = 0 \tag{A1.9}$$

It has been shown previously (see equation [2.37] and discussion following) that $p_0/\sigma^2\rho_0 r^2 \gg 1$, so that the third term, which represents the vertical gravitational acceleration, may not be neglected despite the factor of L_r/L_H. However, in comparison with the second (vertical perturbed pressure gradient) term, both the first (inertial) and fourth (Ω_H coriolis) terms may be neglected. Thus the vertical momentum equation is seen to reduce essentially to an equation of hydrostatic equilibrium in the stellar envelope, and we have shown that the coriolis terms due to Ω_H may be safely neglected in both the horizontal and radial momentum equations.

b) Core scaling

In the core, $\delta\rho$ is given by (2.10") and the discussion is somewhat simplified. The horizontal scale is again given by

$$L_H \sim K_n^{-\frac{1}{2}} r \quad , \tag{A1.5}$$

but, since the analytic core solutions are non-oscillatory, the radial scale is not small. Noting that $\delta p \sim r^{\nu}$ and $v_r \sim r^{\nu-1}$, with $\nu(\nu+1) = K_n$, we take

$$L_r \sim \frac{r}{\nu} \sim K_n^{-\frac{1}{2}} r \sim L_H \quad . \tag{A1.10}$$

As $\delta\rho$ is given in terms of δp rather than v_r in the core, we next consider the horizontal momentum equation (2.8") to obtain an estimate for δp. Noting that $\sigma \sim \Omega_r \sim \Omega_H$, and assuming that the three terms involving these quantities do not cancel one another, we obtain

$$\delta p \sim \sigma \, L_H \, \rho_0 \, v \quad , \tag{A1.11}$$

where v represents the larger of v_r and v_H.

Substitution of this expression for δp in equation (2.10") for $\delta\rho$ yields an estimate for the first term in the continuity equation (2.9'):

$$\sigma \delta\rho \sim \left(\frac{\sigma^2 \rho_0 r^2}{p_0} \right) \frac{L_H}{r^2} \, \rho_0 v \quad . \tag{A1.12}$$

By equation (2.37), the quantity in parentheses is small, and $L_H/r^2 \sim K_n^{-\frac{1}{2}}/r \sim (K_n L_H)^{-1}$, so this term may again be neglected in comparison

with the other terms in the continuity equation. However, since $L_r \sim L_H \sim K_n^{-\frac{1}{2}} r$ in the core, we must now conclude from the continuity equation that

$$v_r \sim v_H \tag{A1.13}$$

in contrast to the result (A1.7) which holds in the envelope. Therefore, all three velocity terms in the horizontal momentum equation are comparable, including the Ω_H coriolis term.

Furthermore, substitution of expressions (2.10") and (A1.11) for $\delta\rho$ and δp into the vertical momentum equation (2.8') reveals that all four terms in this equation are of order $\sigma\rho_0 v_r \sim \sigma\rho_0 v_H$, including the Ω_H coriolis term. Equation (2.8') evidently does *not* reduce to a requirement of hydrostatic equilibrium in the core, as it does in the envelope. By definition, if the core is unstable to convective motions, it cannot support stable quasi-hydrostatic vertical oscillations. An equivalent statement is that the Brunt-Väisälä frequency goes to zero in the convective core.

An accurate solution for the dynamical tide in the core must thus include the Ω_H coriolis terms, and in consequence is not separable in spherical polar co-ordinates.

APPENDIX 2

The separation of the fluid equations

The linearized vector equations (2.8), (2.9), and (2.10), which describe the motion of the fluid in the star under the influence of the perturbing potential δV, are here separated in spherical polar co-ordinates. The final result is the set of scalar ordinary differential equations (2.17), (2.18), and (2.19). The two assumptions listed in section 2b are used, namely (1) that the equilibrium state of the star is spherically symmetric, and (2) that only the radial component of $\underset{\sim}{\Omega}$ is retained in calculating the coriolis force, i.e., $\underset{\sim}{\Omega} = \Omega_r \hat{e}_r$. The temporal and longitudinal dependence of all perturbed quantities is written as $e^{i(\sigma t+m\varphi)}$, where we have set $\sigma_m = \sigma$.

With the introduction of the variable $\underset{\sim}{h}$ (the vector displacement) defined by $\underset{\sim}{v} = i\sigma\underset{\sim}{h}$, and replacing all time derivatives by $i\sigma$, the linearized equations become:

$$-\sigma^2\rho\underset{\sim}{h} = -\nabla\delta p - \delta\rho\nabla V_0 - 2i\sigma\rho_0(\underset{\sim}{\Omega}\times\underset{\sim}{h}) - \rho_0\nabla\delta V \quad , \tag{A2.1}$$

$$\delta\rho = -\nabla\cdot(\rho_0\underset{\sim}{h}) \tag{A2.2}$$

and

$$\frac{1}{p_0}(\delta p + h\, p_0') = \frac{\Gamma}{\rho_0}(\delta\rho + h\,\rho_0') \tag{A2.3}$$

In (A2.3) we have introduced the scalar $h \equiv (\underset{\sim}{h})_r$ and the primes to denote derivatives with respect to r.

After some manipulation, which makes use of the assumed purely radial nature of the vectors ∇V_0 and $\underset{\sim}{\Omega}$, equation (A2.1) may be rearranged to take the explicit form:

$$\sigma^2 \rho_0 \underset{\sim}{h} = \nabla \delta p + \delta\rho \nabla V_0 + \rho_0 \nabla \delta V$$

$$+ (\sigma^2 - 4\Omega_r^2)^{-1} \left[2i\sigma \underset{\sim}{\Omega} \times \nabla_H (\delta p + \rho_0 \delta V) + 4\Omega_r^2 \nabla_H (\delta_p + \rho_0 \delta V) \right] \tag{A2.4}$$

The symbol '∇_H' represents the non-radial component of the ∇ operator. Also, the radial component of (A2.1) is

$$\sigma^2 \rho_0 h = \frac{\partial \delta p}{\partial r} + \rho_0 \frac{\partial \delta V}{\partial r} - \frac{\delta \rho}{\rho_0} p_0' \quad , \tag{A2.5}$$

where ∇V_0 has been replaced by $- p_0'/\rho_0$.

Taking the divergence of (A2.4), making use of (A2.5), and substituting the result into equation (A2.2), we obtain

$$\sigma^2 \delta\rho + \frac{\sigma^2}{r^2} \frac{\partial}{\partial r} (r^2 \rho_0 h) = - \nabla_H^2 \Psi -$$

$$\nabla_H \cdot \left\{ (\sigma^2 - 4\Omega_r^2)^{-1} \left[2i\sigma \underset{\sim}{\Omega} \times \nabla_H \Psi + 4\Omega_r^2 \nabla_H \Psi \right] \right\} \tag{A2.6}$$

where $\Psi \equiv \delta p + \rho_0 \delta V$. We denote the right hand side of this equation by

$$- \frac{1}{r^2} \mathcal{G}(\Psi) \quad ,$$

and note that the operator $\mathcal{G}$ involves only derivatives with respect to the angular co-ordinates θ and φ.

Equation (A2.3) is used to eliminate $\delta\rho$ from (A2.6), which becomes

$$\frac{\sigma^2 \rho_0}{p_0^{1/\Gamma}} \frac{\partial}{\partial r} \left(r^2 p_0^{1/\Gamma} h \right) + r^2 \frac{\sigma^2 \rho_0}{\Gamma p_0} \delta p = - \mathcal{G}(\Psi) \quad . \tag{A2.7}$$

Similarly, (A2.5) becomes

$$p_0^{1/\Gamma} \frac{\partial}{\partial r} \left(p_0^{-1/\Gamma} \delta p\right) - \rho_0(\sigma^2 - N_V^2)\, h = -\rho_0 \frac{\partial \delta V}{\partial r} \quad , \tag{A2.8}$$

where

$$N_V^2 \equiv -\frac{p_0'}{\rho_0} \frac{d}{dr}\left[\ell n \left(p_0^{1/\Gamma}/\rho_0\right)\right] \tag{2.20}$$

These two equations are separable in our spherical polar co-ordinate system. We set

$$\left.\begin{aligned} h(r,\theta,\varphi) &= h_1(r)\, h_2(\theta)\, e^{im\varphi} \quad , \\ \delta p(r,\theta,\varphi) &= \delta p_1(r)\, \delta p_2(\theta)\, e^{im\varphi} \quad , \\ \text{and} \qquad \delta V(r,\theta,\varphi) &= \delta V_1(r)\, \delta V_2(\theta)\, e^{im\varphi} \quad . \end{aligned}\right\} \tag{A2.9}$$

Equation (A2.8) evidently requires that

$$h_2(\theta) = \delta p_2(\theta) = \delta V_2(\theta) \equiv \Theta(\theta) \quad , \tag{A2.10}$$

becoming then the ordinary differential equation:

$$p_0^{1/\Gamma} \frac{d}{dr}\left(p_0^{-1/\Gamma}\, \delta p_1(r)\right) - \rho_0(\sigma^2 - N_V^2)\, h_1(r) = -\rho_0 \frac{d\delta V_1(r)}{dr} \quad .$$

This is the first of our final equations - (2.17).

From (A2.10) we have

$$\Psi(r,\theta,\varphi) = \left[\delta p_1(r) + \rho_0 \delta V_1(r)\right] \Theta(\theta)\, e^{im\varphi} \quad , \tag{A2.11}$$

and

$$\mathcal{G}(\Psi) = \left[\delta p_1(r) + \rho_0 \delta V_1(r)\right] \mathcal{G}(\Theta)\, e^{im\varphi} \quad . \tag{A2.12}$$

Substituting this result in (A2.7), and dividing both sides of the equation by $[\delta p_1 + \rho_0 \delta V_1]\Theta$, we see that (A2.7) does indeed separate to produce the two ordinary differential equations:

$$\frac{\sigma^2 \rho_0}{r^2 p_0^{1/\Gamma}} \frac{d}{dr}\left(r^2 p_0^{1/\Gamma} h_1(r)\right) - \left(\frac{K}{r^2} - \frac{\sigma^2 \rho_0}{\Gamma p_0}\right) \delta p_1(r) = \frac{K}{r^2} \rho_0 \delta V_1(r) \quad ,$$

and

$$\mathcal{G}[\Theta(\theta)] + K\ \Theta(\theta) = 0 \quad , \tag{A2.13}$$

where K is an arbitrary separation constant. The first of these is our final equation (2.18), with $K = K_{mn}$.

The expression $\mathcal{G}[\Theta(\theta)]$ may be written most conveniently in terms of the variable $\mu = \cos\theta$. Setting $\underset{\sim}{\Omega} = \Omega_r \hat{e}_r = (\Omega\mu)\hat{e}_r$, and introducing the constant $f = \sigma/2\Omega$, we obtain the following explicit expression after considerable manipulation:

$$\mathcal{G}[\Theta(\theta)] = f^2 \frac{d}{d\mu}\left(\frac{1-\mu^2}{f^2-\mu^2} \frac{d\Theta}{d\mu}\right) - \frac{f^2}{f^2-\mu^2}\left[\frac{m^2}{1-\mu^2} + \frac{m(f^2+\mu^2)}{f(f^2-\mu^2)}\right]\Theta \quad . \tag{A2.14}$$

Substitution of this result in (A2.13) produces the third of our ordinary differential equations, (2.19).

In general, the solutions of equation (2.19) are singular at $\mu = \pm 1$, i.e., $\theta = 0$ and π, and thus physically unacceptable. However, for a discrete set of values of the arbitrary constant K, which depend on the parameters m and f, the function Θ is bounded for all θ in the range $0 \le \theta \le \pi$. These values are designated $K_{mn}(f)$, with corresponding solutions Θ_{mn}, and are discussed in sections 2c and 2d. The most general, physically acceptable solution to equations (2.8), (2.9), and (2.10) must thus be a sum of solutions of the

form (A2.9):

$$h_m(r,\theta,\varphi) = \sum_n h_{mn}(r)\,\Theta_{mn}(\theta)\,e^{im\varphi} \quad , \qquad \text{(A2.15)}$$

and $$\delta p_m(r,\theta,\varphi) = \sum_n \delta p_{mn}(r)\,\Theta_{mn}(\theta)\,e^{im\varphi} \quad ; \qquad \text{(A2.16)}$$

with $$\delta V_m(r,\theta,\varphi) = \sum_n \delta V_{mn}(r)\,\Theta_{mn}(\theta)\,e^{im\varphi} \quad . \qquad \text{(A2.17)}$$

Equations (2.14) and (2.15) of section 2b are just (A2.16) and (A2.15). If the functions Θ_{mn} form a complete set on $0 \le \theta \le \pi$ (see section 2c), then any arbitrary potential function of the form $f(r)g(\theta,\varphi)$ may be written as (A2.17).

The separation of the linearized equations outlined in this appendix is due to Dr. Peter Goldreich.

APPENDIX 3

Projection Coefficients for $|f| \ll 1$

For $|f| \ll 1$, Hough functions of the first class take the approximate form (Longuet-Higgins, 1967):

$$\Theta_{m\nu}(\theta) \simeq A_\nu \left(\frac{d}{d\mu} + \frac{m\mu}{f} \right) e^{-\eta^2/2} H_\nu(\eta) \qquad \text{(A3.1)}$$

$$\nu = 0, 1, 2, \ldots \quad ,$$

where $\eta \equiv (K/f^2)^{\frac{1}{4}}\mu$, $H_\nu(\eta)$ is an Hermite polynomial, and A_ν is a normalization constant. The corresponding eigenvalues $K_{m\nu}$ are given by

$$K_{m\nu} \simeq \frac{(2\nu+1)^2}{f^2} \quad , \qquad \text{(A3.2)}$$

so

$$\eta_\nu \simeq (2\nu+1)^{\frac{1}{2}}\, \mu/|f| \quad . \qquad \text{(A3.3)}$$

From (A3.1) and (A3.3) it is apparent that the Hough functions are essentially confined to the region

$$-(2\nu+1)^{-\frac{1}{2}}|f| < \mu < (2\nu+1)^{-\frac{1}{2}}|f| \quad ,$$

which is a narrow equatorial band for small values of $|f|$.

The index ν is related to the usual Hough function index n by the relations

$$\begin{array}{lll} f > 0: & \left\{ \begin{array}{ll} n = -m & \text{for } \nu = 0 \\ n = m + \nu - 1 & \text{for } \nu = 1,2,3,\ldots \end{array} \right. ; \\ f < 0: & n = m + \nu + 1 \quad \text{for } \nu = 0,1,2,\ldots \quad . \end{array} \qquad \text{(A3.4)}$$

As may be seen from figure 1, which corresponds to $m = 2$, the $\nu = 0$ Hough function for $f > 0$ actually belongs to the second class of solutions to Laplace's tidal equation.

The projection coefficients are defined by equation (2.34):

$$\mathscr{C}_n = \int_{-1}^{1} \overline{P_2^2}(\mu)\ \Theta_{2,n}(\theta)\ d\mu \qquad , \quad n = 2,4,6,\ldots$$

when $\Theta_{2,n}$ is normalized by (2.30):

$$\int_{-1}^{1} \left[\Theta_{2,n}(\theta)\right]^2 d\mu = 1 \qquad .$$

Applying this normalization condition, we obtain

$$A_\nu = \left[\frac{f}{(2\nu+1)^{3/2}\ \pi^{1/2}\ 2^{\nu-1}\ \nu!}\right]^{1/2} \qquad . \tag{A3.5}$$

Substitution of expression (A3.1) for $\Theta_{m\nu}$ into the equation for the projection coefficients, and a subsequent integration by parts, leads to the result

$$\mathscr{C}_n \simeq A_\nu \left(\frac{15}{16}\right)^{1/2} \frac{f(m+2f)}{2\nu+1} \int_{-\infty}^{\infty} \eta\ H_\nu(\eta)\ e^{-\eta^2/2}\ d\eta \quad , \tag{A3.6}$$

$$\text{with} \quad \begin{cases} m = 2 \\ \nu = n - 1 \\ 0 < f \ll 1 \end{cases} \qquad .$$

A second term in the expression for $\mathscr{C}_n$ has been neglected, as it is smaller by a factor of $\sim f$.

The above integral has been evaluated for n = 2,4, and 6:

$$\int_{-\infty}^{\infty} \eta\ H_1(\eta)\ e^{-\eta^2/2}\ d\eta = 2\sqrt{2\pi} \qquad ,$$

$$\int_{-\infty}^{\infty} \eta_1 \, H_3(\eta_1) \, e^{-\eta_1^2/2} \, d\eta_1 = 12\sqrt{2\pi} \quad ,$$

$$\int_{-\infty}^{\infty} \eta_1 \, H_5(\eta_1) \, e^{-\eta_1^2/2} \, d\eta_1 = 120\sqrt{2\pi} \quad ;$$

to produce the projection coefficients

$$\mathscr{C}_2 \simeq \frac{\sqrt{30}\,(3\pi)^{1/4}}{9} \, f^{3/2}(1+f)$$

$$= 1.066 \, f^{3/2}(1+f) \quad ,$$

$$\mathscr{C}_4 \simeq \frac{3\sqrt{5}\,(7\pi)^{1/4}}{49} \, f^{3/2}(1+f)$$

$$= 0.296 \, f^{3/2}(1+f) \quad ,$$

and

$$\mathscr{C}_6 \simeq \frac{15\,(11\pi)^{1/4}}{242} \, f^{3/2}(1+f)$$

$$= 0.150 \, f^{3/2}(1+f) \quad .$$

These three expressions are plotted as the solid curves in figure 3. The derivation of equation (A3.6) is due to Dr. Peter Goldreich.

REFERENCES

Abramowitz, M. and Stegun, L.A. (1970): (Editors) Handbook of Mathematical Functions, U.S. National Bureau of Standards.

Abt, H.A., Conti, P.S., Deutsch, A.J., and Wallerstein, G. (1968): Astrophys. J. 153, 177.

Allen, C.W. (1973): Astrophysical Quantities, 3rd edition, University of London, Athlone Press.

Batten, A.H. (1967): Pub. Dominion Astrophys. Obs. 13, 119.

Chandrasekhar, S. (1933): Mon. Not. R.A.S. 93, 390, 449.

Chapman, S. and Lindzen, R.S. (1970): Atmospheric Tides, Gordon and Breach, New York.

Cowling, T.G. (1941): Mon. Not. R.A.S. 101, 367.

Cox, J.P. and Giuli, R.T. (1968): Principles of Stellar Structure, Gordon and Breach, New York.

Eckart, C.H. (1960): Hydrodynamics of Oceans and Atmospheres, Pergamon Press, Oxford, New York.

Flattery, T.W. (1967): Hough Functions, Ph.D. thesis, University of Chicago.

Hough, S.S. (1898): Phil. Trans. Roy. Soc. London (A) 191, 139.

Koch, R.H., Olson, E.C., and Yoss, K.M. (1965): Astrophys. J. 141, 955.

Kopal, Z. (1959): Close Binary Systems, John Wiley and Sons, New York.

Levato, H. (1976): Astrophys. J. 203, 680.

Longuet-Higgins, M.S. (1967): Phil. Trans. Roy. Soc. London (A) 262, 511.

Olson, E.C. (1968): Pub. Astron. Soc. Pacific 80, 185.

Plavec, M. (1970): in Stellar Rotation , A. Slettebak (ed.), D. Reidel, Dordrecht-Holland.

Zahn, J.-P. (1966): Ann. Astrophys. 29, 313, 489, 565.

Zahn, J.-P. (1975): Astron. Astrophys. 41, 329.

Zahn, J.-P. (1977): Astron. Astrophys. 57, 383.

PART 2

THE RINGS OF URANUS: RESULTS OF THE 1978 APRIL 10 OCCULTATION.

P. D. Nicholson

S. E. Persson

K. Matthews

P. Goldreich

G. Neugebauer

To be published in the Astronomical Journal, October 1978.

I. INTRODUCTION

The Uranus ring system was discovered on 1977 March 10, by Elliot, et al. (1977), during observations of an occultation by the planet of the star SAO 158687 ($V \sim 8.8$). Other observers obtained less complete data, but nevertheless confirmed the existence of four narrow ($\leqslant 10$ km) essentially circular co-planar rings, christened α, β, γ, and δ, and the wider (~ 100 km) non-circular or inclined ϵ ring (Millis, Wasserman, and Birch 1977; Bhattacharyya and Kuppuswamy 1977a; Churms 1977; Zellner 1977; Mahra and Gupta 1977). Subsequently, Elliot et al. (1978) have identified four more rings: η, 4, 5, and 6. On 1977 December 23, Millis and Wasserman (1978) observed a partial occultation by the ring system of BD-15°3969 ($V = 10.4$). Despite poor observing conditions near dawn, they detected and timed occultations by the ϵ, δ, γ, and (possibly) α rings on one side of the planet.

Predictions of further occultations by the Uranian system were made by Klemola and Marsden (1977). This paper reports observations of the events of 1978 April 4 and 10, designated #4 and #5 respectively by Klemola and Marsden (1977). Both observations were made at a wavelength of 2.2 μm, where a strong methane band greatly depresses the reflected light from the planet. Table I gives the V and 2.2 μm magnitudes of Uranus and the two

stars[1].

The results from the 1978 April 10 occultation are the main subject of this paper. The 1978 April 4 occultation yielded little meaningful data on the rings.

TABLE I

Magnitude of Uranus and Occulted Stars

Object	Magnitude	
	V	[2.2 μm]
Uranus	5.5	12.9 ± 0.2[1]
Star #4	13.4[2]	11.9
Star #5	11.6[2]	10.1

1) See footnote 1.

2) Liller (1977).

[1]On 1978 January 8, the 2.2 μm magnitude of Uranus was measured to be 12.9 ± 0.2 with a 5" diameter aperture which excluded any direct contribution by the rings (diameter ~ 8"). Subsequent observations on 1978 May 7 with a 16" aperture gave [2.2 μm] = 11.6 ± 0.2. Joyce et al. (1977), using an unspecified aperture size, have also reported a 2.2 μm magnitude of 11.5 to 12.0 for Uranus. These results suggest that the integrated 2.2 μm magnitude of the ring system is ~ 12.0. If the average effective width of the rings is 90 km, this implies a geometric albedo at this wavelength of 0.025.

II. OBSERVATIONS

The observations were made using an infrared photometer mounted on the 2.5 m DuPont telescope at Las Campanas Observatory in Chile. A standard K filter (λ_o = 2.20 μm; $\Delta\lambda$ = 0.4 μm) was used with an InSb detector cooled to 55 K. Sky subtraction was performed by chopping at 15 Hz to a secondary beam located 30" to the north.

Star #5 is considerably brighter than the Uranus system (planet + rings) at 2.2 μm: bright enough to give a signal-to-noise ratio of ~ 10 with a time resolution of ~ 0.1 second. The noise was due almost completely to background radiation from the telescope and sky, and it was thus necessary to use a small focal plane aperture centered on the star. An aperture diameter of 7".5 was selected to reduce thermal background noise without introducing noise from guiding and seeing effects. Fortunately, the observing conditions were excellent and the seeing less than 1". The star was centered by finding the half-power points of the 2.2 μm signal one hour before the first ε ring occultation, and centering was maintained thereafter by using an offset guider/Quantex television system. The chopped signal from the detector was demodulated in a conventional lock-in amplifier and recorded on a strip chart, with an overall system time constant of 0.1 second. Absolute timing accurate to <0.3 sec was obtained from WWV.

Star #4 is of comparable brightness to the Uranus system at 2.2 μm, and the signal-to-noise ratio at a time resolution of 0.1 sec was ~ 1. The dawn sky rendered guiding impossible about 10 minutes after planetary emersion.

III. RESULTS

The apparent tracks of the two occulted stars behind Uranus and its rings are shown in Figure 1. For comparison, the 1977 March 10 and 1977 December 23 tracks are shown also. On 1978 April 10 the inclination of the ring plane (assumed to be the satellites' orbit plane) to the sky was 32°.85.

On 1978 April 10, two complementary sets of nine ring occultations were recorded. All of the ring occultations, as recorded on the strip chart, are displayed in Figure 2. Analysis of the data (Section IV (a)) reveals that these nine rings correspond in radius to the nine rings described by Elliot et al. (1978), and they have been identified accordingly. In an initial report of these observations (Persson et al. 1978), the designations θ, ζ and K were used for the rings referred to as 4, 5, and 6 respectively by Elliot et al (1978). To avoid confusion, the terminology of the latter authors is used throughout this paper. Table II gives the times, durations, and fractional depths of the occultations. The depths have not been corrected for the presence of any planetary or ring component in the observed 2.2 μm flux, but this component is ≤ 10% of the total. Relative timing is accurate to ~ 0.1 sec, and absolute timing to < 0.3 sec. Continuous observations were obtained between $5^{hr}09^{min}$ and $7^{hr}05^{min}$ UT, except for ≤ 30 sec gaps at $6^{hr}39^{min}$ and $6^{hr}48^{min}$, but the data do not reveal any further significant occultations which might correspond to those

Fig. 1 - 1977-78 aspect of Uranus and rings. The η ring lies between β and γ, while 4, 5, and 6 are just inside α. The straight lines show the apparent paths of the occulted stars behind the ring system, as they were observed from the various earth stations. The upper track labeled 10 March '77 corresponds to Perth, Western Australia and the lower track to the Kuiper Airborne Observatory.

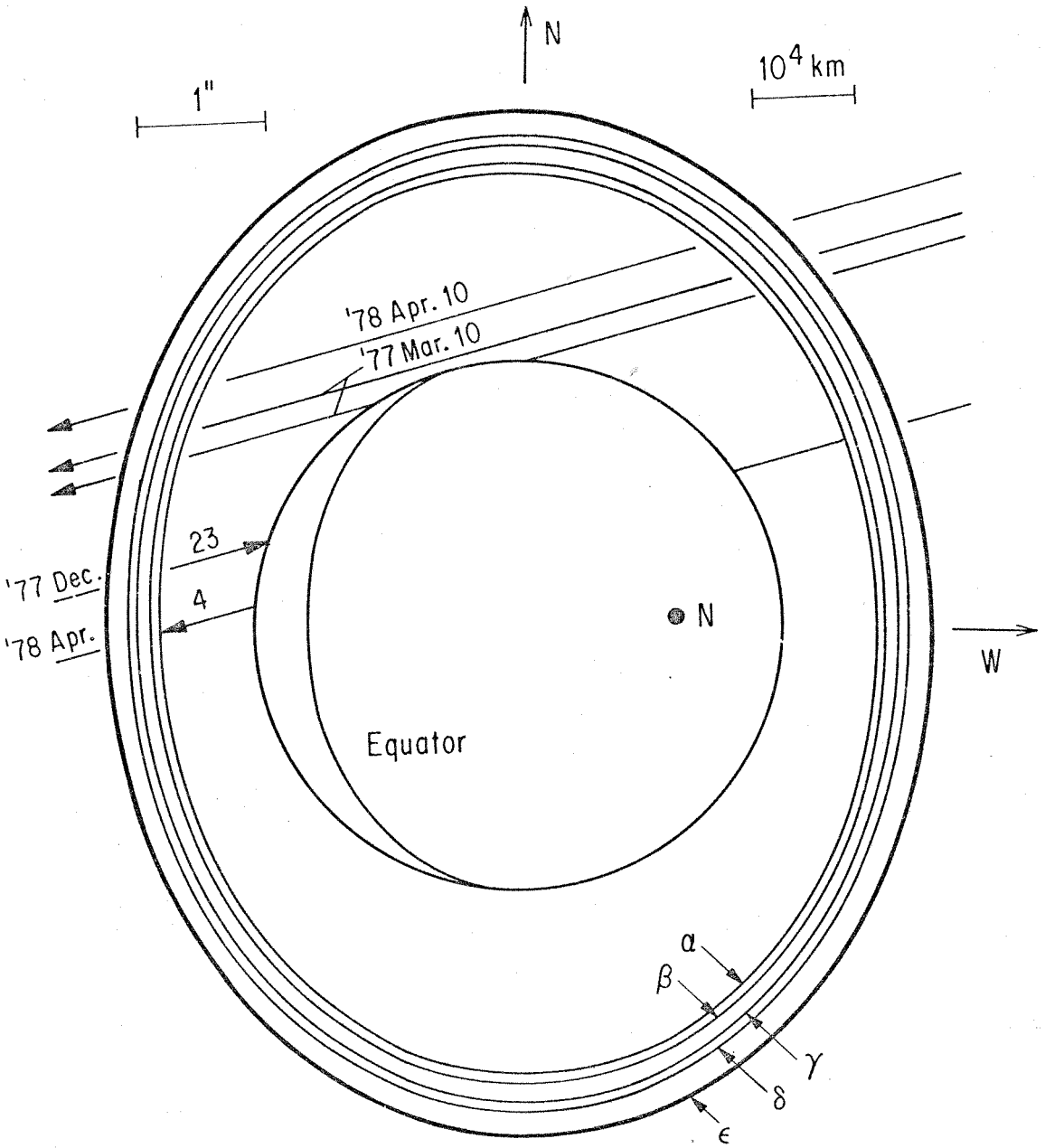
N
1"
10^4 km
'78 Apr. 10
'77 Mar. 10
23
4
'77 Dec.
'78 Apr.
N
W
Equator
α
β
γ
δ
ϵ

Fig. 2 - Excerpts from the strip-chart recording of the 1978 April 10 occultation, showing all identified ring occultations. The time axis of the emersion records has been reversed, so that they may be more readily compared with the immersion records above them. Occultation times, as indicated by the tick marks, are given in Table II. Note that the ϵ ring occultations were, in reality, not symmetrically placed in time with respect to the other occultations.

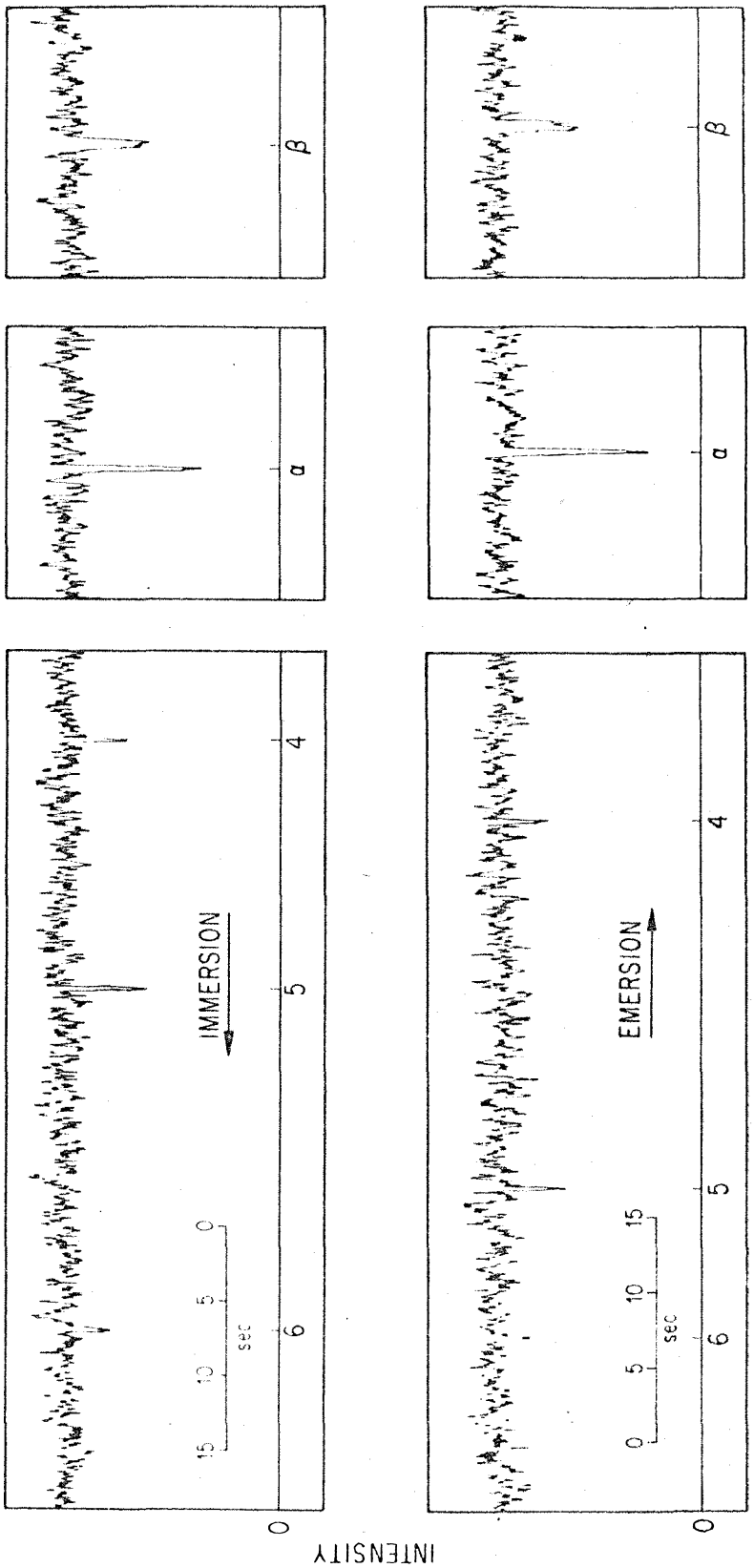
β
α
IMMERSION
EMERSION
sec
INTENSITY

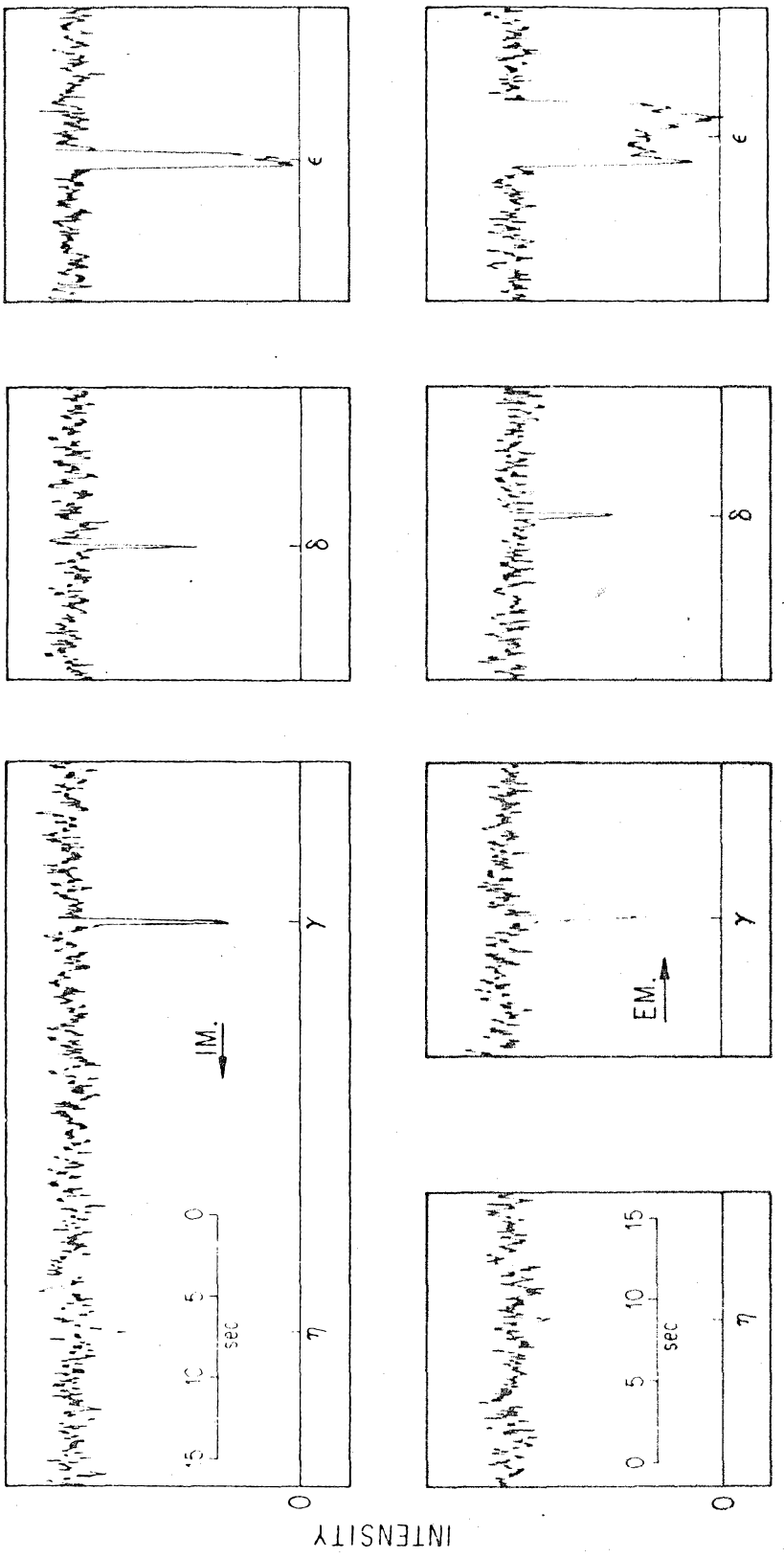
IM.
EM.
sec
sec
INTENSITY
0
0
15
10
5
0
0
5
10
15
η
γ
δ
ε

TABLE II

Ring Occultation Observations

Ring Identification	Immersion			Emersion		
	UT h m s	Duration† (sec)	Fractional Depth of Occultation	UT h m s	Duration† (sec)	Fractional Depth of Occultation
6	5:32:49.6*	0.3*	0.20	6:12:28.5	0.3	0.20
5	5:32:26.5	0.3	0.35	6:12:38.4	0.3	0.35
4	5:32:09.8	0.3	0.25	6:13:03.0	0.3	0.25
α	5:29:57.5	0.5	0.60	6:15:12.2	0.5	0.75
β	5:29:01.4	0.9	0.40	6:16:10.0	0.8	0.40
η	5:27:35.3	0.3	0.20	6:17:35.2	0.3	0.20
γ	5:27:10.3	0.4	0.70	6:18:00.3	0.4	0.75
δ	5:26:32.5	0.3	0.50	6:18:38.0	0.3	0.55
ϵ	5:24:19.0	1.2	0.95	6:21:21.3	4.0	0.6 to 1.0

*Relative uncertainty in times and durations is 0.1 sec.

†Total duration, not FWHM.

reported by Churms (1977) and Millis and Wasserman (1978) during the 1977 March and 1977 December events. The record shows no evidence at the 5% level of any smoothly varying background absorption. No planetary occultation occurred, consistent with the prediction.

On 1978 April 4, a planetary occultation with a duration between half-light points of 44min 48 ± 10 sec occurred at Las Campanas. The mid-point of this event, at $10^{hr}09^{min}50 \pm 10^{sec}$ UT, was 4 min ahead of the prediction by Klemola and Marsden (1977). Only one convincing ring occultation, at $9^{hr}31^{min}00^{sec}$ UT, is identifiable in the very noisy record. This occultation lasted ~ 1 sec and presumably represents the ϵ ring. Guiding became impossible in the dawn twilight before the predicted time of the second ϵ ring occultation. The poor signal-to-noise ratio of the record precludes any useful analysis of the planetary occultation profiles, except perhaps to determine average atmospheric scale heights.

IV. ANALYSIS

a) Overall Ring Geometry

Because only a single set of observations of the 1978 April 10 occultation is available, it is not possible to solve internally for corrections to the star's position or to Uranus' ephemeris, and hence perform an independent calculation of ring radii, etc. However, if the γ and δ rings are, in fact, circular, as suggested by the 1977 March occultation (Elliot et al., 1978), then their known radii can be used to solve for the position of the star relative to the path of Uranus across the sky.

As a check on the assumption of circularity, the mid-time for each pair of ring occultations is given in Table III: a set of concentric circles (or similar, aligned central ellipses) with a common inclination should all exhibit the same mid-time Evidently, the γ and δ rings satisfy this requirement to the accuracy of the timing measurements; consequently they define the adopted mid-time of $5^{hr}52^{min}35.25^{sec}$ UT. We make the plausible assumption that these two rings are both coplanar and circular. The mid-times of the α and β rings are measurably different from the adopted value, indicating either departures of $\geq$ 10 km from circularity, or small inclinations relative to γ and δ. Of the remaining five rings, only η exhibits a mid-time consistent with both circularity and zero relative inclination. For the remainder of the analysis, we shall,

TABLE III

Mid-times and Close-approach Distances

Ring	Occultation Mid-time (UT) h m s		Assumed Radius (km) (Elliot et al., 1978)	Close Approach Distance (km)	
6	5:52:39.0 ± 0.1*				
5	:32.4				
4	:36.4				
α	:34.8		44,844	31,018 ± 3	
β	:35.7		45,799	30,988	average = 30,985
η	:35.2				
γ	:35.3	†	47,746	30,985	
δ	:35.2		48,423	30,981	
ε	:50.1				

* Relative uncertainty

† Adopted mid-time = 5:52:35.25

however, assume that all of the rings are coplanar (though not necessarily circular), and furthermore, that they lie in the common orbital plane of Uranus' five satellites.

From Earth-Uranus geometry as given in the American Ephemeris and Nautical Almanac, together with mean radii for the α, β, γ, and δ rings calculated by Elliot et al. (1978) from the 1977 observations, and the timing data in Table II, the projected close-approach distance of the center of each ring to the star is determined. The adopted topocentric velocity of Uranus, projected on the sky, is 20.056 km/sec. The results are given in the fourth column of Table III. The consistency of the results for β, γ, and δ shows that our observations of these three rings are consistent with their mean radii as determined by Elliot, et al. (1978). The discrepant result for the α ring suggests that it departs from circularity by at least 40 km.

Finally, the average close-approach distance of 30,985 km defined by the β, γ, and δ rings is used with the timing data to calculate the positions in the ring plane of all of the occulting ring segments. The results are given in Table IV. The last two columns of Table IV give, for comparison, the mean radii derived by Elliot et al. (1978). It is emphasized that our absolute radii depend, through the close-approach distance, on the radii of β, γ, and δ adopted by these workers. Any systematic error in these adopted radii will thus also be present in the radii in Table IV. The ring widths are discussed in section IV (b).

TABLE IV

Ring Radii, Azimuths, and Radial Widths

Ring	West Side			East Side			Mean Radius (Elliot et al., 1978)	
	Radius (km)	Azimuth	Width (km)	Radius (km)	Azimuth	Width (km)	West Side	East Side
6	42,002±4	53°.16±0°.01	~5	42,123±4	137°.21±0°.01	~5	42,017	41,943
5	42,370	52°.61	~5	42,280	137°.44	~5	42,415	42,304
4	42,638	52°.22	~5	42,675	138°.02	~5	42,683	42,643
α	44,827	49°.28	9	44,814	140°.88	9	44,834	44,867
β	45,789	48°.12	16	45,805	142°.08	14	45,807	45,780
η	47,299	46°.44	~5	47,299	143°.74	~5	47,323	47,322
γ	47,745	45°.97	7	47,747	144°.22	7	47,747	47,745
δ	48,425	45°.28	~5	48,425	144°.91	~5	48,425	48,421
ε	50,881	42°.98	21	51,439	147°.69	72	51,703	51,056

Radius calculated in orbital plane of satellites, assuming close-approach distance of 30,985 km. Azimuth measured in a prograde direction from ascending node of ring on Earth equator of date. Widths are radial, assuming zero thickness, and are not corrected for diffraction and instrumental response time.

As indicated in section III, a comparison of the radii in Table IV shows that the nine rings observed on 1978 April 10 may indeed be identified with the nine rings reported by Elliot et al. (1978). However, the large variation in radii for rings 6 (180 km) and 5 (135 km) compared with their mutual separation of 300 to 400 km throws some doubt on their existence as two complete rings, rather than as a collection of incomplete arcs. Aside from the well-known α, β, γ, δ and ϵ rings, rings 4 and 5 have also been reported by Millis et al. (1977), and rings η, 4, and 5 by Bhattacharyya and Bappu (1977) (as their spikes #4, 5, and 6 respectively).

Radii calculated for rings 4 and α differ by up to 45 and 53 km respectively, suggesting eccentricities $e \geqslant 0.0005$, or equivalent small relative inclinations. The β ring shows a somewhat smaller range in radius of 27 km ($e \geqslant 0.0003$), while the γ and δ rings are essentially circular. All of these results are quite consistent with the conclusions of Elliot et al. (1978). However, the η ring has appeared circular on both 1977 March 10 and 1978 April 10, but with radii differing by $\sim$ 23 km. Elliot et. al. (1978) have also reported a width of $\sim$50 km for this ring, at variance with our estimate of $\leq$5 km (see IV(b)). The ϵ ring is discussed separately in section IV(d).

The apparent path of the star projected on the ring plane had a minimum radius of $\sim$ 31,000 km ($\sim$5,000 km above the planet's

atmosphere) and maximum radii of 69,400 km on the west side and 107,500 km on the east side. For comparison, the innermost known satellite, Miranda, has a semi-major axis of 130,000 km, and Uranus' Roche limit lies at ~ 70,000 km.

The analysis of the single 1978 April 4 ring occultation is deferred to section IV(c).

b) Ring Widths and Profiles

The observed radial widths of the ring segments projected onto the satellite orbital plane are given in Table IV. These widths have not been corrected for any of the following important broadening mechanisms:

(1) finite time resolution of the system electronics (equivalent to $\sim$ 2 km);

(2) diffraction of starlight around the edges of the rings (Fresnel scale $\sim$ [λ (distance from Earth to Uranus)]$^{1/2}$ = 2.4 km);

(3) finite angular diameter of the star (equivalent to $\sim$ 0.6 km at Uranus, as estimated from the B-V color and V magnitude given by Liller (1977)).

To examine the effect of (1) and (2), the dominant factors for this occultation, the model profile shown in Figure 3 was computed. The model consists of an opaque ring 5 km wide, whose observed profile is modified by diffraction at a wavelength of 2.2 μm and smoothed with an exponential time constant of 0.1 sec. No correction for the 0.4 μm spectral bandwidth of the observations has been included. This model profile, with a width of 8 km and a relative depth of 0.85, is a reasonable representation of the α, γ, and δ profiles if allowance is made for some variation in true widths and opacities. Millis and Wasserman (1978)

Fig. 3 - Theoretical 2.2 μm occultation profile of a 5 km wide opaque ring at the distance of Uranus. The profile was obtained by computing the appropriate Fresnel diffraction pattern, assuming an infinitely distant point source of starlight, and passing this spatial pattern at a velocity of 18 km/sec through a filter with an exponential time constant of 0.1 second. This filter approximately simulates the response of the system electronics.

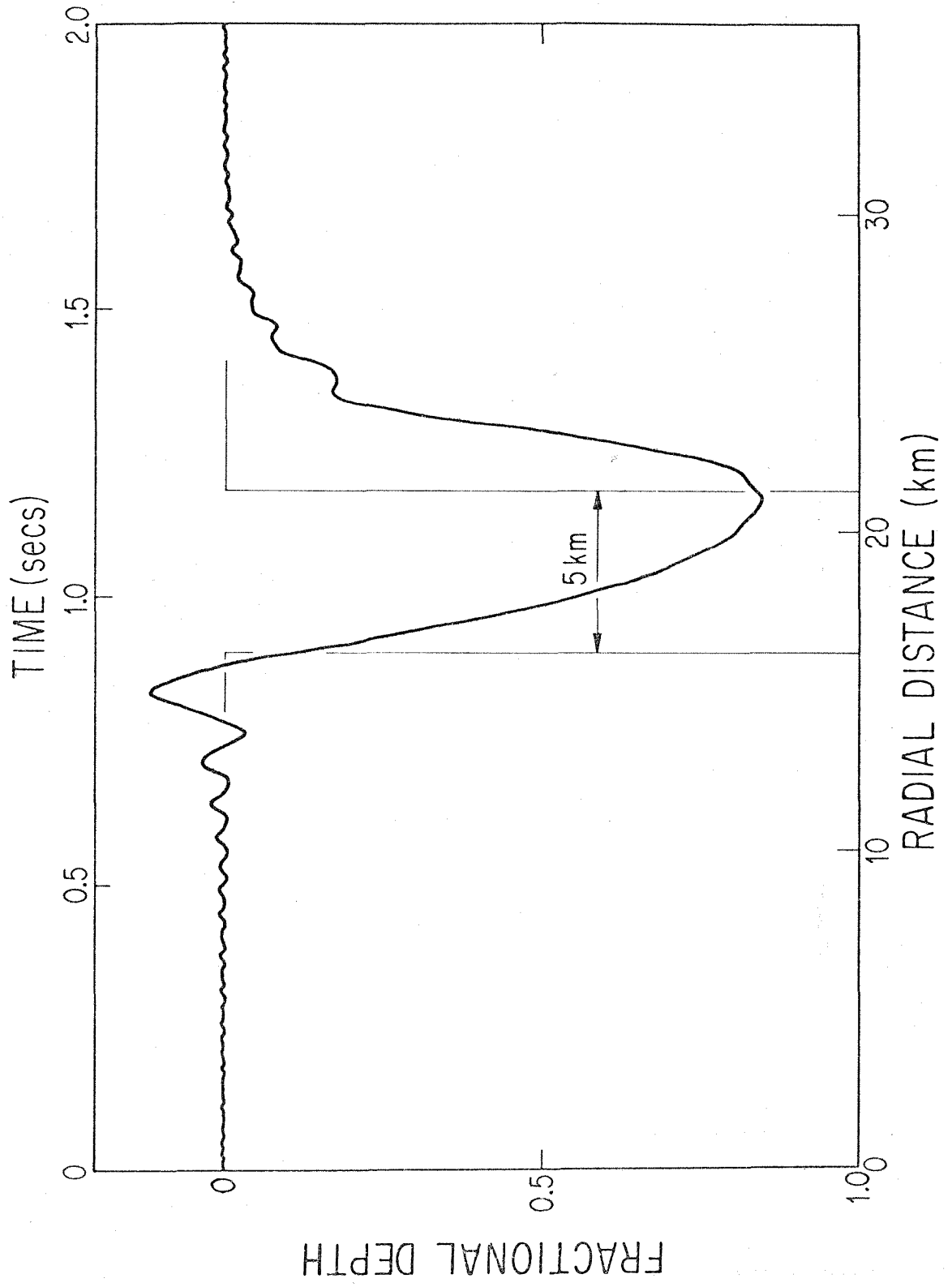
TIME (secs)
0
0.5
1.0
1.5
2.0
5 km
RADIAL DISTANCE (km)
0
10
20
30
FRACTIONAL DEPTH
0
0.5
1.0

reported apparent widths of ~ 8 km for γ and δ in 1977 December, broadened largely by the effects of diffraction at λ = 0.86 μm (~ 1.5 km) and the stellar diameter (~ 1 km at Uranus).

The β ring is clearly resolved in the 1978 April 10 data (see Figure 2), and has an intrinsic width of ~ 15 km. This is consistent with Millis et al.'s (1977) measurement of ~ 1.5 sec for the duration of the β occultation on 1977 March 10. Elliot et al.'s (1977) estimates of ~ 1 sec (implying ~ 10 km width) for the α, β, γ, and δ occultation durations were severely affected by the comparatively large angular diameter (~ 6 km at Uranus) of SAO 158687. This large size does, however, place a useful lower limit of ~ 2 km on the width of any ring which obscured a significant fraction of the starlight, as the α, β, γ, and δ rings did.

We conclude that rings α, γ, and δ are probably quite opaque and have widths of 2 to 5 km. The optical depth and width of the β ring are ~ 0.5 and ~ 15 km respectively. The widths of rings η, 4, 5, and 6 evidently lie in the range 0.5 to 5 km, the lower limit being set by the occultation depths and the angular diameter of star #5. Their optical depths are, at present, indeterminate.

The only published observation at odds with these conclusions is Elliot et al.'s (1978) reported width of ~ 50 km for the η ring in 1977 March, already alluded to in IV(a). There is no evidence in Figure 2 for such a broad feature at the location of the η ring.

c) The 1978 April 4 Ring Occultation

The radius of the single ring identified in the 1978 April 4 occultation data can be estimated from the timing observations and an assumed radius of Uranus. The projected topocentric velocity of Uranus relative to star #4 was 18.466 km/sec, which gives a planetary occultation chord of 49,640 ± 190 km. Elliot et al. (1978) determined a radius of 26,200 km for Uranus from the 1977 March 10 occultation. The derived radius of the occulting material is then 50,670 ± 220 km, where the uncertainty represents mainly the 10 sec uncertainty in the mid-time of the planetary occultation. The oblateness of Uranus, which is of the order of 0.01 (Danielson et al. 1972), has been neglected as it introduces corrections to this radius of only ~ 20 km. A radial width of the ring segment of 20 ± 10 km follows from the ~ 1 sec duration of the occultation.

Evidently, these observations refer to the ε ring, and the derived radius and width are reasonably consistent with the observations obtained six days later (at the 1978 April 10 occultation immersion) for a nearby part of that ring.

d) The ε Ring

The most interesting of the rings of Uranus is the outermost ε ring. On 1977 March 10, the two observed segments of this ring exhibited different, well-resolved widths, and, if the ring is coplanar with the others, radii that differed by ~ 700 km (Elliot et al. 1977, 1978). On 1977 December 23, Millis and Wasserman (1978) observed the ε ring to have intermediate width and radius. In this instance, only pre-immersion observations were obtained. The observations on 1978 April 10 now add two more points to this data set, and the noisy 1978 April 4 data provide another, less accurate, point. These six observations of radial width and radius of the ε ring are plotted in Figure 4, and show a linear relation down to a width of ~ 20 km. Any inclination of $\leqslant 10°$ relative to the other rings would not significantly change the calculated widths; neither are the widths appreciably affected by diffraction or the other broadening effects discussed above in section IV(b).

In light of the relation exhibited in Figure 4, the concept of the ε ring as a set of fragmentary circular arcs (e.g., Dermott and Gold 1977) is clearly untenable. Furthermore, it now seems highly unlikely that the apparent variation in radius can be explained by an inclined circular ring (e.g., Millis and Wasserman 1978), since this would require a rather fortuitous combination of varying width around the ring and Earth-Uranus

Fig. 4 - Radial width plotted against radius for the ε ring for the six occultations observed to date. The multiple observations obtained on 1977 March 10 are represented as two average points. The uncertainty of the 1978 April 4 point is discussed in the text. Error limits on the other points are only slightly larger than the points themselves. The radius scale could contain a systematic error of ~ 100 km.

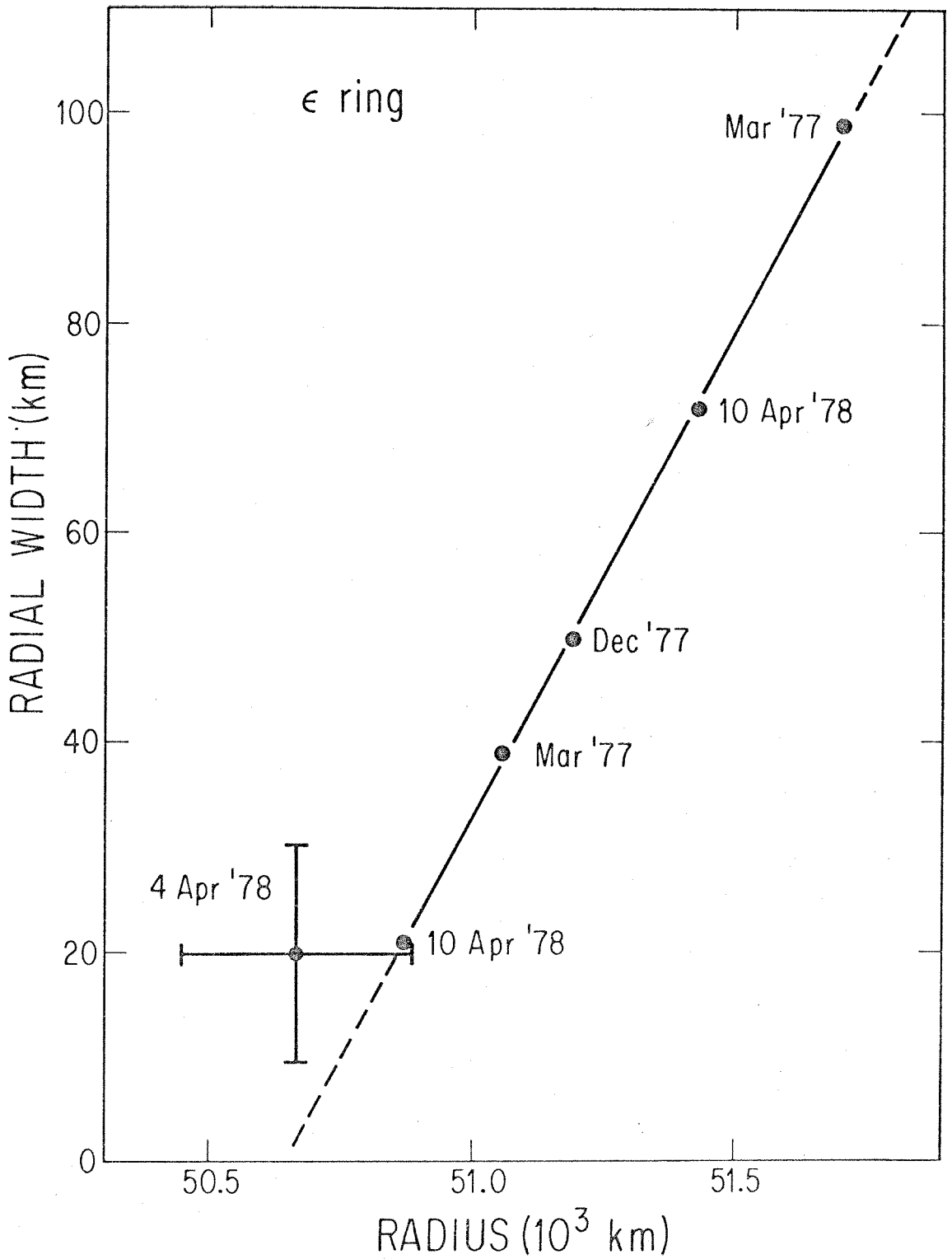
ϵ ring
Mar '77
10 Apr '78
Dec '77
Mar '77
4 Apr '78
10 Apr '78
100
80
60
40
20
0
50.5
51.0
51.5
RADIAL WIDTH (km)
RADIUS (10³ km)

observational geometry. The linear relation is, however, consistent with an elliptical ring, coplanar with the other rings, whose inner and outer boundaries are two Keplerian ellipses with slightly different semi-major axes and eccentricities. A model of this type which accurately fits the observations is described below in section IV(e).

Further information on the nature of the ϵ ring is provided by a comparison of occultation profiles obtained at different times. Figure 5 shows the 99 km wide immersion profile obtained by Millis et al. (1977) on 1977 March 10, and the 72 km wide emersion profile of 1978 April 10. The two profiles are very similar, even in the finer details of the structure. Although the optical depths appear to be comparable, no correction has been made to the 1978 April 10 profile to allow for the $\sim$ 10% contribution of the planet and rings to the observed flux. Such a correction would increase the optical depth for this occultation by $\sim$ 25%, and thus support the conclusion of Elliot et al. (1978) that the integrated optical depth of the ϵ ring is independent of its width. Figure 5 also shows that the edges of the ring remain sharp, even at improved resolution.

The similarity of these two profiles, observed 13 months apart, is rendered truly remarkable when the orbital and precessional motion of the ring particles is considered. The orbital period of the particles is 8.4 ± 0.1 hours, the uncertainty corresponding to the observed range of radii, so that each

Fig. 5 - Comparison of two wide profiles of the ε ring, obtained on 1977 March 10 (Millis et al. 1977) and 1978 April 10. Differing width scales are due to different projected velocities of Uranus relative to the two stars. A temporary loss of data on 1977 March 10 is indicated by a dashed line. The ~ 10% contribution by the planet and rings to the observed 2.2 μm flux has not been subtracted from the 1978 April 10 profile.

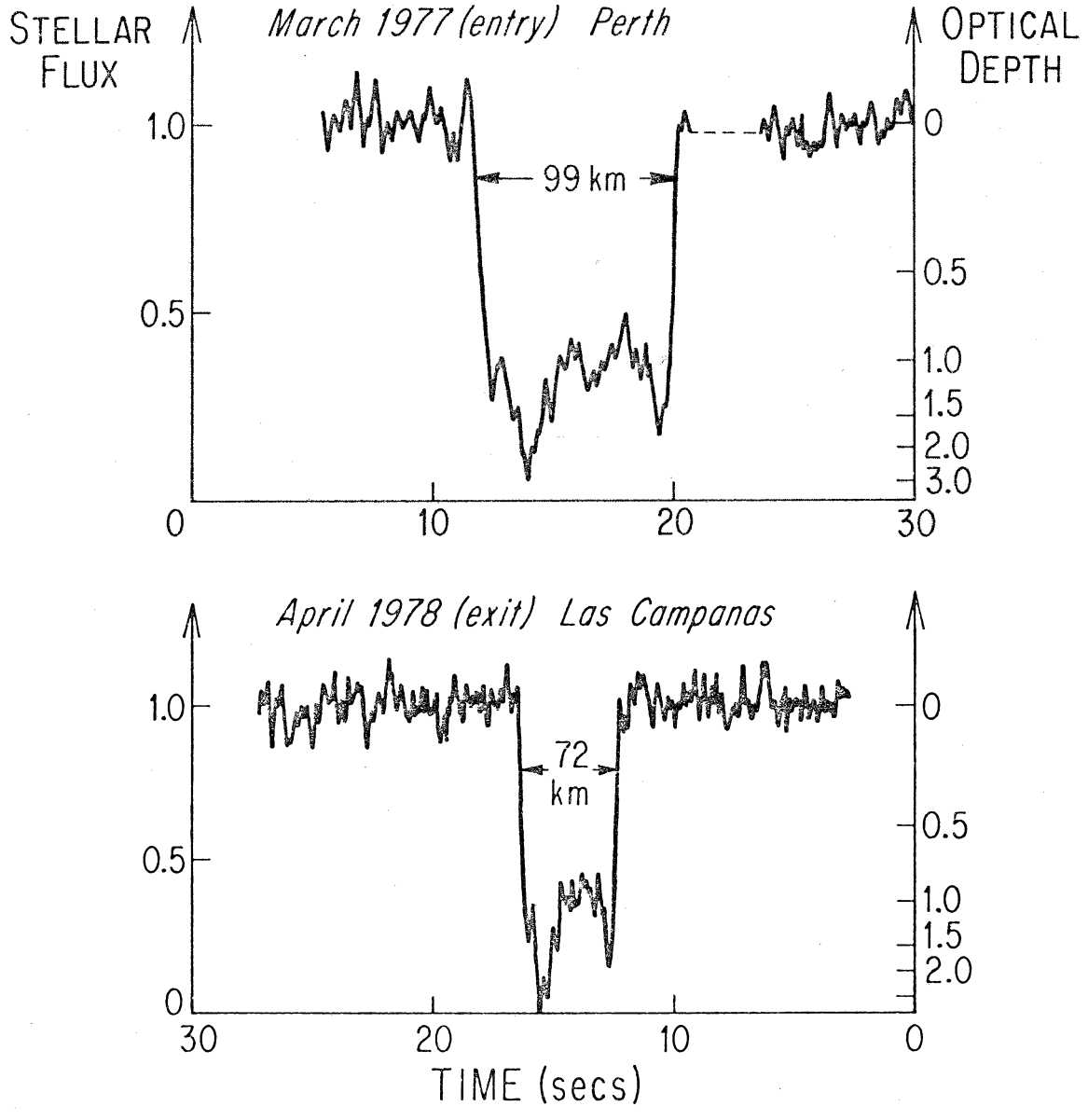
STELLAR FLUX
March 1977 (entry) Perth
OPTICAL DEPTH
1.0
0.5
0
99 km
0
0.5
1.0
1.5
2.0
3.0
0
10
20
30
April 1978 (exit) Las Campanas
1.0
0.5
0
72 km
0
0.5
1.0
1.5
2.0
30
20
10
0
TIME (secs)

particle has completed $\sim$ 1100 orbits in the intervening time. Differential Keplerian motion between the inner and outer edges of the ring (i.e., $\Delta r/r \sim$ 50km/50,000 km) amounts to at least one complete revolution. Differential precession of the apsidal lines of the elliptical particle orbits (or of the nodal lines of circular orbits) would be expected to further smear and broaden the ring, although it is possible that interparticle collisions act to prevent this and maintain instead a uniform average precession rate. Despite these motions, negligible change has occurred in the shape of the ring profile.

(e) A Model of the ε Ring

An attempt was made to construct an elliptical model of the ε ring which would satisfy the available observations. The simplest physically plausible model consists of a Keplerian ellipse which lies in the satellites' orbital plane, and whose apsidal line precesses due to the oblateness of Uranus[2]. As discussed above, the observed profiles and widths of the ε ring suggest that the whole ring precesses as a unit. We therefore chose to fit the model to the centerline of the ring, rather than to the outer and inner edges separately.

Four parameters were adjusted - the semi-major axis, eccentricity, orientation, and apsidal precession rate - to give the best least-squares fit to the observed radii and azimuths of the ε ring. Figure 6 presents the ten available data points and the best fitting model. The data are taken from Table 7 of Elliot et al. (1978) (using the average of their radii for the inner and outer edges of the ring); Millis and Wasserman (1978); and Table IV. The 1978 April 4 point is of much lower accuracy than the others and has been omitted from the fit. Also, numerous attempts to match all four 1977 March 10 immersion

---

[2] Dr. Guiseppe Colombo (private communication) first demonstrated that such an ellipse, given the right precession rate, is a reasonable representation of the observations.

points failed; only their average location could be fitted. For the final fit, shown in Figure 6, the Kavalur and Peking points at radii of 51,713 and 51,740 km were omitted, and only the Perth and KAO points at ~51,678 km were used[3]. This omission makes little difference to the residuals of the other five points, and produces only minor changes in the model parameters. The elements of the model ellipse for epoch 1977 March 10, 20^{hrs} UT (JD 244 3213.33 are:

$\bar{a}$ (semi-major axis) = 51,284 ± 6 km

$\bar{e}$ (eccentricity) = (7.80 ± 0.12) x 10^{-3}

Azimuth of periapse = 212° ± 2°

$\dot{\tilde{\omega}}$ (apsidal precession rate) = $1^{\circ}.374 \pm 0^{\circ}.006$ day^{-1}.

Azimuth is measured in the ring plane, assumed to be the satellite orbit plane, in the prograde direction from the ascending node of this plane on the earth equator of date. The r.m.s. deviation in radius of the seven data points from the model is 7 km, well within the uncertainties. Since this solution might not be unique, initial estimates of $\dot{\tilde{\omega}}$ covering

---

[3] If the Peking occultation time reported (New Scientist (1977) 74, 584) referred to the beginning of the 9.5 sec occultation, rather than to the central time as assumed by Elliot et al. (1978), then the corresponding radius should be reduced by ~ 52 km, bringing the point into excellent agreement with the model. Several different times have been reported for the Kavalur ε ring occultation (Bappu 1977; Bhattacharyya and Kuppuswamy 1977a,b; Bhattacharyya and Bappu 1977; Elliot et al. 1978) and conceivably some error remains in the time adopted by Elliot et al. (1978).

Fig. 6 - Observed radius vs. azimuth for the ϵ ring, and the precessing Keplerian ellipse model which best fits these data. Open symbols represent the observed points, while the corresponding filled symbols at the same radii represent these same points corrected to a common epoch (1977 March 10, 20^{hrs} UT) by removal of precession. The arrows indicate the direction in which the observed points were moved.

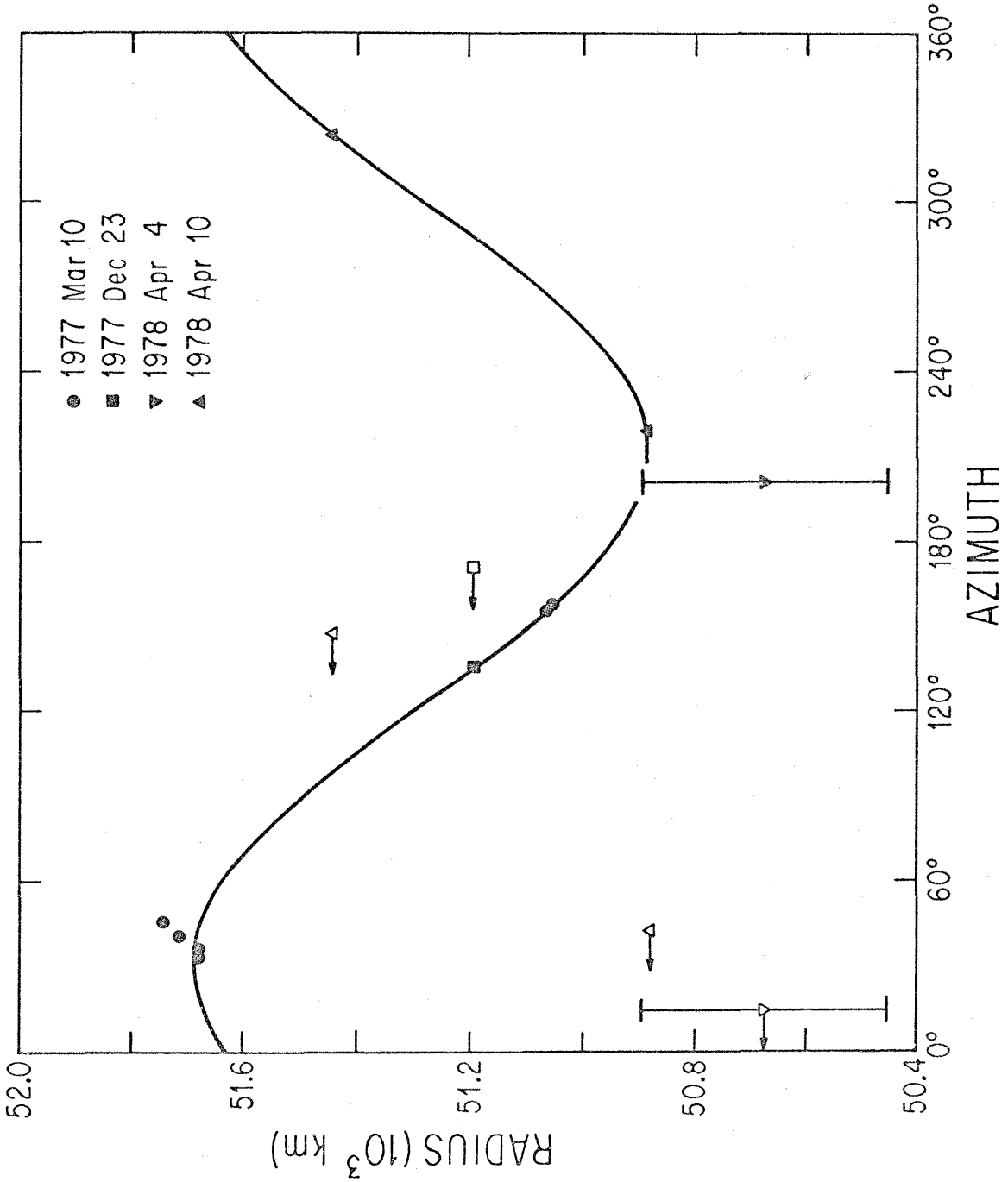
1977 Mar 10
1977 Dec 23
1978 Apr 4
1978 Apr 10
52.0
51.6
51.2
50.8
50.4
RADIUS (10³ km)
0°
60°
120°
180°
240°
300°
360°
AZIMUTH

the range 1° day^{-1} to 10° day^{-1} were used in the least-squares analysis. Ten more solutions were discovered in this manner, but all exhibited r.m.s. deviations $\geq$ 26 km, and typically $\sim$ 75 km. The validity of this model for the ϵ ring can be readily tested by future occultations, since the apparent precision of $\dot{\tilde{\omega}}$ should permit extrapolation of the precession for at least ten years.

Combination of the elements $\bar{a}$ and $\bar{e}$ determined above with the width-radius relation of Figure 4 leads to elements for the ellipses which form the outer and inner edges of the ϵ ring. If these ellipses have semi-major axes and eccentricities $\bar{a} \pm \Delta a$ and $\bar{e} \pm \Delta e$, the radial width W of the ring, as a function of central radius $\bar{r}$, is given to first order in $\bar{e}$ by:

$$W = 2\Delta a + 2(\Delta a/\bar{a} + \Delta e/\bar{e})\ (\bar{r} - \bar{a}) \quad .$$

Fitting this linear relation to Figure 4 yields:

$$\Delta a = 30 \text{ km}$$

$$\Delta e = 0.36 \times 10^{-3} \quad .$$

Finally, Uranus' J_2 (the dimensionless second gravitational harmonic coefficient), can be derived from the apsidal precession rate, since contributions to $\dot{\tilde{\omega}}$ by satellite perturbations should be negligible. Assuming a planetary equatorial radius of 26,200 km (Elliot, et al. 1978), we obtain

$$J_2 = (3.43 \pm 0.02) \times 10^{-3} \quad .$$

The quoted uncertainty is a formal probable error associated with

the least-squares fitting procedure; it does not allow for any systematic errors in the occultation analyses. It is assumed the the ϵ ring is inded a freely precessing Keplerian ellipse, unaffected by resonant interactions. Subject to this assumption, this value of J_2 can be used to predict apsidal precession rates for the other supposed elliptical rings:

$$\dot{\tilde{\omega}}_4 = 2^\circ.61 \text{ day}^{-1} \quad ,$$

$$\dot{\tilde{\omega}}_\alpha = 2^\circ.20 \text{ day}^{-1} \quad ,$$

and $$\dot{\tilde{\omega}}_\beta = 2^\circ.04 \text{ day}^{-1} \quad .$$

When reduced to a common epoch with these precession rates, the available radius-azimuth data for these three rings are consistent with elliptical models. The α ring data show a variation in radius much larger than the uncertainties and are well distributed in orbital phase, defining an elliptical model with the elements:

$$a = 44{,}839 \pm 1 \text{ km}$$

$$e = (0.63 \pm 0.03) \times 10^{-3}$$

azimuth of periapse = $325^\circ \pm 2^\circ$ (epoch 1977 March 10, 20^{hrs} UT).

The r.m.s. deviation in radius of the eight points from this model is 1.6 km. Models for rings 4 and β are less well-defined, because of poor orbital phase distribution of the data. Previous estimates of J_2 have been based on determinations of the apsidal precession of the satellites Ariel (Dunham 1971) and Miranda (Whitaker and Greenberg 1973), which yielded values of 12×10^{-3} and 5×10^{-3} respectively. Such determinations of J_2 are complicated by the effects of the satellites' mutual interactions.

V. CONCLUSIONS

(1) The nine rings observed on 1978 April 10 are the same as those described by Elliot et al. (1978) in their analysis of the 1977 March 10 observations. No additional rings were observed, out to a radius limit of 107,000 km, and no evidence was found for background absorption exceeding 5%.

(2) Observations of the η, γ, and δ rings are consistent with these three rings being coplanar and circular, although the present η ring data are inconsistent in both radius and width with the 1977 March results (Elliot et al. 1978).

(3) Minimum eccentricities for rings 4, α, and β, based on the 1977 and 1978 occultations, are 0.0005, 0.0005, and 0.0003 respectively, under the assumption that all of the rings are coplanar.

(4) Calculated radii for rings 5 and 6 exhibit ranges of $\sim$ 150 km, comparable to the spacing between these two rings. Further occultation observations are necessary to sort out the structure of this region.

(5) Occultation profiles suggest that rings α, γ, and δ are rather opaque and have radial widths in the range 2 to 5 km. The β ring is clearly resolved, and has an average optical depth of $\sim$ 0.5 and width of $\sim$ 15 km. The widths of rings η, 4, 5, and 6 probably lie between 0.5 and 5 km, but see (2) above.

(6) The width and radius of the ϵ ring exhibit a linear relation, which strongly suggests that it is a single, continuous,

non-circular ring.

(7) The optical depth profile of the ε ring, including the sharp edges, has remained essentially unchanged in 13 months, despite differential orbital motion and precession.

(8) Observations of the ε ring obtained in 1977 March, 1977 December, and 1978 April all fit a model of a Keplerian ellipse whose apsidal line is advancing at a rate of $1^{\circ}.37\ day^{-1}$. This rate gives a value of Uranus' J_2 of 3.43×10^{-3}, if resonant interactions are unimportant.

REFERENCES

Bappu, M.K.V. (1977): IAU Circ. No's. 3051 and 3068.

Bhattacharyya, J.C. and Bappu, M.K.V. (1977): Nature 270, 503.

Bhattacharyya, J.C. and Kuppuswamy, K. (1977a): Nature 267, 332.

Bhattacharyya, J.C. and Kuppuswamy, K. (1977b): IAU Circ. No. 3058.

Churms, J. (1977): IAU Circ. No. 3051.

Danielson, R.E., Tomasko, M.G., and Savage, B.D. (1972): Astrophys. J. 178, 887.

Dermott, S.F. and Gold, T. (1977): Nature 267, 590.

Dunham, D.W. (1971): Ph.D. Thesis, Yale University.

Elliot, J.L., Dunham, E. and Mink, D. (1977): Nature 267, 328.

Elliot, J.L., Dunham, E., Wasserman, L.H., Millis, R.L., and Churms, J. (1978): Astron. J. 83, 980.

Joyce, R.R., Pilcher, C.B., Cruikshank, D.P., and Morrison, D. (1977): Astrophys. J. 214, 657.

Klemola, A.R. and Marsden, B.G. (1977): Astron. J. 82, 849.

Liller, W. (1977): Astron. J. 82, 929.

Mahra, H.S. and Gupta, S.K. (1977): IAU Circ. No 3061.

Millis, R.L. and Wasserman, L.H. (1978): Astron. J. 83, 993.

Millis, R.L., Wasserman, L.H., and Birch, P.V. (1977): Nature 267, 330.

Persson, S.E., Nicholson, P.D., Matthews, K., Goldreich, P., and Neugebauer, G. (1978): IAU Circ. No. 3215.

Whitaker, E.A. and Greenberg, R.J. (1973): M.N.R.A.S. 165, 15 p.

Zellner, B. (1977): IAU Circ. No. 3058.

PART 3

ON THE RESONANCE THEORY OF THE RINGS OF URANUS.

P. Goldreich

and

P. D. Nicholson

Published under the title "Revenge of Tiny Miranda", Nature 269 (1977) pp. 783-785.

Dermott and Gold[1] have proposed a resonance model for the rings of Uranus. They assume the rings are, in fact, arcs composed of small particles librating about stable resonances determined by pairs of satellites, either Ariel and Titania or Ariel and Oberon. Dermott and Gold dismiss, as insignificant, resonances involving tiny Miranda. We find that, by a wide margin, the strongest resonances are all associated with Miranda. Furthermore, we show that the hypothesis that the rings are made up of librating particles, while original and ingenious, is incorrect.

Before considering the quantitative analysis of the resonance model, we make two minor points. First, when allowance is made for the orbital motion (assumed prograde) of the ring material between occultations, it is found that the two occulting regions of each ring were physically only 35° (α ring) to 46° (ϵ ring) apart. Thus, only short arcs are required to fit the observations. Second, while large systematic errors may remain in the calculated absolute ring radii, the spacings between the rings are well determined and must be accurately predicted by a resonance theory. In Table 1, the spacings predicted by Dermott and Gold are compared with those deduced by Elliot et al.[2] and Marsden[3]. The discrepancies appear to be larger than observational error and exhibit no systematic trend.

TABLE 1

Observed vs. Resonant Ring Spacings

Ring pair	Spacing (km)*			Difference (km)
	Marsden[3]	Elliot et al.[2]	Resonance model[1]	
α, β	949	926	1026	+ 89
γ, δ	680	672	800	+ 124
ϵ_1, ϵ_2	632	~ 600	483	~ - 130

* Calculated values are averages of occultation entry and exit results.

We have calculated the strengths of the resonances between a ring particle in circular orbit and either a single satellite or a pair of satellites. The resonance strength is expressed as the magnitude of the resonant term in the disturbing potential, $\mathcal{R}$, felt by the ring particle. Figure 1 shows the strengths of the most important resonances in the radial range 42×10^3 km $< a < 54 \times 10^3$ km, which spans the ring radii. The only two-body resonances included in Figure 1 are the 4:1 and 5:1 resonances with Miranda. Two-body resonances involving other satellites also lie in the range of the rings, but their strengths are too small for them to appear in Figure 1.

The strongest resonances are the two-body resonances with Miranda which occur where

$$4n_M - n - 3\frac{d\tilde{\omega}_M}{dt} = 0$$

or

$$4n_M - n - \frac{d\tilde{\omega}_M}{dt} - 2\frac{d\Omega}{dt} = 0 \quad .$$

Here, n_M and n are the mean motions of Miranda and the ring particle, Ω is the longitude of the ascending node of the ring on the orbit of Miranda, and $\tilde{\omega}_M$ is the longitude of Miranda's periapse. The resonance strengths are given by Brouwer and Clemence[5]:

$$\mathcal{R}_1^4 = \frac{GM}{48a}\frac{m_M}{M}\frac{a}{a_M}\, e_M^3 \left[-256\alpha + \left(142 + 114\alpha\frac{d}{d\alpha} + 21\alpha^2\frac{d^2}{d\alpha^2} + \alpha^3\frac{d^3}{d\alpha^3}\right) b_{1/2}^{(1)}(\alpha)\right]$$

Fig. 1 - The strengths of two and three-body resonances in the neighborhood of Uranus' rings. ⊗'s represent the 4:1 and 5:1 resonances with Miranda discussed in the text and identified by $e = e_M$ and $\sigma = \sin(i/2)$; circles represent the three-body resonances for $q = 1$ and values of p as indicated. The resonances previously[1] associated with the rings are shown as crosses.

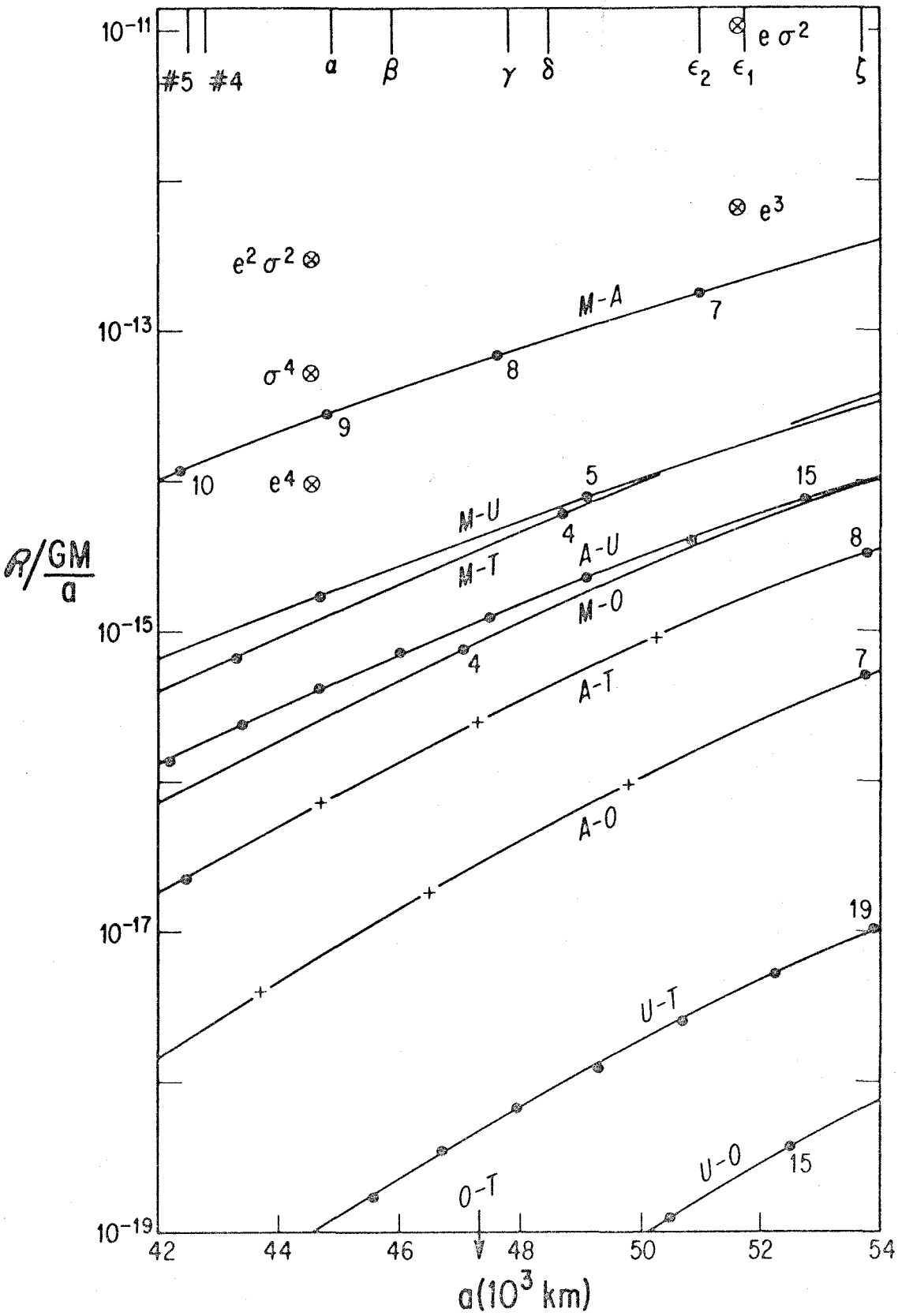
10^{-11}
10^{-13}
10^{-15}
10^{-17}
10^{-19}
$\mathcal{R}/\frac{GM}{a}$
#5 #4 a β γ δ ϵ_2 ϵ_1 ζ
$\otimes e\sigma^2$
$\otimes e^3$
$e^2\sigma^2\otimes$
$\sigma^4\otimes$
$e^4\otimes$
M-A
M-U
M-T
M-0
A-U
A-T
A-0
U-T
U-0
O-T
42 44 46 48 50 52 54
$a(10^3\ km)$

and

$$\mathcal{R}_2^4 = \frac{GM}{4a}\frac{m_M}{M}\frac{a}{a_M} e_M (\sin i/2)^2 \left[\left(8 + \alpha \frac{d}{d\alpha}\right) b_{3/2}^{(2)}(\alpha)\right] ,$$

where M is the mass of Uranus, m_M and e_M the mass and eccentricity of Miranda, i the mutual inclination of the ring and Miranda's orbit, and $\alpha = a/a_M$. The functions $b_s^{(j)}$ are Laplace coefficients. There are three 5:1 resonances, corresponding to

$$5n_M - n - 4\frac{d\tilde{\omega}_M}{dt} = 0 ,$$

$$5n_M - n - 2\frac{d\tilde{\omega}_M}{dt} - 2\frac{d\Omega}{dt} = 0 ,$$

and

$$5n_M - n - 4\frac{d\Omega}{dt} = 0 .$$

Using formulae given by Peirce[6], we obtain the resonance strengths:

$$\mathcal{R}_1^5 = \frac{GM}{384a}\frac{m_M}{M}\frac{a}{a_M} e_M^4 \left[-3125\alpha + \left(1569 + 1556\alpha\frac{d}{d\alpha} + 402\alpha^2\frac{d^2}{d\alpha^2} + 36\alpha^3\frac{d^3}{d\alpha^3} + \alpha^4\frac{d^4}{d\alpha^4}\right) b_{1/2}^{(1)}(\alpha)\right]$$

$$\mathcal{R}_2^5 = \frac{GM}{16a}\frac{m_M}{M}\frac{a}{a_M} e_M^2 (\sin i/2)^2 \left[\left(85\alpha + 20\alpha^2\frac{d}{d\alpha} + \alpha^3\frac{d^2}{d\alpha^2}\right) b_{3/2}^{(2)}(\alpha)\right]$$

$$\mathcal{R}_3^5 = \frac{3GM}{8a}\frac{m_M}{M}\frac{a}{a_M} (\sin i/2)^4 \left[\alpha^2 b_{5/2}^{(3)}(\alpha)\right] ,$$

where a and α now refer to the position of the 5:1 resonance. All of these strengths depend sensitively on the uncertain values of e_M and i. Greenberg[4] has determined that $e_M \simeq 0.012$ and $i \simeq 4°$, though he regards the latter as "extremely model dependent". Using these values, and noting, therefore, that only $\mathscr{R}_1^4$ and $\mathscr{R}_1^5$ are likely to be reasonably accurate, we obtain

$$\mathscr{R}_1^4 \simeq 6.6 \times 10^{-13} \frac{GM}{a} ,$$

$$\mathscr{R}_2^4 \simeq 1.1 \times 10^{-11} \frac{GM}{a} ,$$

$$\mathscr{R}_1^5 \simeq 9.1 \times 10^{-15} \frac{GM}{a} ,$$

$$\mathscr{R}_2^5 \simeq 3.0 \times 10^{-13} \frac{GM}{a} ,$$

and

$$\mathscr{R}_3^5 \simeq 5.2 \times 10^{-14} \frac{GM}{a} .$$

Next, we consider three-body resonances of the form

$$qn - (p + q)n_B + pn_A = 0 ,$$

where p and q are integers and the n's are mean motions with the subscripts A and B denoting the outer and inner satellites. Both satellite orbits are assumed to be circles and to be outside the rings. The dominant resonant term in the disturbing

potential arises as follows. Outer satellite A perturbs the orbit of inner satellite B, producing oscillatory variations in its radius and longitude with frequencies $p(n_A - n_B)$. The potential at the ring due to B moving on its perturbed orbit contains terms with frequencies $qn - (p + q)n_B + pn_A$. These include the resonant term and many short period terms. Additional, but smaller (by a factor $\leqslant 0.1$), resonant terms arise from the attraction of A moving on an orbit perturbed by B. Finally, there are much smaller resonant terms due to the interaction between the direct perturbations of the ring by each satellite moving on its unperturbed circular orbit. The dominant resonant term is easily shown to be

$$\mathcal{R}_{pq} = \frac{GM}{2a}\,\frac{m_A m_B}{M^2}\,\frac{a_A a^2}{a_B^3}\,\frac{n_A^2}{\left[p^2(n_B - n_A)^2 - n_B^2\right]}\;x$$

$$\left\{h_q(\alpha)\left[f_p(\beta) - \frac{2n_B}{p(n_B - n_A)}\,g_p(\beta)\right] +\right.$$

$$\left. g_q(\alpha)\left[\left(1 + \frac{3n_B^2}{p^2(n_B - n_A)^2}\right)g_p(\beta) - \frac{2n_B}{p(n_B - n_A)}\,f_p(\beta)\right]\right\},$$

where the a's are orbital radii, the m's are satellite masses and $\alpha = a/a_B$, $\beta = a_B/a_A$. The functions f_k, g_k, and h_k may be

expressed in terms of Laplace coefficients[5], $b_s^{(j)}$ by

$$f_k(x) = x\, b_{3/2}^{(k)}(x) - \frac{1}{2}\left[b_{3/2}^{(k+1)}(x) + b_{3/2}^{(k-1)}(x) \right] + \delta_{k1} \quad ,$$

$$g_k(x) = \frac{1}{2}\left[b_{3/2}^{(k-1)}(x) - b_{3/2}^{(k+1)}(x) \right] - \delta_{k1} \quad ,$$

$$h_k(x) = \frac{1}{2}\left[b_{3/2}^{(k-1)}(x) + b_{3/2}^{(k+1)}(x) \right] - b_{3/2}^{(k)}(x)/x + 2\delta_{k1} \quad .$$

We have calculated the strengths of all q = 1 resonances due to each pair of satellites using power series approximations for the Laplace coefficients and satellite parameters from Greenberg[4]. The results are displayed in Figure 1, with a smooth curve connecting the resonances due to each satellite pair. It is apparent that resonances involving tiny Miranda, the innermost satellite, dominate the field. The Ariel-Titania and Ariel-Oberon resonances advocated by Dermott and Gold[1] are relatively weak and presumably incapable of determining the ring locations.

Examination of Figure 1 reveals that the strong Miranda-Ariel resonances lie close to four of the rings: Millis et al.'s[7] #5 and Elliot et al.'s[2] α, γ and ϵ_2. Differences between Marsden's[3] calculated positions for these rings and the resonances corresponding to p = 10, 9, 8 and 7 are 155, 96, 157 and 111 km,

respectively, for an assumed $J_2 = 0.013$ for Uranus. As a consequence of the approximate Laplace relation satisfied by the mean motions of Miranda, Ariel and Umbriel[8], several weaker Miranda-Umbriel and Ariel-Umbriel resonances also approximately coincide with the above rings. Furthermore, the 4:1 resonance with Miranda is located about 114 km inside Marsden's[3] position for the ϵ_1 ring.

Despite the near coincidences between the locations of the strongest resonances and some of the rings, the rings cannot be made up of librating material. The maximum radial width of an arc of librating particles is

$$W = 8\left(\frac{a\mathscr{R}}{3GM}\right)^{1/2} a \quad .$$

From the resonance strengths, we obtain $W \approx 0.7$ km for the 4:1 resonance and $W \leqslant 0.07$ km for the strongest Miranda-Ariel resonances. By comparison, the widths of the observed rings range from 1-10 km for the inner rings and 30-100 km for the ϵ ring or rings. Furthermore, libration occurs about a relative maximum of the potential energy in the frame rotating with the resonant mean motion. Thus, inelastic collisions among the particles would be destabilizing and lead to the dissolution of a compact arc of librating material. We conclude that if the ring positions are determined by resonances, the control

is more subtle than previously suggested. One possibility is that the rings are the crests of nonlinear density waves in an optically thin disk of particles. Calculations of the resonant excitation of density waves in Saturn's rings have shown that even weak resonances produce nonlinear waves[9].

REFERENCES

1. Dermott, S.F., and Gold, T. Nature 267, 590-593 (1977).
2. Elliot, J.L., Dunham,E., and Mink, D. Nature 267, 328-330 (1977).
3. Marsden, B.G. IAU Circular 3061 (1977).
4. Greenberg, R. Icarus 24, 325-332 (1975).
5. Brouwer, D., and Clemence, C.M. Methods of Celestial Mechanics, Academic Press, New York, pp. 490-494 (1961).
6. Peirce, B. Astron. J. 1, 1-8, (1849).
7. Millis, R.L., Wasserman, L.H., and Birch, P.V. Nature 267, 330-331 (1977).
8. Sinclair, A.T. Mon. Not. R. Astr. Soc. 171, 59-72 (1975).
9. Goldreich, P., and Tremaine, S. Icarus 34, 240-253 (1978).